Chromosome arrangement and dynamics in the budding bacterium *Hyphomonas neptunium*

Dissertation
zur Erlangung des Doktorgrades
der Naturwissenschaften
(Dr. rer. Nat.)

dem Fachbereich Biologie
der Philipps-Universität Marburg
vorgelegt

von
Alexandra Jung
aus Berlin

Marburg, im Mai 2016

Die Untersuchungen zur vorliegenden Arbeit wurden von Februar 2013 bis Oktober 2015 am Max-Planck-Institut für terrestrische Mikrobiologie und an der Philipps-Universität Marburg unter der Leitung von Professor Dr. Martin Thanbichler durchgeführt.

Vom Fachbereich Biologie der Philipps-Universität Marburg (HKZ: 1180)
als Dissertation angenommen am 22. 08. 2016

Erstgutachter: Prof. Dr. Martin Thanbichler
Zweitgutachter: Prof. Dr. Lotte Søgaard-Andersen

Tag der mündlichen Prüfung: 24. 08. 2016

Publications

Jung A, Eisheuer S, Cserti E, Leicht O, Strobel W, Möll A, Schlimpert S, Kuhn J, Thanbichler M. 2015. Molecular toolbox for genetic manipulation of the stalked budding bacterium *Hyphomonas neptunium*. Appl Environ Microbiol **81:**736-744.

Jung A, Raßbach A, Heinrich K, Thanbichler M. Chromosome arrangement and dynamics in the budding bacterium *Hyphomonas neptunium*. In preparation.

To my family

Zusammenfassung

Korrekte Chromosomenreplikation und die akkurate Segregation des Chromosoms sind essentiell für alle lebenden Zellen und müssen gut mit anderen Prozessen des Zellzyklus, wie z.B. der Zellteilung, abgestimmt sein. Unser bisheriges Wissen über prokaryotische Chromosomendynamik basiert auf Studien einiger weniger Modellorganismen, welche sich durch binäre Teilung fortpflanzen und meist eine stäbchenförmige Morphologie besitzen. Um unser Wissen über bakterielle Chromosomensegregation zu erweitern, wurde vor kurzem in unserem Labor begonnen, die Chromosomendynamik im marinen Alphaproteobakterium *Hyphomonas neptunium* zu untersuchen. *H. neptunium* teilt sich durch Knospung an der Stielspitze und verwendet seinen Stiel als reproduktive Struktur. Diese Art der Teilung unterscheidet *H. neptunium* von den bisher untersuchten Modellorganismen und macht es zu einem interessanten Kandidaten für die Analyse der Chromosomendynamik in Bakterien, da das duplizierte Chromosom zunächst den Stiel durchqueren muss, um die neu gebildete Tochterzelle zu erreichen. Neueste Studien zeigen, dass die Chromosomensegregation in einem einzigartigen, zweistufigen Mechanismus abzulaufen scheint. Zunächst wird die duplizierte centromer-ähnliche Region innerhalb der Mutterzelle, möglicherweise durch einen ParABS-abhängigen Mechanismus, an deren gestielten Pol segregiert und verweilt dort, bis sich eine sichtbare Knospe an der Stielspitze gebildet hat. Anschließend wird die centromer-ähnliche Region in einem zweiten Schritt durch den Stiel in die Knospe transportiert. Verschiedene Anhaltspunkte deuten darauf hin, dass dieser zweite Segregationsschritt durch einen neuen, bisher unbekannten Mechanismus vermittelt wird. Chromosomenreplikation und -segregation finden in Bakterien gewöhnlich gleichzeitig statt. Der zweiteilige Segregationsmechanismus lässt allerdings darauf schließen, dass die Chromosomenreplikation und die Segregation durch den Stiel, ähnlich wie bei der eukaryotischen Mitose, zeitlich entkoppelt sind.

In dieser Arbeit wurde die Rolle des ParABS-Systems in der Chromosomensegregation in *H. neptunium* genauer analysiert. Es konnte gezeigt werden, dass das ParABS-System essentiell für die Lebensfähigkeit der Zelle sowie für die Chromosomensegregation ist. Die Beeinträchtigung der Funktionalität von ParA führte zu einer Veränderung der Zellmorphologie sowie zu einer unvollständigen Segregation der centromer-ähnlichen Region innerhalb der Mutterzelle, was dazu führte, dass auch die Segregation durch den Stiel nicht mehr stattfand. Dies zeigt, dass das ParABS-System die Segregation der centromer-ähnlichen Region in der Mutterzelle vermittelt und dass es sich bei der Segregation innerhalb der Mutterzelle und durch den Stiel um sequenzielle Prozesse handelt. Weiterhin wurde die Rolle von PopZ und SMC in *H. neptunium* untersucht, da diese Proteine in anderen Bakterien eine zum Teil wichtige Rolle in der Chromosomensegregation spielen. PopZ lokalisiert in der entstehenden Knospe am Pol gegenüber des Stiels und es konnte gezeigt werden, dass es eine untergeordnete Rolle in der Positionierung der ParABS-Segregationsmaschinerie spielt. SMC scheint essentiell in *H. neptunium* zu sein und zeigt ein ähnliches Lokalisationsmuster wie ParB (centromer-ähnliche Region).

Die Analyse sieben verschiedener genomischer Loci in neugeborenen Zellen zeigte, dass das Chromosom entlang der Längsachse der Zelle ausgerichtet ist, wobei die centromer-ähnliche Region am flagellierten und die Terminusregion am gegenüberliegen Zellpol liegt. Die anderen Loci zeigen eine lineare Anordnung zwischen den Zellpolen, welche mit ihrer Position in der chromosomalen Sequenz korreliert. Weiterhin wurde gezeigt, dass der ParB/*parS*-Komplex als erstes innerhalb der Mutterzelle und anschließend durch den Stiel segregiert wird, was die zentrale Rolle des Komplexes im Segregationsprozess verdeutlicht.

Wie bereits erwähnt, deutet der zweiteilige Segregationsmechanismus auf eine zeitliche Entkopplung von Chromosomenreplikation und -segregation durch den Stiel hin. Um die Koordination dieser Prozesse genauer zu untersuchen, wurden Fluoreszenzfusionen verschiedener Replisomkomponenten generiert und deren Lokalisationsmuster analysiert. Die Replikationsmaschinerie zeigte eine dynamische Lokalisation innerhalb der Mutterzelle: in Zellen, die sich sehr wahrscheinlich am Übergang vom Schwärmer- zum

Stielzellstadium befinden, sowie in gestielten Zellen wird das Replisom am Pol gegenüber des (zukünftigen) Stiels assembliert und bewegt sich über die Zellmitte in die Nähe des gestielten Pols, wo es anschließend wieder deassembliert wird. Dieses Lokalisationsmuster korreliert mit der Lage der Ursprungs- und Terminusregion innerhalb der Zelle. Die beiden Replisomen scheinen unabhängig voneinander entlang der beiden Chromosomenarme zu wandern. Die Kolokalisation von ParB (centromer-ähnliche Region) und DnaN (Replisom) zeigte, dass häufig ein Großteil des Chromosoms bereits repliziert ist, bevor dessen Segregation durch den Stiel erfolgt. Dies bedeutet, dass die Replikation zum Teil zeitlich von der Segregation durch den Stiel entkoppelt ist.
Zusammenfassend erweitern diese Beobachtungen unseren Einblick in die Chromosomendynamik in *H. neptunium* und deuten darauf hin, dass dieser Organismus bereits beschriebene Segregationsmechanismen, wie das ParABS-System, mit einem neuartigen Mechanismus kombiniert, den es aufzuklären gilt.

Abstract

Faithful chromosome replication and segregation are essential for every living cell and must be tightly coordinated with other cell cycle events such as cell division. Our knowledge about prokaryotic chromosome dynamics is based on studies of only a few model organisms that divide by binary fission and are mostly characterized by a rod-like morphology. To broaden our insight into bacterial chromosome segregation, our lab has recently started to analyze chromosome dynamics in the marine alphaproteobacterium *Hyphomonas neptunium*, which divides by budding at the tip of the stalk and uses its stalk as a reproductive structure. This mode of reproduction distinguishes *H. neptunium* from so far studied model organisms and renders it an exciting candidate for the study of chromosome dynamics, since the duplicated chromosome must transit the stalk to reach the newly generated daughter cell. Recent work has revealed that the *H. neptunium* chromosome is segregated in a unique two-step process. At first, one of the duplicated origins is segregated within the mother cell, possibly in a ParABS-dependent manner, and remains at the stalked mother cell pole until a visible bud has formed at the tip of the stalk. In a second step, it is then segregated through the stalk into the bud. Several lines of evidence suggest that the transport through the stalk is mediated by a novel, yet unidentified, segregation mechanism. Commonly, chromosome replication and segregation occur concomitantly in bacteria. However, this two-step segregation mechanism implies a temporal uncoupling of chromosome replication and segregation through the stalk, reminiscent of eukaryotic mitosis.

In this work, we analyzed the role of the ParABS system in chromosome segregation of *H. neptunium*. The ParABS system was shown to be essential for cell viability and chromosome segregation. Impairment of ParA functioning leads to morphological alterations and incomplete origin segregation within the mother cell and, consequently, hampers chromosome segregation through the stalk. This shows that the ParABS system mediates origin segregation within the mother cell. It also implies that chromosome segregation within the mother cell and through the stalk are sequential processes. Furthermore, we analyzed the role of PopZ and SMC in *H. neptunium,* since these proteins were shown to be involved in chromosome segregation in other bacteria. PopZ localizes to the pole opposite the stalk in the newly generated bud and appears to play only a minor role in the positioning of the ParABS partitioning machinery. SMC seems to be essential in *H. neptunium* and shows a similar localization pattern as ParB. Determination of the location of seven genomic loci in new-born cells revealed that the chromosome shows a longitudinal arrangement with the origin located at the flagellated pole and the terminus at the opposite cell pole. The other loci are arranged between both cell poles in a linear order that correlates with their position on the genomic map. Moreover, analysis of chromosome dynamics indicates that the ParB/*parS* complex is the region to be segregated first within the mother cell and also through the stalk, emphasizing its central role in the segregation process. As mentioned above, the observed two-step chromosome segregation mechanism suggested a temporal uncoupling of chromosome replication and its segregation through the stalk. To investigate the coordination between these two processes in more detail, we followed replisome dynamics by fluorescence labeling of different replisome components. The replication machinery shows a dynamic localization within the mother cell: in cells that are most likely at the swarmer-to-stalked cell transition as well as in stalked cells, it assembles at the pole opposite the (future) stalk and moves, via midcell, close to the stalked cell pole, where it disassembles again. This localization pattern is consistent with the observed location of the origin and terminus region. Furthermore, the replisomes appear to track independently along the two chromosome arms. Co-localization of ParB (origin) and DnaN (replisome) revealed that a large part of the chromosome is replicated before its segregation through the stalk commences, indicating that these processes are partially temporally uncoupled. Collectively, these observations expand our insight into chromosome dynamics in *H. neptunium* and suggest that it combines previously described segregation mechanisms, such as the ParABS system, with a novel segregation mechanism that awaits discovery.

Abbreviations

aa	amino acid
Anti-GFP	anti-green fluorescent protein
Anti-RFP	anti-red fluorescent protein
AP	alkaline phosphatase
ATCC	American Type Culture Collection
bp	base pair(s)
DAP	diaminopimelic acid
DAPI	4',6-diamidino-2-phenylindole
DEPC	diethylpyrocarbonate
DIC	differential interference contrast
DMSO	dimethyl sulfoxide
DNA	deoxyribonucleic acid
dNTP	any of the triphosphates of the four naturally occurring coding deoxynucleosides
DTT	dithiothreitol
EDTA	ethylenediaminetetraacetate
EdU	5-ethynyl-2'-deoxyuridine
HRP	horseradish peroxidase
IgG	immunoglubulin G
kb	kilo base pair(s)
kDa	kilo Dalton
LB	Luria-Bertani
MB	Marine Broth
NCBI	National Center for Biotechnology Information
nt	nucleotide(s)
OD_{600}	optical density at 600 nm
PAA	polyacrylamide
PAGE	polyacrylamide gel electrophoresis
PCR	polymerase chain reaction
PG	peptidoglycan
Poly (dI-dC)	Poly(deoxyinosinic-deoxycytidylic) acid sodium salt
PVDF	polyvinylidene fluoride
RNA	ribonucleic acid
rpm	revolutions per minute
SDS	sodium dodecyl sulphate
TEMED	*N*, *N*, *N*', *N*'-tetramethylethylenediamine
Tris-HCl	Tris(hydroxymethyl)aminomethane hydrochloride
WT	wild type
x g	multiple of acceleration of gravity

Contents

1 Introduction

Faithful duplication and segregation of genetic material is essential for every living cell. Unlike in eukaryotes, chromosome replication and segregation occur concurrently in bacteria, implying that these processes need to be tightly regulated and coordinated. Importantly, the bacterial chromosome must be compacted more than 1000-fold to fit the size of a bacterial cell and, at the same time, must be accessible for processes such as transcription, replication, repair, and segregation. In the last years, advances in live cell imaging and the development of new techniques provided new insights into bacterial chromosome organization and dynamics and revealed that bacterial chromosomes show a defined structure with dedicated mechanisms for compaction, replication, and segregation. This confirms once more that bacterial cells, despite their small size, are not simply cells that are randomly packed with DNA and proteins, but highly organized and structured organisms.

1.1 Chromosome organization in bacteria

In contrast to eukaryotes, bacteria lack a nucleus. Instead, bacterial chromosomes together with its associated factors reside in a defined region within the cell, called the nucleoid. Most bacteria possess a single circular chromosome with a size of ~1-9 Mb. However, there are also bacteria that harbor multipartite genomes (e.g. *Vibrio cholerae*, *Brucella abortus*, or *Sinorhizobium meliloti*) and/or linear chromosomes (e.g. *Streptomyces coelicolor, Agrobacterium tumefaciens*, or *Borrelia burgdorferi*). Chromosome replication starts at a defined site known as the origin of replication (*oriC*), occurs bidirectionally along the chromosomal arms, and finishes in the so-called terminus (*ter*) region (see Figure 1-1 A) (1).
The bacterial chromosome is a highly structured and organized entity that shows a helical organization (2). Various factors such as macromolecular crowding, negative supercoiling, small nucleoid associated proteins (NAPs), and the bacterial condensin-like SMC (structural maintenance of chromosome) protein contribute to the global compaction of the chromosome (reviewed in (2)). NAPs (e.g. H-NS, IHF, HU, and Fis) are small and highly abundant DNA binding proteins that bend, bridge, and wrap DNA. The bacterial SMC complex is involved in both chromosome segregation (see 1.3.3) and compaction (2, 3). It has been proposed that it operates as a DNA clamp that captures DNA within a ring structure and keeps distinct regions of the chromosome in close proximity (3-5).

Two major patterns of spatial chromosome organization were identified in bacterial cells using fluorescent repressor operator systems (FROS) and plasmid-based ParB/*parS* systems: a longitudinal organization pattern (also called *ori-ter*) and a transverse organization pattern (left-*ori*-right pattern) (reviewed in (6)). For the longitudinal organization pattern, the origin region is located at the old cell pole and oftentimes anchored by a polar landmark protein (see 1.3.1). The terminus resides at the opposite cell pole and the two chromosomal arms lie side by side between *ori* and *ter*. During chromosome segregation, one of the duplicated origins is segregated to the opposite cell pole followed by the remainder of the newly replicated DNA and the displacement of the terminus towards midcell. Hence, predivisional cells display an *ori-ter ter-ori* configuration and the *ori-ter* pattern is established for the next generation (see Figure 1-1 B) (reviewed in (6)). For the transverse organization pattern, the origin region is found at midcell, while the two chromosomal arms occupy the two different cell halves connected by the terminus region. Here, the duplicated origins are segregated to the quarter positions of the cell followed by the replicated chromosomal arms and the left-*ori*-right pattern is thus regenerated in the future generation (see Figure 1-1 C) (6-8). Chromosome organization has so far mostly been analyzed in rod-shaped bacteria and it appears that the longitudinal organization pattern, as found in *Caulobacter crescentus*, *Myxococcus xanthus*, and *V. cholera*, is the most common one (6, 9-11). The transverse organization pattern was described for slow-growing *Esche-*

richia coli cells, whereas in fast-growing *E. coli* cells an *ori-ter*-like pattern was observed (7, 8, 12). However, evidence exists that slow growing *E. coli* cells might switch between the left-*ori*-right and the *ori-ter* pattern during their cell cycle (13). Interestingly, *Bacillus subtilis* also switches between these two patterns during its cell cycle and developmental states. In sporulating cells, the duplicated chromosomes adopt an *ori-ter* pattern, whereas in vegetative cells the chromosome switches between these patterns in the course of the cell cycle (6, 14-17). Interestingly, the ParABS partitioning system together with polar landmark proteins that are involved in the correct positioning of the segregation machinery help to generate and/or maintain the *ori-ter* pattern (see 1.3.1) (6). In contrast, generation of the left-*ori*-right pattern requires the SMC complex (17, 18).

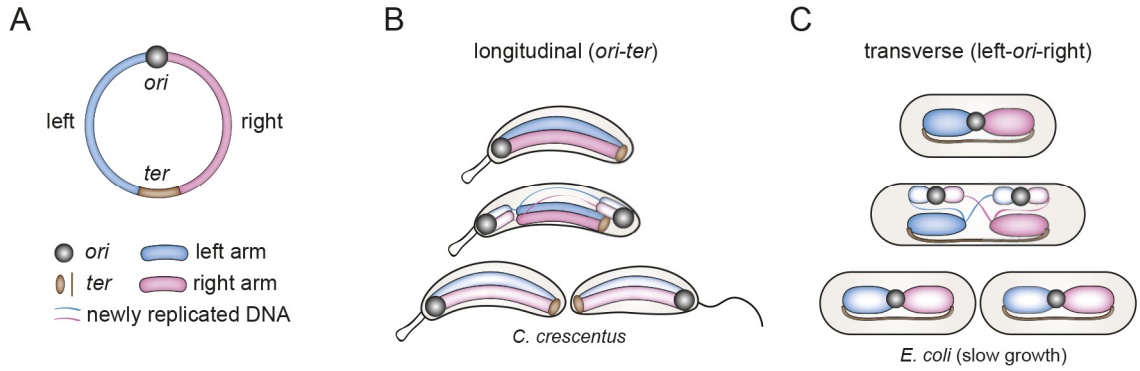

Figure 1-1: Chromosome arrangement in bacteria. Schematics of A) a circular chromosome with origin of replication (*ori*), terminus (*ter*), and left and right chromosomal arms (left and right), B) longitudinal arrangement (*ori-ter*) pattern exemplified in *C. crescentus*, C) transverse (left-*ori*-right) organization pattern in slow growing *E. coli* cells. Please refer to text for details. Adapted from (6).

Furthermore, a comprehensive study in *C. crescentus*, in which more than 100 chromosomal loci were labeled using FROS, revealed that the chromosome has a conserved arrangement within the cell and that this arrangement is immediately restored after segregation. Interestingly, it was also shown that the subcellular localization of chromosomal loci correlated linearly with their position on the genomic map (9). This has been also observed for many other bacterial species, supporting the notion that bacterial chromosomes are spatially and temporally highly organized (10, 11, 19-21).

Bacterial chromosomes are further organized into macrodomains or chromosomal interaction domains. Fluorescence *in situ* hybridization (FISH) and λ recombination-based assays revealed that the *E. coli* chromosome is organized into four Mb-sized macrodomains (*ori*, *ter*, left, and right) and two non-structured regions adjacent to the *ori* macrodomain. Macrodomains are characterized by a high frequency of contacts between chromosomal loci and a similar subcellular localization (19, 22). The *ter* macrodomain was shown to be organized and compacted by the DNA-binding protein MatP. MatP specifically binds to *matS* sites, which are exclusively found in the *ter* macrodomain, and brings together distal MatP/*matS* complexes by its bridging ability (23, 24).

Chromosome conformation capture analysis in combination with deep sequencing (Hi-C) revealed that the *C. crescentus* chromosome consists of multiple highly self-interacting regions called "chromosome interaction domains" (CIDs) that are ~30-420 kb long and largely spatially independent. CID boundaries are thought to be generated to some extent by highly expressed genes (25). Recently, CIDs were also identified in *B. subtilis* as well as three global domains (*ori*, central, and *ter*), whose formation requires ParB/*parS* and the SMC complex (26, 27). Of note, genome labeling in combination with 3D-structured illumination microscopy (SIM) in *B. subtilis* revealed an additional organizational unit designated "high-density chromosomal region" (HDR). These regions of higher density are larger than average CIDs, and it was proposed that HDRs might represent a stochastic union of CIDs (27).

Macrodomains and CIDs are further organized into independent supercoiled domains that fold into plectonemic loops and emerge from the central body of the chromosome, reminiscent of bottlebrush bristles (2, 25, 28, 29). Experiments in *E. coli* and *Salmonella typhimurium* revealed that these topological domains have an average size of ~10 kb (28, 30). In recent years, it became more and more evident that the 3D architecture and dynamic properties of the chromosome impact diverse cellular processes and display another, yet largely unexplored, level of encoded information (31). For instance, chromosome conformation and topology were shown to be involved in regulating the initiation of replication (32). The process of bacterial chromosome replication and its regulation will be briefly summarized in the following chapter.

1.2 Chromosome replication in bacteria

The duplication of the genetic material must be tightly regulated to ensure that it is precisely coordinated with other cell cycle events and occurs only once per cell cycle. Replication initiates at a single, well-defined structure designated origin of replication (*oriC*) and requires the initiator protein DnaA, which binds to several DnaA binding motifs in the origin region (33). Upon ATP binding, DnaA forms helical oligomeric structures that trigger the local unwinding and melting of the DNA at an AT rich DNA unwinding element (DUE) (34). This open complex provides an entry site for components of the DNA replication machinery. The helicase complex is then recruited in a DnaA-dependent manner to set up the replication fork followed by the other replication proteins that together form the replisome (35). The two sister replisomes then track, presumably independently, along the chromosomal arms (10, 17, 36, 37). Replication finishes in the terminus region, the replisomes disassemble, and the two sister chromosomes are separated by resolution of interlinked chromosomes or chromosome dimers if required (see 1.3.4). The subcellular sites of replisome assembly and disassembly depend on the arrangement of the chromosome, i.e. the subcellular location of the origin and the terminus region (36, 38). To ensure that replication initiation occurs at the right time and only once in the cell cycle, the accessibility of DnaA to *oriC* as well as the DnaA activity is tightly regulated. For instance, DNA-binding proteins that interact with *oriC* modulate DnaA binding by competing for binding sites, sequestration of *oriC*, and/or by changing the architecture of the origin region (by e.g. DNA bending). Furthermore, it was shown that they are also involved in regulating *dnaA* transcription (39). Moreover, DnaA activity is controlled by regulation of its nucleotide state (40). In recent years, it became increasingly evident that DNA topology, architecture, and methylation of the origin region display important factors for replication initiation control (32, 34).

1.3 Chromosome segregation in bacteria

In eukaryotes, chromosome replication and segregation are temporally uncoupled and occur in different phases of the cell cycle. After replication, sister chromatids experience a long cohesion period (S-, G2- and part of M-phase) that is often mediated by cohesin proteins. After the completion of chromosome replication, the chromosomes undergo an additional condensation step to prepare for chromosome segregation, which is mediated by a mitotic spindle apparatus that pulls the duplicated chromosome simultaneously to opposite cell halves (reviewed in (41, 42)).

In bacteria, chromosome replication and segregation occur concurrently, which implies that these processes need to be tightly regulated in time and space. Chromosomal loci are replicated and, after a short period of sister chromatid cohesion (fraction of S-phase), immediately segregated to their final destination in the newly formed daughter cell apparently without the help of a spindle apparatus (2, 41, 42).

How chromosome segregation is mediated in bacteria is not completely understood and it appears that different mechanisms exist among bacterial species. In general, chromosome segregation can be divided into three steps: 1) segregation of the origin region, 2) bulk chromosome segregation, and 3) segregation

of the terminus region (2). The ParABS system and the SMC complex have been mainly implicated in origin segregation (3, 43). How bulk chromosome segregation is achieved, is currently not well understood. Entropic forces, the release of chromosome cohesion, transcription, and (lengthwise) condensation have been suggested to contribute to bulk chromosome segregation (2, 29, 44-48). The DNA translocase FtsK was shown to mediate terminus separation and segregation (49).

1.3.1 The ParABS system in bacterial chromosome segregation

Much of our knowledge about ParABS-mediated DNA segregation mechanisms is derived from studies of low copy number plasmids, where ParABS was shown to be essential for plasmid maintenance (50). A large part of the sequenced bacterial genomes encodes related ParABS partitioning systems that contribute, to varying extents, to active segregation and positioning of newly replicated origins (2, 43, 51). This tripartite system consists of a centromere-like *parS* site, the DNA-binding protein ParB, which binds to the *parS* sites in the origin region and further spreads along the DNA forming a large nucleoprotein complex (partitioning complex), and the Walker-type ATPase ParA (2, 52-55). ParA is characterized by a low intrinsic ATPase activity and binds non-specifically to DNA in its ATP-bound state. Binding of the ParB/*parS* complex to nucleoid associated ParA-ATP triggers ATP hydrolysis, and monomeric ParA is released from the structure. The ParB/*parS* complex then encounters neighbouring ParA molecules and the cycle of binding, hydrolysis, and release repeats, resulting in movement of the origin region (2, 50, 56). However, the exact mechanism of how the translocation force and directionality are generated is still under debate and different models have been proposed based on different lines of evidence. In the "filament pulling model", ParA was proposed to polymerize into a large filamentous structure across the cell that retracts upon interaction with ParB/*parS* and, hence, pulls the duplicated origin region to the opposite cell pole (57-60). On the other hand, in the "diffusion-ratchet model", ParA-ATP dimers bind non-specifically over the nucleoid without forming any higher order structures and the ParB/*parS* complex diffuses gradually along a local ParA gradient in a ratchet-like mechanism (61-64). Recent research in *C. crescentus* supported a "DNA relay model" that complements the "diffusion-ratchet model". Based on mathematical modelling combined with experimental data, it was argued that diffusion of the partitioning complex alone is not sufficient to ensure the observed directionality and speed of the ParB/*parS* translocation (65). Lim *et al.* suggested that the elastic dynamics of the chromosome contribute to relay the ParB/*parS* complex from one DNA region to another by using ParA-ATP dimers as temporary tethers. Furthermore, the study provides evidence that the abundance and distribution of ParA, the movement of the ParB/*parS* complex *in vivo* as well as *in vitro* data are inconsistent with the previous proposed "filament pulling model" (65).
Chromosome-encoded ParABS-based partitioning systems are widely conserved among bacterial species and are mostly encoded in close proximity to the origin of replication. However, the well-studied model organism *E. coli* for instance does not harbor a chromosome-encoded ParABS system (51) (see below). The contribution of ParABS to origin segregation and positioning differs among bacteria and it was shown that ParAB and *parS* are also implicated in additional cellular processes. The following sections will give an overview about the role of the ParABS partitioning system in different model organisms.

C. crescentus

ParABS-mediated chromosome segregation has been extensively studied in *C. crescentus* and it was shown that *parABS* are essential for chromosome segregation and cell viability (66-68). As mentioned above, origin-proximal *parS* sites bound by ParB display a centromere-like structure, on which force is exerted during segregation and which thus is the region to be segregated first (67, 68). It was shown that the *parS* displacement to origin-distal sites of the genome leads to a global reorientation of the chromosome in a

way that *parS* sites still localize to the cell pole but not the origin (69). Moreover, segregation is delayed until the replication of the origin-distal *parS* sites is accomplished (68). Depletion of ParB inhibits Z-ring formation and cell division resulting in filamentous cells (66). Overexpression of either ParA or ParB also resulted in cell division as well as chromosome segregation defects. Interestingly, simultaneous overexpression of both ParA and ParB only led to mild division defects, suggesting that the ratio of both proteins is critical for their proper function (66, 67). Besides its role in origin segregation, ParB is also indirectly involved in correct Z-ring positioning by interaction with the Z-ring inhibitor MipZ (70). This tight coordination of chromosome segregation with cell division presumably explains the essentiality of ParABS in this organism. Furthermore, a recent study suggests that binding of the replication initiator DnaA to the centromere region enables chromosome segregation, indicating a close link between chromosome replication and segregation (71).

As mentioned above, the *C. crescentus* chromosome displays a longitudinal arrangement with the origin region located at the flagellated/stalked pole and the terminus at the opposite cell pole (9, 72, 73). At the beginning of the cell cycle, the origin region is anchored to the old cell pole via an interaction of ParB (binding to the origin-proximal *parS* sites) with the pole-organizing protein PopZ (see Figure 1-2) (67, 74, 75). At the onset of chromosome segregation, the origin region is released from the PopZ matrix, replicated, and one of the duplicated origins is then moved to the opposite cell pole in a ParABS-dependent manner. In brief: dimeric ParA-ATP binds non-specifically to the dynamic nucleoid, forming a gradient away from the ParB/*parS* partitioning complex. When the ParB/*parS* complex encounters ParA-ATP dimers, it binds to them and triggers ATP-hydrolysis of ParA, leading to the release of monomeric ParA. The ParB/*parS* complex is loosened and can interact with neighbouring nucleoid-bound ParA dimers. This binding cycle promotes the movement of the ParB/*parS* complex to the opposite cell pole with the help of the dynamic motion of the chromosome. Before the ParB/*parS* complex arrives at the new cell pole, PopZ adopts a bipolar localization ready to anchor the segregated ParB/*parS* complex at the new cell pole (see Figure 1-2) (56, 58, 65, 68, 74-79). Apart from its role in immobilizing the origin region at the new cell pole, PopZ is required to capture monomeric ParA and possibly regenerate ParA dimers. Hence, PopZ is needed for both the directionality of the segregation process and the correct positioning of the segregation machinery (77).

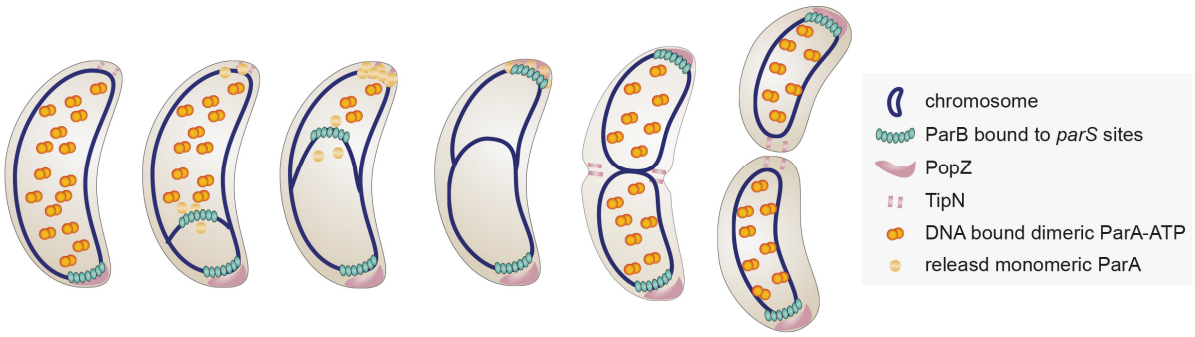

Figure 1-2: Schematic representation of chromosome segregation in *C. crescentus*. The origin region is actively segregated by the ParABS system. Please refer to text for detailed description. Adapted from (78, 80, 81).

PopZ is a small protein that can form large polymeric networks at the cell poles. It acts as a polar landmark that, next to its role in the positioning of the segregation machinery, is involved in the polar recruitment of cell cycle regulators (74-76). Deletion of *popZ* causes an aberrant localization of ParAB and cell division defects, resulting in the formation of filamentous cells and minicells (74, 75).
ParA interacts additionally with the polarity factor TipN at the new cell pole (see Figure 1-2). Deletion of *tipN* causes pleiotropic cell polarity defects and compromised ParAB dynamics, but only a mild cell division defect (58, 78, 82, 83). Interestingly, deletion of *popZ* and *tipN* is synthetically lethal, while overpro-

duction of TipN in a *popZ* deletion strain supresses the cell filamentation phenotype and rescues the ParAB mislocalization phenotype (75, 77, 78). Therefore, it was suggested that TipN and PopZ act synergistically in capturing and/or modulating of the activity of free ParA at the new cell pole (78). However, a more outstanding role for PopZ in the regulation of the directionality and positioning of the segregation machinery has been proposed (77).

V. cholerae

V. cholerae represents one of the most important model organisms for the study of multipartite genomes, since it possesses two circular chromosomes, chr1 (~ 3 Mb) and chr2 (~ 1.1 Mb), that each harbor a ParABS partitioning system (84). Both chromosomes show a longitudinal arrangement: the centromere region (ParB/*parS*) of chr1 is anchored to the new cell pole by the polar landmark protein HubP via an interaction with ParA1, whereas the centromere of chr2 resides at midcell. The terminus regions of both chromosomes are arranged at the new cell pole and appear to be organized by the MatP/*matS* system (11, 85, 86). Segregation of chr1 was shown to occur asymmetrically with one of the duplicated centromeres (ParB/*parS*) moving to the opposite cell pole. Interestingly, similar to *C. crescentus*, ParA1 of *V. cholerae* also forms a retractable cloud-like structure between the centromere region and the cell pole (57). In contrast, chr2 segregation occurs symmetrically with the duplicated centromeres being transported from midcell to the cell quarter positions (11, 57).
The Par systems of the two chromosomes differ and were shown to act independently of each other in chromosome segregation (87). ParAB of chr1 are similar to other chromosome-encoded Par proteins, whereas ParAB of chr2 are similar to plasmid-encoded ParAB (88, 89). The ParABS1 system is not essential. Deletion of *parA1* leads to the loss of polar localization of *ori*1, but the chromosomes are still effectively segregated to the daughter cells, suggesting the existence of a redundant system for the segregation of the chr1 origin (57, 90). Consistently, deletion of *parB1* also results in failure of polar *ori*1 localization and additionally causes an overinitiation phenotype of chr1 that is *parA1* dependent, suggesting a link to chromosome replication, possibly by a direct interaction of ParAB1 with DnaA (91). In contrast, the ParABS2 system is essential for segregation and maintenance of chr2 (87). In this case, a connection between chromosome replication and segregation also exists, since it was shown that ParB2 is involved in the regulation of replication initiation at the origin of chr2 (92, 93).

B. subtilis

In *B. subtilis*, the ParABS system makes only a minor contribution to chromosome segregation, since only < 2 % anucleate cells were observed upon deletion of *parB* (*spoOJ*). Moreover, no increase in the frequency of anucleate cells could be detected in the absence of *parA* (*soj*) (94, 95). However, double deletion of *parB* and *smc* lead to a significant increase in anucleate cells (compared to the respective single knockouts) (95, 96). This could be explained by the discovery that the ParB/*parS* complex is required to efficiently recruit the SMC complex to the origin region, where it is then loaded onto the DNA (97, 98). In *B. subtilis*, SMC was shown to be required for proper origin segregation and chromosome organization (see below) (97-100). It is important to mention that also the double deletion of *smc* and *parA* resulted in an increased frequency of anucleate cells (compared to single deletions) (95, 100).
Interestingly, a recent study reported that ParA, and probably the whole ParABS machinery, enables the segregation of the ParB/*parS* complex from midcell to the nucleoid periphery (17). It appears that template DNA in *B. subtilis* shows a left-*ori*-right pattern (with *ori* at midcell), while newly replicated DNA is segregated to the nucleoid periphery, adopting an *ori-ter* pattern (17). In the absence of ParA, origin movement was not directional anymore and if the duplicated origins reached the nucleoid periphery, they oftentimes moved back to midcell (17). Hence, it was proposed that the ParABS system actively segregates the duplicated origins from midcell to the nucleoid edge and is therefore important to establish and main-

tain the *ori-ter* pattern (17). This is consistent with the observation from earlier studies that deletion of *parA* and *parB*, respectively, results in impaired positioning of replicated origins in a subpopulation of cells (95, 98). In summary, the ParABS system and the SMC complex appear to have complementary roles in origin segregation. Usually, the ParABS system seems to have a supporting role in *ori* segregation but becomes crucial for chromosome partitioning in the absence of SMC (100).
Apart from its role in *ori* segregation, ParA was shown to regulate the initiation of replication by directly interacting with DnaA (101). Monomeric ParA inhibits the initiation of replication by preventing the oligomerization of DnaA, which is a prerequisite for the initiation. By contrast, dimeric ParA, which is capable to bind DNA, acts as an activator of DnaA, possibly by promoting oligomerization of DnaA and, thus, initiation of replication (101, 102). It has been demonstrated that ParB triggers ATP hydrolysis by ParA and thereby prevents the formation of ParA dimers (103). However, what triggers the switch from a ParA monomer (inhibitor) to a dimer (activator) is currently not known.
Hereby, ParAB also indirectly regulate sporulation since transcription of Sda, an inhibitor of sporulation, is positively regulated by the active form of DnaA. Thus, this checkpoint ensures that sporulation is not initiated in cells that undergo DNA replication (104, 105). Consistently, sporulation is disturbed in the absence of ParB and this phenotype is supressed by deletion of *parA* (94).

M. xanthus and others

Recent research in *M. xanthus* has revealed that the ParABS system, as in *C. crescentus*, is essential for chromosome segregation and cell viability in this organism (10, 106). Depletion of ParB resulted in growth defects and severe chromosome segregation defects, with cells dividing over the nucleoid or producing anucleate daughter cells. Interestingly, cell filamentation was not observed, suggesting that division site selection, but not cell division per se, is impaired in the absence of ParB (10, 106). It was shown that Z-ring positioning is mediated by the positive regulator PomZ in *M. xanthus* (107). It will be interesting to further elucidate how chromosome segregation and cell division are coupled in this organism.
ParAB were shown to adopt a unique subcellular localization. The ParB/*parS* complex localizes at a certain distance from the cell pole, while ParA forms subpolar patches that span the distance from the cell pole to ParB (10, 106). Recently, it was shown that the bactofilins BacNOP form extended polar scaffolds that are required for the subpolar localization and positioning of ParAB. ParA was shown to bind along the entire length of the bactofilin structures via a newly identified adaptor protein, whereas ParB directly interacts with the scaffold at its pole-distal end (108). During asymmetrical origin segregation from the old to the new cell pole, ParA additionally forms a shortening cloud-like structure between the segregating origin and the bactofilin scaffold at the new pole as also observed in *C. crescentus* and *V. cholerae* (ParA1) (10, 57, 58, 108).

The ParABS system has also been studied in diverse actinobacteria, such as *Corynebacterium glutamicum*, *Mycobacterium smegmatis*, *Mycobacterium tuberculosis*, and *Streptomyces coelicolor*, that are characterized by polar growth (43, 109). Interestingly, in all the above organisms, except for *M. tuberculosis*, where transposon mutagenesis indicated that ParAB could be essential, the ParABS system is dispensable (43, 110). However, deletion of components of the ParABS system results in chromosome segregation defects as indicated by an increased number of anucleate cells (111-114).
In *C. glutamicum*, the ParB/*parS* complex localizes to the cell pole and is anchored by the polar growth determinant DivIVA (115). An interaction between ParB and DivIVA was also shown for other actinobacteria (115). Furthermore, *C. glutamicum* ParA forms foci at the cell poles and larger patches between the cell poles. Deletion of *parA* or *parB* lead to a multitude of phenotypes including a high frequency of anucleate cells, cells that divide over the chromosome, growth defects, and variable cell lengths (111, 116). Moreover, ParB was shown to mislocalize in the absence of ParA. Hence, it has been suggested that origin segregation is mediated in a ParABS-dependent manner and that cell growth and division site selection are

coupled to chromosome segregation (111, 116). Similar observations have also been made in *M. smegmatis* (112, 113). Interestingly, it was shown that the double deletion of *parAB* can suppress the segregation defects of the respective single mutants in this organism. Moreover, the DivIVA homolog Wag31 interacts with ParA in *M. smegmatis* (113). Of note, a recent study in *M. tuberculosis* revealed that phosphorylation of ParB abolishes ParB binding to the *parS* sites and ParA. However, further studies are required to elucidate the biological relevance and its impact on chromosome segregation *in vivo* (117).
In S. *coelicolor*, ParAB are required for the partitioning of its linear chromosomes and septation during sporulation (118, 119). Deletion of *parA* or *parB* leads to a frequent formation of anucelate spores and in the absence of *parA* sporulation septation is impaired (118, 119). *S. coelicolor* exhibits a complex developmental cycle that starts with the formation of a vegetative mycelium and culminates in the formation of reproductive aerial hyphae that are characterized by extensive chromosome replication and that finally turn into long chains of spores (120). Once growth of the aerial hyphae has stopped, the multiple chromosomes are synchronously segregated and condensed, which is accompanied by the formation of a ladder of uniformly spaced septa, ensuring that each prespore contains one chromosome (114). ParA is recruited to the tip of the aerial hyphae by Scy, which is part of the tip organizing centre that mediates tip growth (121, 122). ParA forms long filamentous structures and promotes the equal and synchronous distribution of ParB along the hyphae by possibly acting as a scaffold (114, 118). It was proposed that Scy regulates the initiation of ParA polymerization, thereby linking polar growth with chromosome segregation (121). Furthermore, next to ParB and Scy, the actinobacteria-specific protein ParJ was found to interact with ParA and to negatively regulate ParA polymerization prior to sporulation (123).

In *Pseudomonas aeruginosa*, deletion of *parA* or *parB* also leads to severe chromosome segregation defects (20 % anucleate cells), impaired motility, as well as growth defects (20, 124, 125). Interestingly, the absence of ParA or ParB alters the overall chromosome organization, since not only the origin region but also the terminus region is mislocalized (20). Hence, deletion of *parA* or *parB* led to a plethora of phenotypes as also observed in other organisms. Consistently, transcriptional profiling of *par* mutants revealed global changes in gene expression, suggesting that ParAB directly or indirectly modulate gene expression and thereby connect chromosome segregation with other cellular processes (126).

In summary, studies of the ParABS system in various bacterial species revealed that its contribution to chromosome segregation differs and that it is oftentimes also implicated in other cellular processes such as initiation of replication, cell division or chromosome compaction (2, 43). Hence, the ParABS system links chromosome segregation with the cell cycle. However, the fact that deletion of components of the segregation machinery often causes pleiotropic phenotypes has hampered the identification of additional functions of ParAB. Furthermore, it was shown that in many organisms, in which the chromosome adopts a longitudinal organization, the ParABS machinery is positioned and immobilized at the cell pole by polar landmarks such as PopZ, HubP, DivIVA or bactofilins (2, 108, 127).

1.3.2 Par-independent chromosome segregation

Despite the high abundance of the ParABS system, many bacteria also lack or encode incomplete ParABS systems (51). *Streptococcus pneumoniae*, for instance, encodes *parB* and *parS* close to the origin of replication but lacks *parA* (128). However, it was shown that ParB is recruited to the *parS* sites forming a nucleoprotein complex. Similar to *B. subtilis*, this complex also recruits SMC, another system known to be involved in origin segregation (129). However, neither ParB nor SMC are essential in *S. pneumoniae* and their deletion only leads to mild chromosome segregation defects (~ 3 % anucleate cells). Hence, it was suggested that additional factors might exist that mediate active origin separation and segregation (129). It was shown that transcription contributes to chromosome segregation in *S. pneumoniae*, but is not essential for

the initial separation of the replicated origins (47). Additionally, ParB modulates competence development in *S. pneumoniae* by spreading around the *parS* sites and thereby blocking expression of an operon that was shown to mediate competence development. Competence represents the ability of bacteria to accommodate environmental DNA, which can confer adaptive advantages (130). However, ParB does not modulate transcription at a global level (130)

As mentioned above, *E. coli* lacks a ParABS system, suggesting that other factors might be at play to mediate origin segregation towards opposite cell poles. It is still not clear how organisms without ParABS segregate their origin regions. Over a decade ago, a 25 bp sequence close to *oriC*, called *migS*, was suggested to be involved in origin segregation in *E. coli* (131). However, no major chromosome segregation defects were observed in the absence of *migS*, and later studies did not even reveal an impact of *migS* on *ori* segregation (131-133). On the other hand, many active and passive segregation processes have been described to contribute to or drive efficient chromosome segregation in *E. coli*, including an involvement of MukBEF (functional analog to SMC), the Min system, entropic forces, or the release of build-up tension by prolonged cohesion (45, 48, 134-137). Interestingly, certain regions on the *E. coli* chromosome, including the origin region, were shown to experience longer cohesion times than others followed by abrupt separation. It was proposed that extended periods of sister chromosome cohesion build up tension that is followed by an abrupt separation of sister loci when the tension becomes too strong (48, 134, 135) . However, it remains elusive how some of these processes contribute to active origin segregation and if another, yet unidentified, mechanism is involved.

1.3.3 The role of SMC in chromosome organization and segregation

SMC complexes are ubiquitous protein complexes that can be found in all domains of life and are implicated in a variety of processes such as chromosome segregation, condensation, repair, and cohesion (138). Bacteria commonly possess one type of SMC complex that is similar to eukaryotic condensin and thought to be involved in chromosome compaction and segregation (3). SMC consists of a long antiparallel coiled-coil connected to a hinge (dimerization) domain at one end and an ATPase domain at the other end (139). SMC forms a homodimer that associates with its accessory proteins ScpA and ScpB to form a ring-like structure that can encircle DNA in an ATP-dependent manner (see Figure 1-3 A) (5, 140-143). SMC complexes are proposed to act as molecular clamps by bringing distant stretches of DNA in close proximity, but the exact mechanism and mode of action still remain elusive (4, 144).
Recent work in *B. subtilis* suggests that SMC promotes separation of newly replicated origins and lengthwise cohesion of the left and right chromosome arms (26, 27, 99, 100). SMC is essential for viability under fast growth conditions (temperature sensitive growth in rich medium). Under slow growth conditions, deletion of *smc* results in chromosome organization and segregation defects apparent in the formation of anucleate cells (~ 10 %), aberrant nucleoid morphology, ParB mislocalization as well as growth defects (96, 145). Depletion experiments revealed that separation of newly replicated origins is impaired in the absence of SMC, resulting in overall chromosome segregation defects (99, 100).
It was shown that SMC and ParB clusters overlap or are in close proximity *in vivo* and that the SMC complex is recruited to the origin region in a ParB/*parS*-dependent manner (97, 98). Chromosome conformation capture analysis revealed that the ParB/*parS*-dependent recruitment of SMC to several *parS* sites is required for the precise folding of the origin domain (26, 27). Furthermore, the chromosome shows a longitudinal arrangement in the cell for most of the cell cycle with interarm interactions along the length of the chromosome. In the absence of ParB/*parS* nucleoprotein complexes or SMC, the juxtaposition of the two chromosomal arms is impaired (26, 27). Similarly, deletion of SMC in *C. crescentus* also resulted in decreased interarm interactions (25).

Together, these observations led to a model in which SMC recruitment by several ParB/*parS* complexes structures and compacts the origin region and thereby appears to resolve replicated origins (26, 27). SMC encircles the DNA at its loading site and could then move along the DNA towards the terminus region, possibly by loop extrusion, thereby tethering the two chromosomal arms (see Figure 1-3 B) (4, 26). This hypothesis is consistent with the observation that SMC is enriched around the origin region but also present at lower levels along the chromosomal arms (4, 97). Moreover, single-molecule fluorescence microscopy revealed that two fractions of SMC exist in the cell, a static one and a mobile one that seems to move within the nucleoid (146). Additionally, recent *in vitro* data suggest that SMC can diffuse along and also bridge DNA (147). However, several models are conceivable how SMC mediates the juxtaposition of the two chromosomal arms (26). As mentioned above, chromosome segregation is not severely impaired upon ParB deletion (95). Consistently, a small fraction of SMC complexes still entraps chromosomal DNA in the absence of ParB, which might be sufficient to promote origin separation (5).

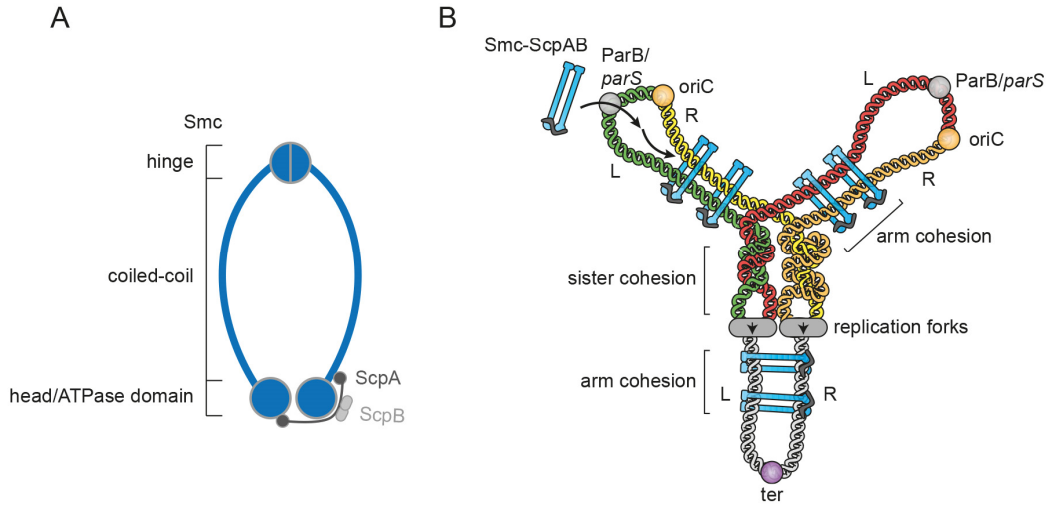

Figure 1-3: The SMC-ScpAB complex. A) Schematic representation of the SMC-ScpAB architecture (without ATP). Adapted from (140, 144, 148). B) Schematic model of origin separation and chromosome organization by SMC-ScpAB in *B. subtilis*. Please refer to text for detailed description. L and R: left and right chromosome arm, respectively. Adapted from (4).

E. coli and other γ-proteobacteria encode a structurally and functionally related complex, called MukBEF, in which MukB represents the SMC protein and MukEF the accessory proteins (3). Deletion of *mukB* also results in temperature-sensitive growth, the formation of anucleate cells, and the loss of the left-*ori*-right organization of the chromosome, indicating that the MukBEF complex is involved in chromosome segregation and organization (18, 149). Like *B. subtilis* SMC, MukB colocalizes with the origin region (18). Recent studies revealed that MukBEF interacts with and recruits topoisomerase IV (TopoIV) to the origin region to mediate the decatenation of newly replicated DNA, and it was shown that this interaction is required for the timely separation of newly replicated origins (150-152). It was suggested that MukBEF-TopoIV interaction might stimulate decatenation by TopoIV (150). However, elucidation of the exact mechanism of this cooperation requires further investigation. Interestingly, it was shown that MukBEF is also associated with the terminus region of the chromosome and interacts there with MatP (153). As mentioned above, MatP, which binds to *matS*, is required to organize the terminus macrodomain (23). MatP appears to remove the MukBEF complex from the terminus region (153). It was proposed that this could promote the association of MukBEF with the origin region instead and modulate the availability of TopoIV at *ter*, thereby enabling the decatenation of this region at the right time (153). Recently, an additional member of the SMC family, named MksBEF, was discovered that is widely conserved among bacterial species (154). It is often found in combination with SMC-ScpAB or MukBEF and also appears to be involved in chromosome organization and segregation (154, 155) .

1.3.4 Terminus segregation by FtsK

In the last stages of chromosome segregation, the terminus regions are segregated into the two different cell halves, clearing the cell division plane from DNA to prevent the guillotining of chromosomes. This process is mediated by the multifunctional DNA translocase, FtsK (49). FtsK is part of the divisome and coordinates the last stages of chromosome segregation with cell division (156-159). It is composed of an N-terminal transmembrane domain, which anchors FtsK to the membrane, a flexible linker, and a C-terminal part that consists of a motor and a DNA binding domain (160). The motor domains of FtsK form hexameric rings around the DNA and pump the chromosome in an ATP-dependent manner towards the *dif* site, a 26 bp defined sequence, present in the terminus region (160-162). Directional movement is achieved by short conserved motifs, so-called KOPS (FtsK-orienting polar sequences). KOPS are present throughout the genome and are oriented towards *dif*. Their orientation mediates the positioning of FtsK on the DNA and, thus, ensures directional DNA translocation towards the *dif* sites (163-165). During chromosome replication and segregation, chromosome dimers and catenanes (interlocked rings) can arise, which need to be resolved before cell division (166, 167). By pumping the chromosomes, FtsK brings the *dif* sites of the two sister chromosomes in close proximity and directly activates the XerCD recombinase that promotes site-specific recombination between *dif* sites to resolve chromosome dimers (168-171). Furthermore, FtsK is thought to bind and activate TopoIV that mediates chromosome decatention (158, 172).
While FtsK is mostly implicated in terminus segregation, the *B. subtilis* FtsK homolog SpoIIIE was shown to mediate bulk chromosome segregation during sporulation by pumping ~75 % of the forespore chromosome into the developing spore (173-175).

1.4 *Hyphomonas neptunium* as a model system for chromosome segregation in stalked budding bacteria

Chromosome replication and segregation are fundamental cellular processes that need to be tightly regulated in time and space. So far, our knowledge on this subject is based on the study of only a few established model organisms that reproduce by binary fission and are typically characterized by a rod-like morphology. To further broaden our understanding of bacterial cell biology and the molecular mechanisms underlying chromosome dynamics in bacteria, we have recently established the marine alphaproteobacterium *Hyphomonas neptunium* as a new model organism in our lab (176).

H. neptunium distinguishes itself from other so far studied organisms by its remarkable mode of reproduction by budding whereby it utilizes its stalk as a reproductive organelle. Cytokinesis gives rise to a motile swarmer cell and a non-motile stalked cell. The stalked mother cell can immediately enter a new round of DNA replication, budding, and cell division, whereas the swarmer cell is initially not able to reproduce and must first differentiate into a stalked cell. By doing so, it loses its flagellum and a stalk starts growing at the opposite cell pole. Once the stalk is generated, a bud emerges at the distal end of the stalk and dilates to form a new flagellated daughter cell (see Figure 1-4). The stalk is part of the cell body that connects the mother cell with the bud. Cell division then takes place at the junction between the stalk and the newly generated bud (80, 177, 178). This dimorphic life style resembles in part the cell cycle of *C. crescentus*, a well-established model organism for bacterial cell biology (see Figure 1-4).
H. neptunium, isolated from the harbor of Barcelona (Spain), was originally described as *Hyphomicrobium neptunium*, due to morphological similarities (177). 16S rRNA-based phylogeny analysis resulted in a reclassification as a member of the order *Rhodobacterales* (179). However, 23S rRNA gene sequence analysis and concatenated protein alignments support a classification as a member of the *Caulobacterales*. Consist-

ently, comparative genomics revealed a close relationship between *C. crescentus* and *H. neptunium* (180, 181). For instance, most key cell cycle regulators found in *C. crescentus* are conserved in *H. neptunium*. It still remains elusive how this similar set of developmental regulators adapted to lead to such a divergent outcome in regard to the mode of reproduction. Moreover, the unique mode of reproduction by budding raises several questions. One intriguing aspect is how chromosome segregation is mediated, since the duplicated chromosome must transit the stalk to reach the newly formed daughter cell compartment. Furthermore, it will be of great interest to elucidate how chromosome replication and segregation are spatio-temporally coordinated with budding and the highly asymmetric cell division (176).

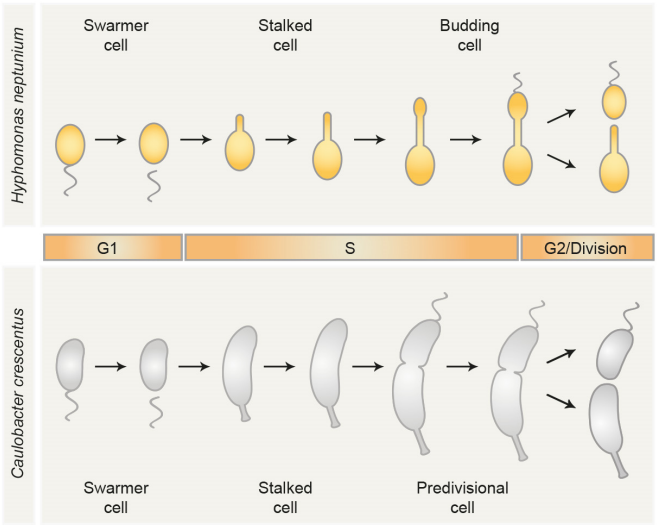

Figure 1-4: Cell cycles of *H. neptunium* and *C. crescentus*. *H. neptunium* reproduces by budding, whereas the closely related model organism *C. crescentus* divides by asymmetric binary fission. Please refer to text for detailed description. Adapted from (80, 176).

1.4.1 Chromosome segregation in *H. neptunium*

As mentioned above, *H. neptunium* divides by budding and uses its stalk as a reproductive structure (177). This mode of reproduction distinguishes *H. neptunium* from so far studied model organisms and renders it an exciting candidate to study chromosome segregation. It possesses a single circular chromosome of around 3.7 Mb that is only replicated once per cell cycle and encodes a ParABS system (80, 180). *In vivo* studies revealed that in *H. neptunium* the centromere-like region, determined by the ParB/*parS* complex, is segregated in a two-step process. At first, one of the duplicated centromere-like regions is moved to the stalked pole of the mother cell and remains there until a clearly visible bud has formed. Subsequently, it is transported through the stalk and immobilized at the flagellated pole of the bud (see Figure 1-5 A) (80, 182). First experiments in phosphate-limited media, in which *H. neptunium* elongates its stalk, revealed that ParB segregation through the stalk can occur rapidly, directedly and over significant distances, indicating the involvement of an active segregation process (182, 183). ParA showed a non-homogenous localization pattern in ~23 % of cells. In the majority of cells, ParA formed either one or two polar foci. In swarmer and stalked cells, ParA was shown to localize at either the pole opposite of the stalk or bipolarly in the mother cell, which is reminiscent of the ParB localization pattern. In the majority of budding cells, ParA localized to the flagellated bud pole (see Figure 1-5) (80). Interestingly, ParA appears to localize at the tip of the stalk either before bud formation initiates or at a very early time point of budding, at which the bud might not yet be clearly visible by microscopy (see Figure 1-5 C). This suggest that ParA localizes to the bud before ParB arrives, which was also confirmed by co-localization studies (80). It is assumed that the ParB/*parS* complex is the region that is the first to be segregated through the stalk and that the stalk is therefore free of DNA before it is traversed by the complex (80, 184). Given that the generic *parABS*-

based partitioning system requires non-specific chromosomal DNA for function, it was proposed that the transport of DNA through the stalk may be driven by a novel DNA segregation mechanism (58, 64, 65, 78, 80).

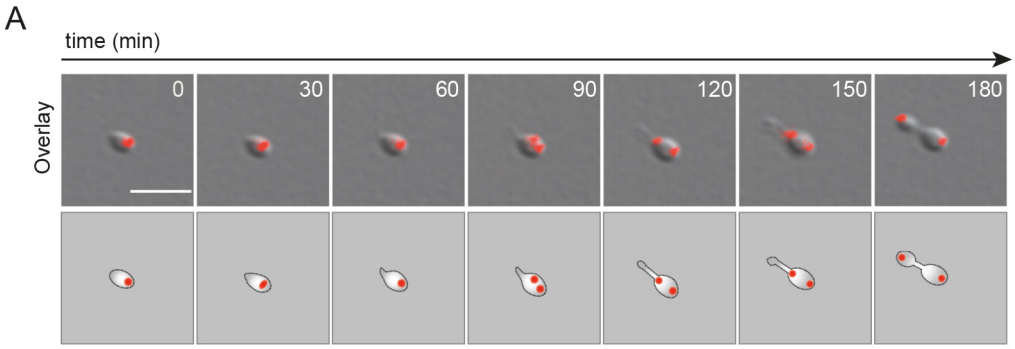

B

	foci [%]		
	0	1	2
swarmer cells	22,6	68,6	8,8
stalked cells	27,5	52,5	20
budding cells	20	66,7	13,3

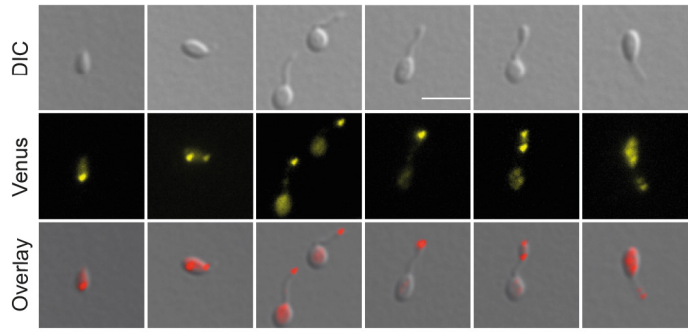

Figure 1-5: Localization of ParAB in *H. neptunium*. A) Segregation of ParB-YFP in a two-step process. Time-lapse microscopy of *H. neptunium* KH22 (*parB-yfp*) on MB agarose pad. Overlays (of DIC and fluorescence images) and scheme are shown. Bar 3 µm. B) Localization of ParA-Venus in *H. neptunium*. Distribution (%) of different ParA localization patterns in swarmer (n= 159), stalked (n=80), and budding cells (n= 60) (adapted from (80)). Cells of strain *H. neptunium* AR33 (P_{Zn}::P_{Zn}-*HNE_3561-venus*) were grown in MB medium and induced for 6 h with 0.3 mM $ZnSO_4$ (80). C) Exemplary micrographs of ParA-Venus localization. Cells of strain AR33 were grown in MB medium and induced for 3 h with 0.5 mM $ZnSO_4$. Bar 3 µm.

In order to find potential candidates involved in chromosome segregation, the *H. neptunium* genome was searched for ParA homologs (80). In bacteria, ParA homologs have been implicated in diverse cellular processes such as DNA partitioning, distribution and localization of proteins, and regulation of Z-ring positioning (81). Deletion and localization studies of identified ParA homologs draw the attention to the orphan *HNE_0708*, which encodes a hypothetical protein. Deletion of *HNE_0708* causes slightly elongated stalks with small bubble-like structures at the stalk tips, as well as impaired origin localization (see Figure 1-6 C & data not shown) (80). Localization of ParB in the *HNE_0708* deletion background revealed multiple ParB foci in budding cells, indicating a defect in either origin segregation or initiation of replication. Furthermore, cryo-electron microscopy revealed DNA accumulation in the stalk in the absence of HNE_0708 (80). So far, no functional fluorescent fusion of this protein is available that could give further hints to a potential function of the protein. An inducible HNE_0708-Venus fusion shows a diffuse localization in the mother and daughter cell compartments and sometimes a patchy pattern in the stalk (see Figure 1-6 B) (80). However, it was observed that, similar to the deletion strain, DNA accumulated in the stalk (80). This indicates that the fusion protein is either not fully functional or that its expression from the zinc-inducible promoter supplementary to the wild-type copy leads to an overexpression effect. Interestingly, HNE_0708 shows a rather unusual domain structure when compared to ParA proteins that are encoded in an operon with ParB, as it possesses an additional N-terminal TIR domain (see Figure 1-6 A) (80). TIR domains are thought to mediate protein-protein interactions in bacteria (185). It

will be highly interesting to further investigate HNE_0708 and its potential role in chromosome segregation.

A promising candidate that could play a role in the transport of the chromosome through the stalk is the the DNA translocase FtsK. As mentioned above, FtsK is a multifunctional protein that is widespread among bacteria and involved in diverse processes such as cell division, dimer resolution, and chromosome segregation (160). *In vivo* analysis showed that in *H. neptunium* FtsK appears to localize not exclusively at the division site but also in the stalk (S. Eisheuer, unpublished). Furthermore, FtsK is essential in *H. neptunium* and production of an ATPase-deficient variant of FtsK in addition to the wild-type protein resulted in chromosome segregation defects in a subpopulation of cells (S. Eisheuer, unpublished). Taken together, this suggests a potential role of FtsK in chromosome translocation through the stalk.

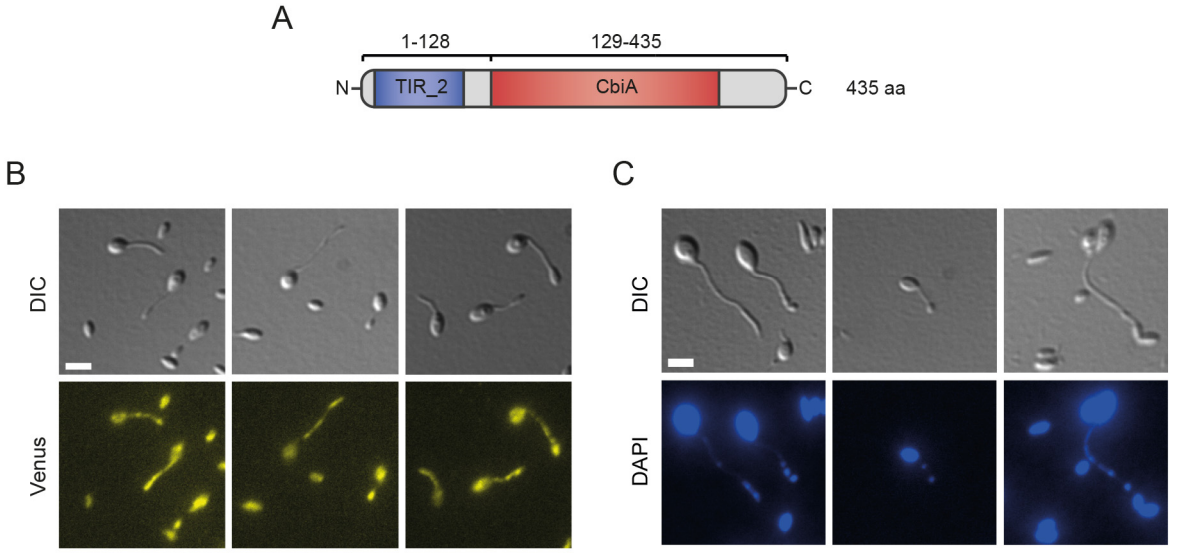

Figure 1-6: Analysis of the ParA homolog HNE_0708 A) Schematic depicting the domain structure of HNE_0708. B) HNE_0708-Venus localization. Cells of strain AR37 (P_{Zn}::P_{Zn}-*HNE_0708-venus*) were grown in MB medium, induced for 6 h with 0.3 mM $ZnSO_4$, and visualized by DIC and fluorescence microscopy. Bar 2 µm. Adapted from (80). C) Deletion of *HNE_0708*. Cells of strain AR46 (Δ*HNE_0708*) were grown in MB medium and stained with DAPI. Subsequently, cells were visualized by DIC and fluorescence microscopy. Bar 2 µm. Adapted from (80).

Another interesting aspect is the arrangement of the origin region in *H. neptunium*. The origin region is often in close proximity to the GC skew change (186). The GC skew depicts the abundance of guanine to cytosine and is generally positive on the leading and negative on the lagging strand. The GC skew changes at the origin and the terminus, where the leading becomes the lagging strand and vice versa (187). In the origin region of many bacteria, the *parABS* cluster is usually in proximity to *dnaA* together with the corresponding DnaA boxes. As mentioned above, DnaA binds to these boxes in the origin region, resulting in an unwinding of the DNA in this region. The replication machinery is then able to assemble in this region, leading to the initiation of replication (34, 43, 51). In *H. neptunium*, the *parAB* operon is also in close proximity to the GC-skew change, but *dnaA* is around 570 kb away from the *parAB* operon (see Figure 1-7 A). Interestingly, it was shown that the ParB/*parS* complex is segregated first within the mother cell and through the stalk, before the region close to *dnaA* (see Figure 1-7 B) (80). It is not clear so far where replication starts – if close to the predicted GC-skew change or close to the *dnaA* locus. In the latter case, this would imply that chromosome replication and segregation are uncoupled. By using one of the DnaA box consensus sequences of *C. crescentus*, an accumulation of *dnaA* boxes was identified close to *dnaA* (see Figure 1-7 A) (80). However, when using the DoriC database of bacterial and archaeal replication origins (http://tubic.tju.edu.cn/doric/), two putative DnaA boxes were identified close to *hemE*. The consensus sequence for *H. neptunium* DnaA boxes is not known. Hence, it is currently unclear at which of the two

potential *oriC*s chromosome replication starts in *H. neptunium*, and an experimental determination will be required. Please note, for simplification, the region close to the GC skew change will be referred to as origin in the course of this study.

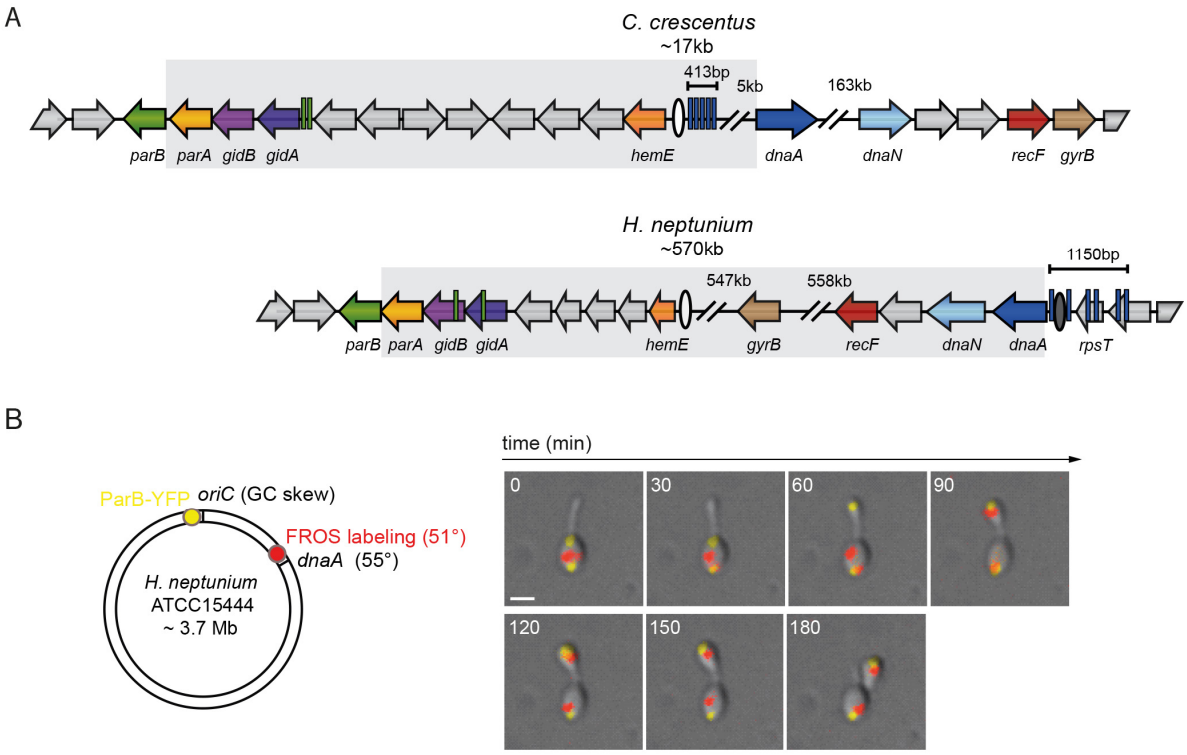

Figure 1-7: Origin region of *H. neptunium*. A) Schematic of the origin arrangement of *C. crescentus* and *H. neptunium*. Green bars indicate *parS* sites, blue bars indicate DnaA boxes. Upper panel: white oval depicts *oriC* of *C. crescentus*. Lower panel: white and dark grey ovals depict the two potential sites for *oriC* in *H. neptunium*. Adapted from (80). B) The ParB/*parS* complex is segregated before the region close to *dnaA*. Left: Schematic of the regions labeled on the chromosome shown in timelapse in right panel. The region close to the GC skew change was labeled by ParB-YFP binding to the *parS* sites (yellow). The region close to *dnaA* (51°) was labeled using FROS (red). Right: Timelapse of KH25 (P_{Zn}::P_{Zn}-*lacI-mCherry*, *lacO* array intergrated at position 51°, *parB-yfp*). Overlay of DIC and fluorescence images is shown. Bar 1 µm. Adapted from (80).

1.5 Aim of study

Up to now, chromosome dynamics has been mainly studied in model organisms that divide by binary fission and are characterized by a rod-like morphology (2). To further broaden our knowledge on this subject, we have recently established the stalked budding bacterium *H. neptunium* as a new model system in our lab (176).

Recent research suggests that chromosome segregation in *H. neptunium* occurs in a two-step process: at first one of the duplicated origin regions is segregated within the mother cell, which is possibly mediated by the ParABS system, the duplicated origin then remains at the stalked mother cell pole until a visible bud has formed, before it is segregated through the stalk (80, 182). This study aims to investigate chromosome organization and segregation in *H. neptunium* by analyzing chromosome arrangement and dynamics, the role of the ParABS system as well as other factors that are possibly implicated in chromosome segregation in *H. neptunium*. Several lines of evidence suggested that the second segregation step, the transport of the chromosome through the stalk, might be driven by a novel active segregation mechanism (80). Hence, we also attempt to identify new factors that are involved in chromosome segregation through the stalk. Chromosome replication and segregation occur concurrently in bacteria. However, the unique mode of reproduction by budding and the observed two-step origin segregation raise the question, if these two processes might be uncoupled in *H. neptunium*. Therefore, we further aim to investigate the temporal co-ordination of chromosome replication and segregation in *H. neptunium*.

2 Results

2.1 The ParABS system in *H. neptunium*

2.1.1 ParB binds to *parS* sites *in vitro*

ParABS-based chromosome partitioning systems are widely conserved among bacterial species (51). The *H. neptunium* genome also possesses a *parAB* operon, and two potential *parS* sites were identified upstream of it (see Figure 2-1 B) (80). To further elucidate the role of the ParABS system in *H. neptunium*, we set to verify that ParB binds to the predicted *parS* sites in the origin region. For this purpose, ParB-His_6 was purified and binding to Cy3-labeled oligonucleotides containing either the wild-type or a mutated *parS* sequence was tested *in vitro* by electrophoretic mobility shift assay (EMSA) (see Figure 2-1 A & C). For wild-type *parS*, a bandshift was observed, indicating the binding of ParB to the *parS* sites. In contrast, binding was abolished when ParB was incubated with the mutated *parS* sites (see Figure 2-1 C). Hence, ParB binds specifically to the corresponding *parS* sites *in vitro*.

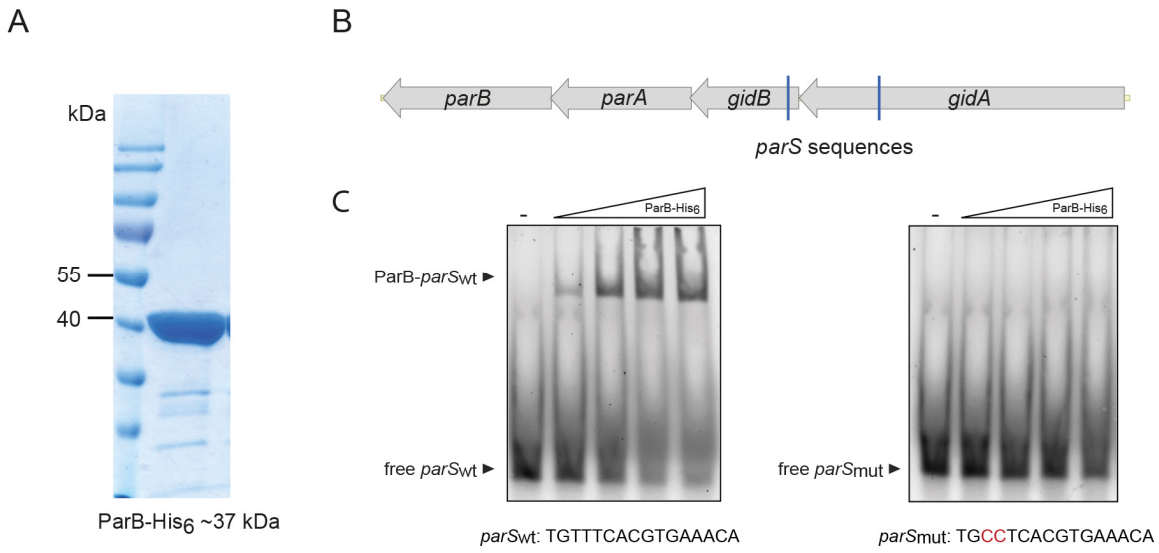

Figure 2-1: Interaction of ParB-His_6 with wild-type and mutated *parS* sites of *H. neptunium*. A) Purification of ParB-His_6. SDS-PAGE analysis of ParB-His_6 stained with Instant Blue. B) Schematic of the *parAB* locus and the two *parS* sites contained in it (blue bars). C) Electrophoretic mobility shift assay. Cy3-labeled oligonucleotides (each 10 nm) with the wild-type *parS* sequence (left) or the mutated *parS* sequence (right), respectively, were incubated without and with varying concentrations of ParB-His_6 (0.05, 0.1, 0.3, and 0.6 µM). Subsequently, free *parS* and *parS* bound to ParB were separated by PAGE and visualized. Red letters indicate substitutions.

2.1.2 The ParB/*parS* complex is segregated in a two-step process

To further elucidate the role of ParB in chromosome segregation, we wanted to analyze its subcellular localization in more detail. As shown previously, ParB is segregated in a two-step process (80, 182). ParB first localizes to the flagellated pole in swarmer cells. Once stalk formation has initiated, the origin region is duplicated and one of the ParB foci is moved to the stalked pole of the mother cell and remains there until the bud is generated. ParB is then moved through the stalk and sequestered at the pole opposite the stalk in the newly formed bud (see Figure 1-5 A). To quantify the exact timing of the different ParB segregation steps (i.e. the duration of segregation within the mother cell, the "waiting time" of ParB at the stalked mother cell pole before its segregation through the stalk, and the duration of segregation through

the stalk), time-lapse microscopy of ParB-YFP with 5 and 1 min resolution, respectively, was performed. The segregation of ParB within the mother cell took 10-55 min, with an average segregation time of 30±13 min (n=19, 5 min intervals) and an average speed of 0.05±0.03 µm/min (n=17, 5 min intervals). In some cells, ParB segregation occurred directedly and progressively within 10-15 min, while in others ParB segregation stalled and even reversed occasionally (data not shown). It will be important to quantify the segregation time in more cells in the future to validate the measured times and exclude, for instance, the possibility that cells with very long segregation times are exceptions. After segregation of one of the duplicated ParB foci within the mother cell, the focus at the stalked mother cell pole remained stationary for 25-105 min with an average "waiting time" of 58±24 min (n=19, 5 min intervals) before segregation through the stalk occurred. Origin segregation through the stalk could occur within 3-4 minutes (see Figure 2-2), confirming that it is a rapid and directed process.

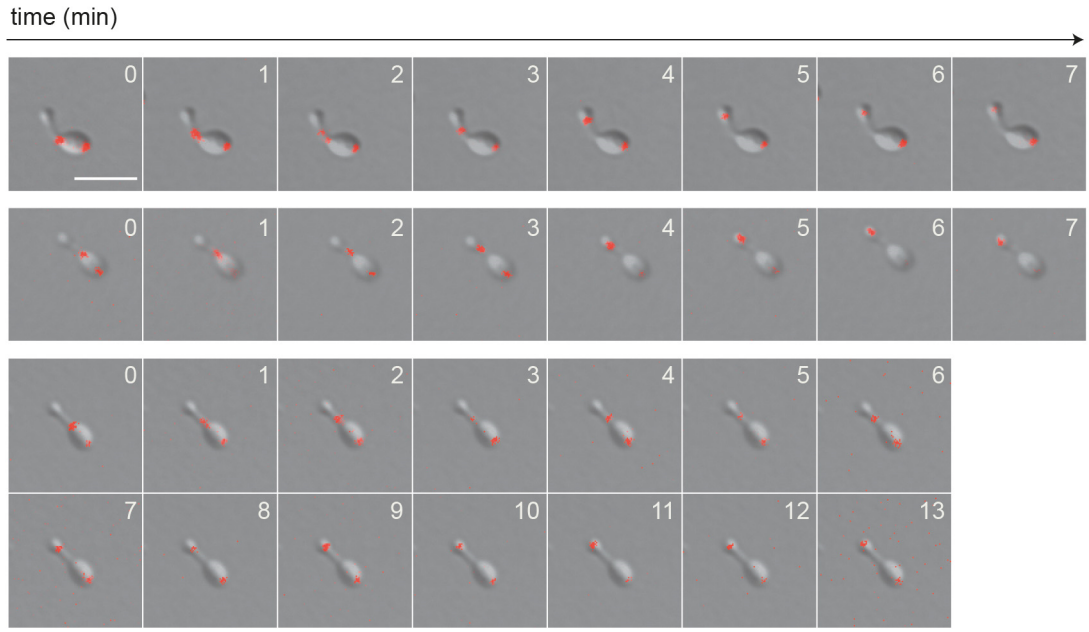

Figure 2-2: Time-lapse analysis of ParB-YFP segregation through the stalk. For time-lapse microscopy, cells of *H. neptunium* KH22 (*parB-yfp*) were grown in MB medium to exponential phase, transferred to an MB agarose pad, and visualized at 1 min intervals by DIC and fluorescence microscopy. Overlays of DIC and fluorescence micrographs are shown. Bar 3 µm.

What determines the "waiting time" of ParB at the stalked mother cell pole and what triggers the start of ParB segregation through the stalk later on? One possibility could be that ParB segregation through the stalk is coupled to chromosome replication in a way that the chromosome is first fully replicated before segregation through the stalk is initiated. The temporal coupling of chromosome replication and segregation will be described in chapter 2.6 in more detail. Furthermore, time-lapse analysis revealed that a bud must be generated before ParB is translocated through the stalk. In order to analyze if bud size correlates with the initiation of ParB segregation through the stalk, we determined the bud and mother cell sizes by measuring the cell width of cells, in which ParB is or has just been transported through the stalk (see Figure 2-3). During ParB translocation, mother cells showed a width of 0.86-1.28 µm (n=57), with an average width of 1.02±0.09 µm. Interestingly, there was no specific bud size at which ParB translocation occurred, since bud width varied between ~46-77 % of the mother cell width (i.e. 0.45-0.82 µm). However, the data suggest that a critical minimal bud size might be required for ParB segregation through the stalk to start, since bud size was never smaller than ~46 % of the mother cell width and 0.45 µm, respectively. Furthermore, it is conceivable that this bud size might also correlate with a specific cell cycle state at which ParB translocation through the stalk occurs.

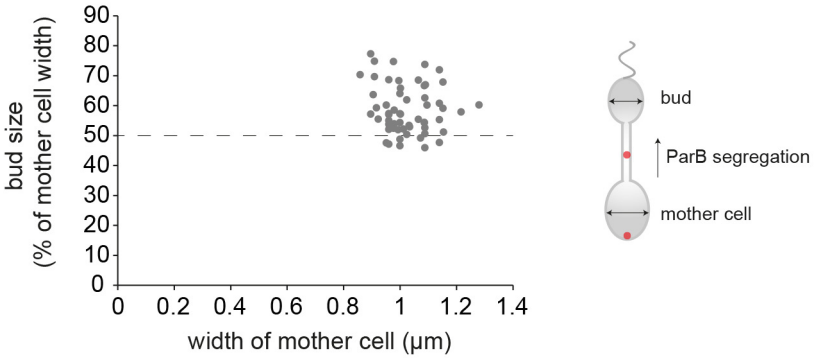

Figure 2-3: Daughter cell (bud) size during ParB translocation through the stalk. Cells of *H. neptunium* KH22 (*parB-yfp*) were grown in MB medium to exponential phase, transferred to an MB agarose pad, and visualized at 5 min intervals by DIC and fluorescence microscopy. The daughter (bud) and mother cell width was measured at the time ParB was detected in the stalk. In cases in which the ParB focus could not be captured within the stalk, the cell width was measured at the time the ParB focus was at first visible in the bud. (n=57).

2.1.3 Identification of ParB interaction partners

The *H. neptunium* stalk appears to be free of DNA before it is traversed by the ParB/*parS* complex. Given that the generic *parABS*-based partitioning system requires non-specific chromosomal DNA for function, the transport of DNA through the stalk may be driven by a novel DNA segregation mechanism (80). However, the ParB/*parS* complex appears to be the region that is at first segregated through the stalk (80). Therefore, we hypothesised that potential candidates involved in mediating origin translocation through the stalk might also interact with ParB. To identify potential candidates we set to search for ParB interaction partners by using an undirected approach. Hence, we performed pull-down analysis with ParB-His_6 as bait coupled to magnetic beads. ESI mass spectrometry analysis (Proteomics Facility, Biology, University Marburg) revealed the DNA-binding protein HU (HNE_2469) and three small hypothetical proteins (HNE_1048, HNE_3182 & HNE_3528) as interesting potential candidates.

To verify an interaction of ParB with the potential candidates, we analyzed their subcellular localization by fluorescence microscopy. In case the potential candidates interact with ParB, we would expect them to show a similar localization pattern as ParB. Therefore, C-terminal Venus fusions of the three hypothetical proteins were generated and further analyzed. *HNE_3528* encodes a 152 aa long, DUF3617 domain-containing protein. However, HNE_3528-Venus produced from its native promoter did not show any fluorescent signal and was not detectable by immunoblot analysis (data not shown). This could indicate that the gene might be wrongly annotated. *HNE_1048,* encoding a 192 aa long, SUFU domain-containing protein only showed a diffuse cytoplasmic signal when produced from its native promoter (see Figure 2-4 B). Please note that the function of the bacterial Sufu domain is unknown (188). *HNE_3182* encodes a 98 aa long, zinc finger domain-containing protein. The inducible HNE_3182-Venus fusion also only exhibited a diffuse localization pattern (see Figure 2-4 A). The size and integrity of HNE_1048-Venus and HNE_3182-Venus were confirmed by immunoblot analysis (see Figure 2-4 C). The diffuse localization pattern makes it currently difficult to draw any conclusion towards a potential function of the proteins or their involvement in chromosome segregation. HU is a non-specific DNA binding protein that is involved in DNA compaction. Moreover, HU was described to be involved in the initiation of replication by stabilizing DnaA oligomers in *E. coli* (reviewed in (34)). However, it requires further investigation if the isolation of HU really indicates an interaction between ParB and HU.

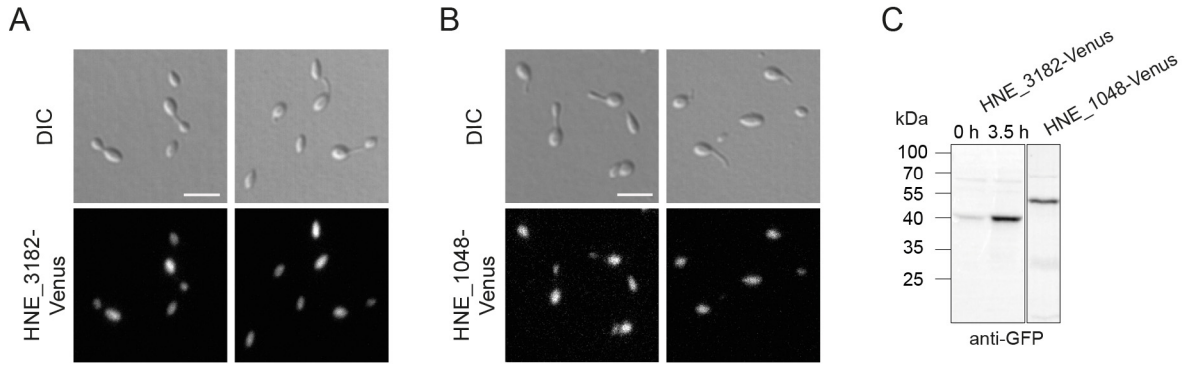

Figure 2-4: Localization studies of hypothetical proteins identified in ParB-His$_6$ pull-down assay. A) Subcellular localization of HNE_3182-Venus. Cells of strain AJ81 (P_{Zn}::P_{Zn}-*HNE_3182-venus*) were grown in MB to exponential phase, induced with 0.3 mM $ZnSO_4$ for 3.5 h, and visualized by DIC and fluorescence microscopy. Bar 3 µm. B) Subcellular localization of HNE_1048-Venus. Cells of strain AJ83 (*HNE_1048::HNE_1048-venus*) were grown in MB to exponential phase, and visualized by DIC and fluorescence microscopy. Bar 3 µm. C) HNE_3182-Venus and HNE_1084-Venus levels of samples described above were analyzed by immunoblot using an anti-GFP antibody.

As described above, the undirected approach did not reveal any interesting potential ParB interaction partners. In the next step, we therefore employed a candidate approach to identify proteins that are involved in chromosome segregation through the stalk. The subcellular localization of bactofilin homologs in *H. neptunium* caught our attention, since they localize to distinct regions of the stalk (E. Cserti, unpublished) and could thus be involved in mediating chromosome translocation through the stalk. Bactofilins are a widespread class of bacterial cytoskeletal elements that have the ability to form polymeric structures without any co-factors. They are involved in diverse cellular processes such as the maintenance of cell shape and virulence, motility or stalk formation by acting as localization factors that recruit other proteins to specific positions in the cell (reviewed in (127)). Recently, it was shown in *M. xanthus* that bactofilins contribute to chromosome organization and segregation by acting as polar landmarks recruiting ParAB to defined subpolar regions (108). *H. neptunium* has two bactofilin homologs, named BacA and BacB, which show a dynamic localization during the cell cycle (E. Cserti, unpublished). Upon the initiation of stalk formation, BacAB colocalize at the stalk base. During stalk growth, they localize in close proximity to the tip of the stalk. The region between the tip of the stalk and bactofilins defines the area of bud formation. Interestingly, in some budding cells, bactofilins localize simultaneously to the junction between the bud and the stalk as well as to the junction between the stalk and the mother cell (E. Cserti, unpublished).

To analyze if bactofilins play a role in chromosome segregation through the stalk, we analyzed ParB (origin) localization in the absence of bactofilins. Deletion of bactofilins leads to a large fraction of amorphous cells (E. Cserti, unpublished). In Δ*bacAB* cells that exhibit a similar morphology as wild-type cells, ParB showed the wild-type localization pattern (see Figure 2-5 A). And even in amorphous cells, ParB was still segregated to the newly formed buds, indicating that BacAB are not involved in origin segregation/positioning (see Figure 2-5). Strikingly, even in highly asymmetric amorphous cells, ParB is segregated to the region where a new bud will be formed. Furthermore, ParB seems to "wait" there until the bud is generated and is subsequently segregated (see Figure 2-5 B, first and second row). This observation suggests the presence of a factor, which might anchor or capture ParB or an origin-proximal DNA region at this specific site.

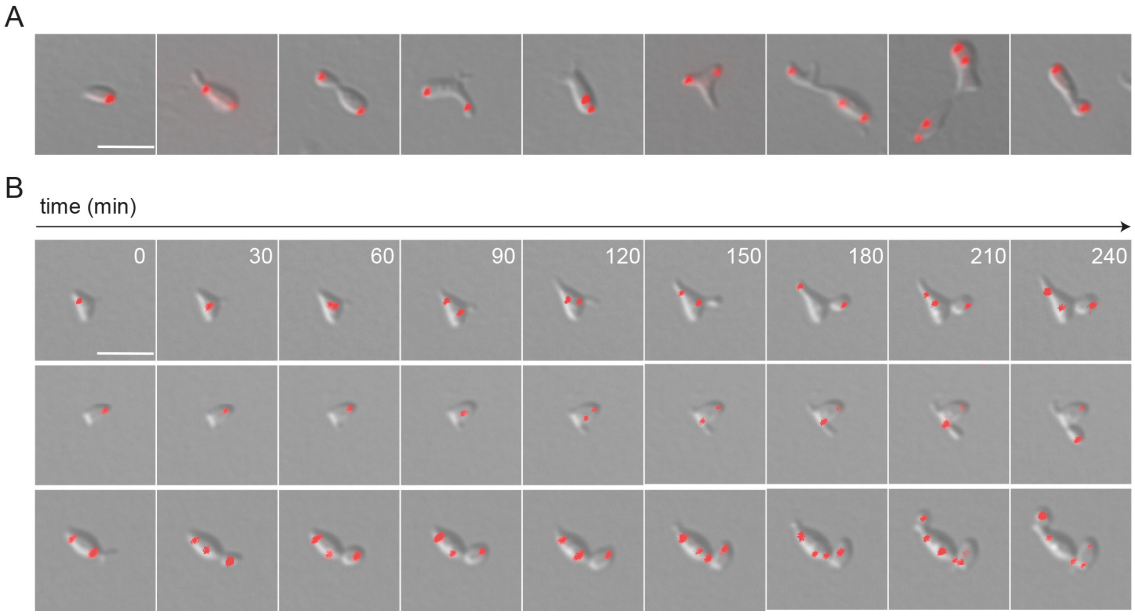

Figure 2-5: Localization of ParB-YFP in the absence of BacAB. A) Cells of strain AJ74 (*ΔbacAB parB::parB-yfp*) were grown in MB to exponential phase, and visualized by DIC and fluorescence microscopy B) For time-lapse microscopy, cells of *H. neptunium* AJ74 were grown in MB medium to exponential phase, transferred to an MB agarose pad, and visualized at 30 min intervals by DIC and fluorescence microscopy. Overlays of DIC and fluorescence micrographs are shown. Bar 3 μm.

2.1.4 ParAB are essential in *H. neptunium*

To further investigate the role of ParAB in chromosome segregation in *H. neptunium*, we intended to generate single in-frame deletions by double homologous recombination. However, we did not succeed in deleting either *parA* or *parB*, which suggests that they are essential for viability in *H. neptunium*.
Therefore, we attempted to create conditional mutants by introducing a fluorescently tagged copy of the respective gene at the locus of the zinc-inducible promoter and deleting the native copy at the endogenous locus. For ParB, no conditional mutant could be generated, since double homologous recombination gave exclusively rise to the wild-type genotype (data not shown). In the case of ParA, we were able to generate a conditional mutant. Microscopic analysis revealed that ParA depletion leads to elongated and misshaped cells with elongated stalks and bud compartments, as corroborated by flow cytometry analysis (see Figure 2-6 B & D and Figure S6-1 A). However, there was also a subpopulation of cells that showed wild-type morphology and cell size (see Figure 2-6 B & D). It should be noted that cells were also able to grow in the absence of inducer due to leaky expression of *parA-venus* from the zinc promoter (see Figure 2-6 C). Hence, long depletion times were required to detect morphological changes. Furthermore, this basal ParA level in the absence of induction might also be responsible for the fraction of cells showing wild-type morphology upon ParA depletion. Production of ParA-Venus from the zinc-inducible promoter mostly complemented the ParA depletion phenotype, since the majority of cells showed wild-type morphology. Nonetheless, the inducible ParA-Venus fusion did not lead to a complete complementation of the phenotype (see Figure 2-6 B & D and Figure S6-1 A). This might be caused by the altered ParA expression level (inducible instead of native promoter) or the ParA-Venus fusion might not be fully functional.

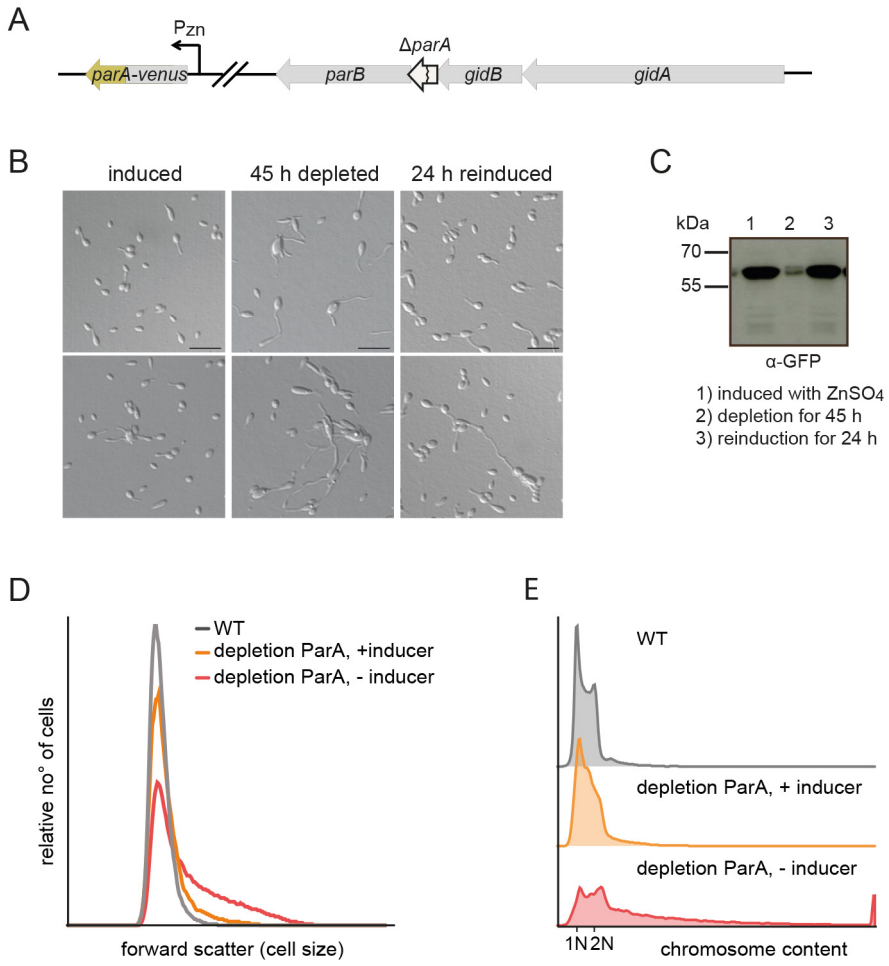

Figure 2-6: Effects of ParA depletion on cell morphology, cell size, and DNA content. A) Construction of strain AJ46. A copy of *parA-venus* was introduced at the site of the zinc-inducible promoter and *parA* was deleted from its native locus. B) Effects of ParA depletion on cell morphology. Cells of strain AJ46 (Δ*parA* P_{Zn}::P_{Zn}-*parA-venus*) were grown in the presence of inducer (0.3 mM $ZnSO_4$), washed, shifted to $ZnSO_4$-free medium, and grown for 45 h. After 16.5 h and 41 h of depletion, cells were diluted 1:10 and 1:3, respectively, in MB medium. For reinduction of ParA, cells were shifted to MB medium supplemented with 0.5 mM $ZnSO_4$. Morphological changes were assessed by DIC microscopy. Bar 5 µm. C) Immunoblot analyses of ParA-Venus levels of samples described in (B). D) & E) Effects of ParA depletion on cell size and chromosome content. Cells of strain AJ46 were grown in MB medium in the presence or absence of 0.3 mM $ZnSO_4$ (inducer). WT: *H. neptunium* wild type was grown in MB. Subsequently, exponentially growing cells were analyzed by flow cytometry. To analyze the DNA content by flow cytometry, cells were stained with Vybrant® DyeCycle™ Orange for 25 min beforehand.

In the next step, we wanted to assess if chromosome segregation was hindered upon ParA depletion. Demographic representation of nucleoid localization in budding cells revealed that DNA segregation was impaired in the vast majority of cells, since no DNA could be detected in the buds (see Figure 2-7). By comparison, DNA was segregated to the bud compartment in the majority of cells in the wild type control (see Figure 2-7). Additionally, flow cytometry analysis of DNA content revealed that many cells had more than one or two chromosomes upon ParA depletion, while wild-type cells contained either one or two chromosomes (see Figure 2-6 E). This indicates that chromosome replication still takes place but, due to impaired segregation, DNA accumulates in the mother cell. However, there was also a fraction of cells, in which DNA segregation occurred normally (see Figure 2-7 B, left panel). This is most likely due to the basal ParA level present in the cells (see above). Furthermore, we could also observe the presence of anucleate cells (see Figure 2-7 A, asterisks & Table 6-5). In most cases, these cells did not have the shape of normal swarmer cells that usually bud off upon cell division, but rather looked like thickened parts of a stalk. This suggests that cell division takes place at low frequency even without chromosome segregation

taking place beforehand. However, the presence of elongated cells indicates that cell division appears to be impaired. As mentioned above, the induction of ParA-Venus from the zinc-inducible promoter did not complement the depletion phenotype completely. Consistently, DAPI staining revealed that chromosome segregation was impaired even upon induction of ParA-Venus in a subpopulation of cells (see Figure 2-7 B, middle panel).

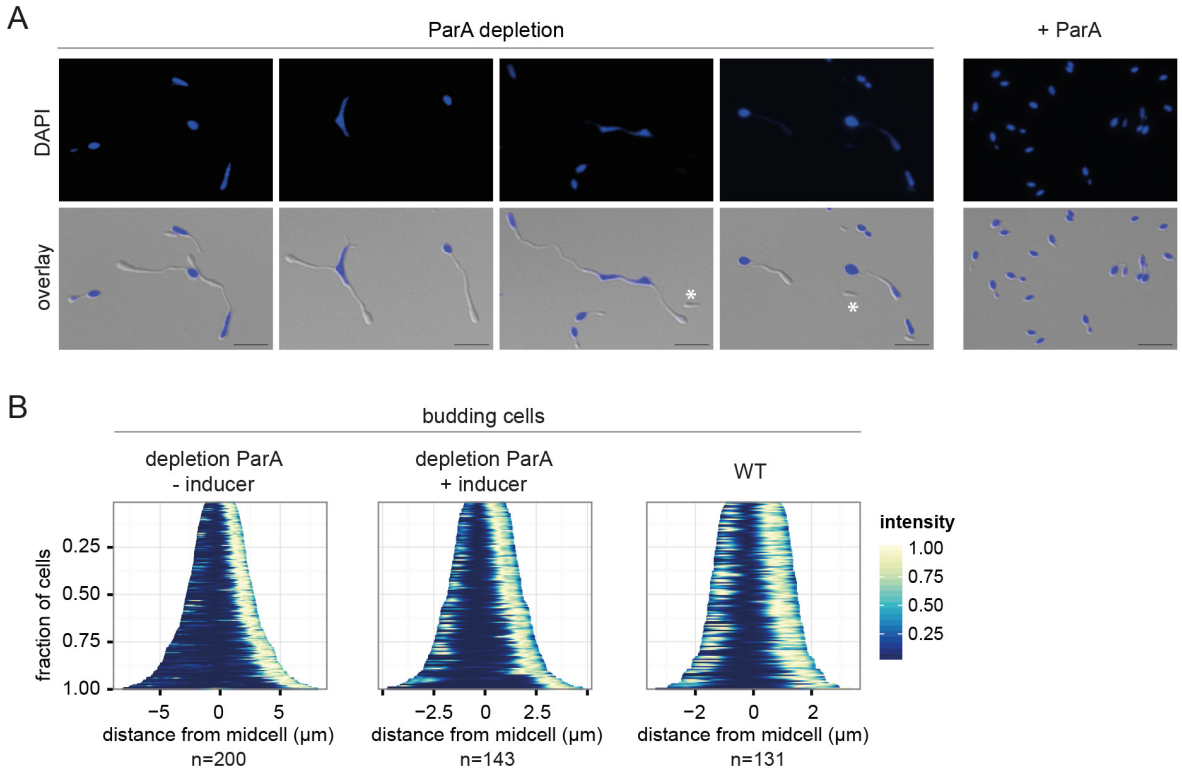

Figure 2-7: Effects of ParA depletion on chromosome segregation. A) Cells of strain AJ46 were depleted of ParA for 45h, subsequently stained with DAPI for 20 min, and visualized by DIC and fluorescence microscopy. Asterisks indicate DNA-free cells. Bar 5 µm. B) Demographic representation of the DAPI (DNA) signal in budding cells of strain AJ46 grown in the presence or absence of inducer (0.3 mM $ZnSO_4$) and in *H. neptunium* wild-type cells. Demographs are aligned with the mother cell on the right and the bud compartment on the left. Cells of strain AJ46 were grown in MB with or without 0.3 mM $ZnSO_4$ and *H. neptunium* wild-type cells were grown in MB to exponential phase, stained with DAPI for 20 min, and visualized by DIC and fluorescence microscopy.

In the next step, we intended to analyze the localization of the origin region in the absence of ParA. However, we did not succeed in introducing a fluorescently tagged version of ParB in the ParA depletion strain. Therefore, and due to the need for very long depletion times to detect morphological changes, we were seeking for an alternative approach to impair ParA functioning.

In *C. crescentus*, a missense mutation in the ATPase domain (K20R) of ParA leads to a dominant negative effect when produced in addition to wild-type ParA, resulting in incomplete chromosome segregation (68). We therefore mutated the *H. neptunium* ParA accordingly (see Figure 2-8 A) and introduced the mutated, fluorescently tagged version under the control of the copper-inducible promoter. To visualize the localization of the origin region, ParB was fluorescently tagged with Cerulean in the same strain. In order to analyze the effects of the ParA mutation on cell morphology and origin localization, we performed time-course microscopy. Before induction of the mutated ParA (ParA K18R), the cells already showed morphological alterations, most likely due to the low basal activity of the copper-inducible promoter (data not shown). Nevertheless, many cells also showed wild-type morphology and origin segregation. After 4 and 6 h of induction of the mutated ParA, cells showed an aberrant morphology with elongated stalks and buds (see Figure 2-8 B and Figure S6-1 B). It appeared that although cell division was impaired, the

budding process did not stop and that the buds somehow grew further into the stalk, resulting in a clubbed morphology (see Figure 2-8 B). Moreover, origin segregation was impaired in these cells, since there was hardly any ParB-Cerulean focus detected in the bud compartment (see Figure 2-8 B). These observations were also confirmed by flow cytometry analysis. Here, many cells had an increased cell size after 4 h of induction of the mutated ParA compared to the wild type, the non-induced control or a control strain carrying a fluorescently tagged, wild-type ParA at the locus of the copper-inducible promoter (see Figure 2-9 C). When the induction time was prolonged, these defects became even more pronounced, resulting in elongated and misshaped cells with multiple ParB foci in the mother cell (see Figure 2-8 B). This phenotype resembles the before mentioned ParA depletion phenotype.
Additionally, microscopic analysis of DAPI stained cells confirmed that no DNA is transported through the stalk to the bud compartment, whereas in the control strains DNA was detected in the bud (see Figure 2-9 A & B). Flow cytometry analysis further revealed that cells contained two or more chromosomes, while wild-type cells had either one or two chromosomes (see Figure 2-9 C). Moreover, as already seen for the conditional ParA mutant, anucleate cells were observed (see Figure 2-8 B & Figure 2-9 A, white asterisks and Table 6-5).

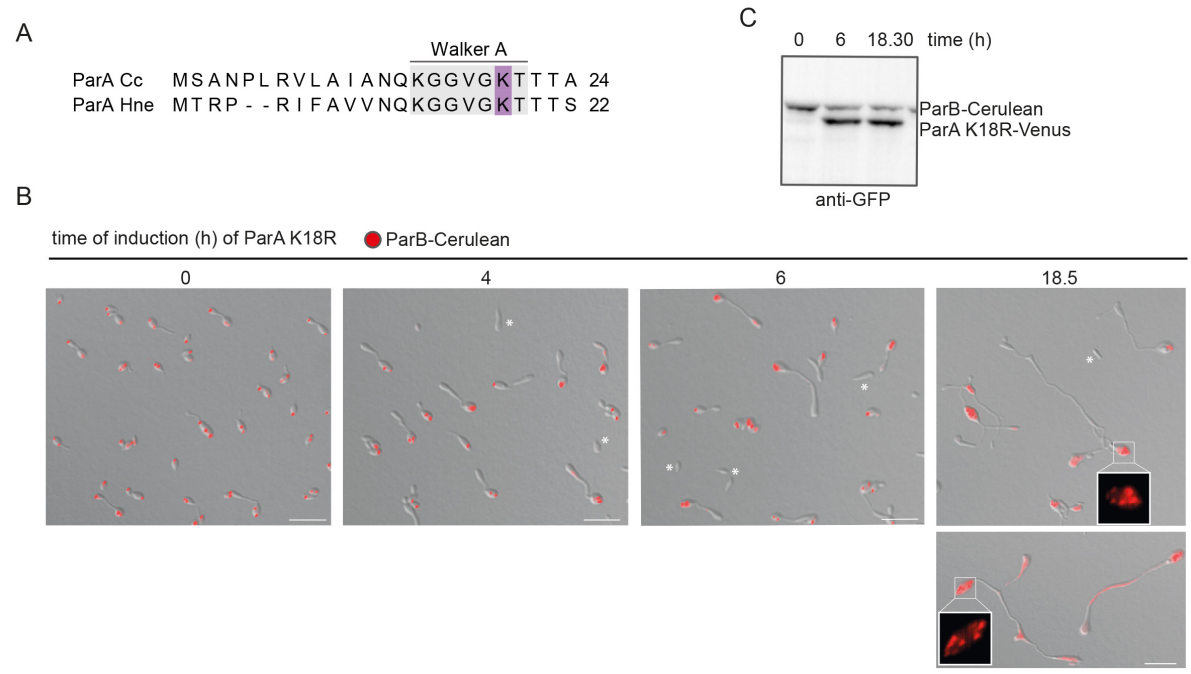

Figure 2-8: Effects of ParA K18R production on cell morphology and origin segregation. A) Alignment of the N-terminal part of the primary sequence of ParA of *C. crescentus* NA1000 and *H. neptunium* ATCC 15444. The Walker A motif is highlighted in light grey. The conserved lysine that was previously mutated in *C. crescentus* (68) and mutated in this work in *H. neptunium* is highlighted in purple. B) Effects of ParA K18R production on cell morphology and origin segregation. Cells of strain AJ79 (*parB-cerulean* P_{Cu}::P_{Cu}-*parA(K18R)-venus*) were grown in MB medium to exponential phase, induced with 0.5 mM $CuSO_4$, and growth was continued for 18.5 h. Samples were taken at the indicated time points. Morphological changes and ParB localization were analyzed by DIC and fluorescence microscopy. Asterisks indicate cells without a ParB-Cerulean signal. Bar 5 µm. C) ParA K18R-Venus and ParB-Cerulean levels in cells grown as described in (A) were analyzed by immunoblot analysis using an anti-GFP antibody.

Overall, we can conclude that the ParAB/*parS* system mediates chromosome segregation in the mother cell, since origin segregation, and DNA segregation in general, are incomplete when ParA functioning is impaired. Furthermore, one could speculate that completion of origin segregation in the mother cell might be required for the initiation of the second step (transport through stalk), indicating that origin segregation is a sequential process. Admittedly, we cannot exclude the formal possibility that ParA itself is required for origin segregation through the stalk. However, this seems rather unlikely, since the generic

ParABS system requires non-specific chromosomal DNA for proper functioning (65, 77) and the stalk appears to be free of DNA before it is traversed by the ParB/*parS* complex. Furthermore, impairment of ParA activity resulted in amorphous and elongated cells, suggesting that chromosome segregation might be coupled, to some extent, to other cell cycle events such as budding and/or cell division.

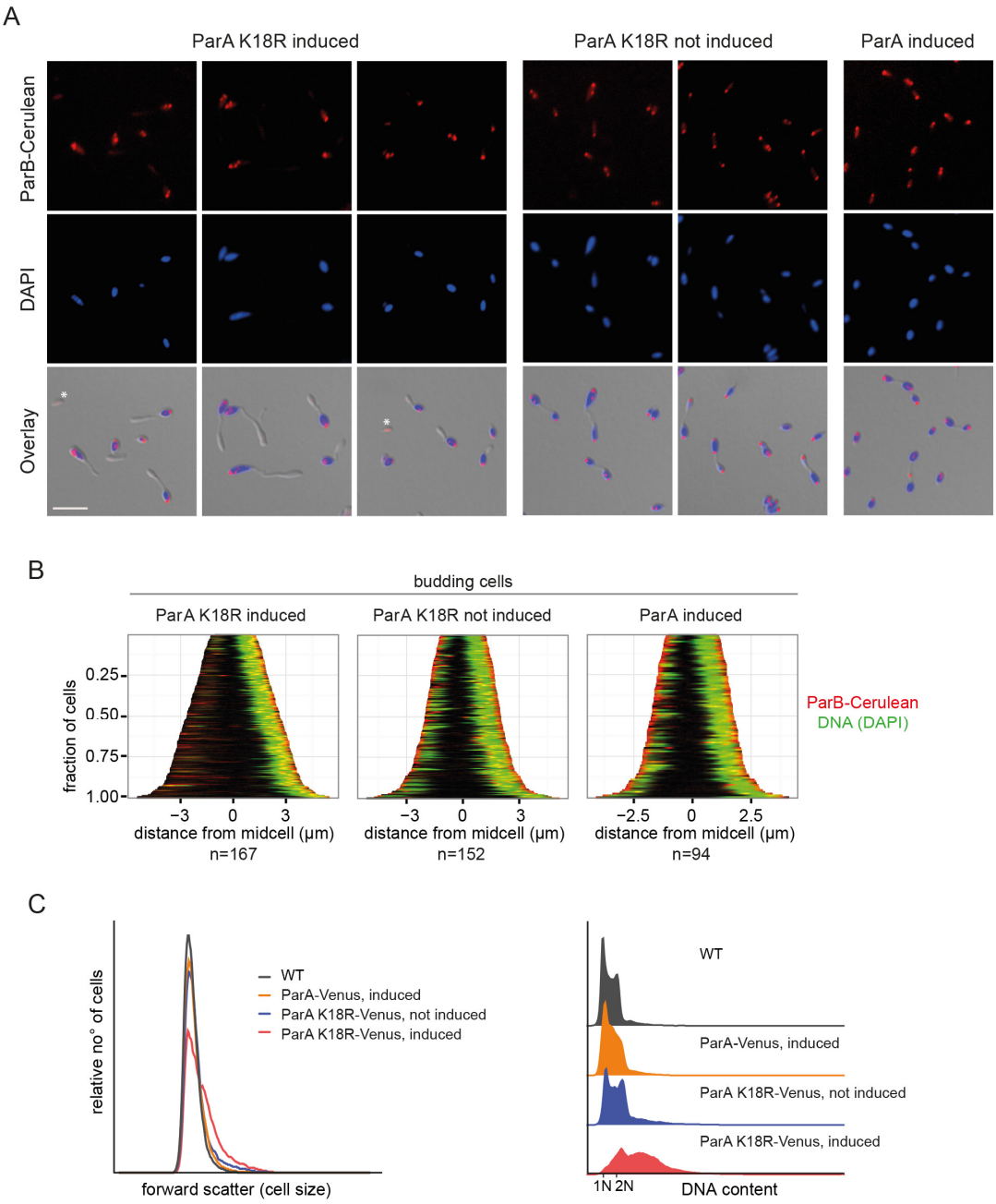

Figure 2-9: Effects of ParA K18R production on cell size and DNA content. A) Effects of ParA K18R production on chromosome segregation. Cells of strain AJ79 (*parB-cerulean* P_{Cu}::P_{Cu}-*parA(K18R)-venus*) and AJ80 (*parB-cerulean* P_{Cu}::P_{Cu}-*parA-venus*) were grown in MB medium to exponential phase, induced with 0.3 mM $CuSO_4$ for 4.5 h, subsequently stained with DAPI for 25 min, and visualized by DIC and fluorescence microscopy. Additionally, cells of strain AJ79 were grown in MB to exponential phase, but growth was continued in MB without inducer for 4.5 h and samples were analyzed accordingly. Asterisks indicate DNA-free cells. Bar 5 µm. B) Demographic representation of DAPI signal and ParB-Cerulean localization in budding cells of strains described in (A). Demographs are aligned with the mother cell on the right and the bud compartment on the left. C) Effects of ParA K18R production on cell size and chromosome content. Cells of strain AJ79 and AJ80 were grown in MB medium to exponential phase and induced with 0.3 mM $CuSO_4$ for 4.5 h. Additionally, cells of strain AJ79 and *H. neptunium* wild type were grown in MB to exponential phase but growth was continued in MB without inducer for 4.5 h. Subsequently, cells were analyzed by flow cytometry. To analyze the DNA content by flow cytometry, cells were stained with Vybrant® DyeCycle™ Orange for 25 min.

2.2 Functional analysis of the pole-organizing protein PopZ

The pole organizing protein PopZ plays an important role in chromosome segregation in the close relative *C. crescentus*. As mentioned before, *C. crescentus* PopZ is required to anchor the origin region to the cell pole and to capture and regenerate monomeric ParA during origin segregation to prevent segregation reversals (77). A previous BLAST analysis identified HNE_1677 as an *H. neptunium* PopZ homolog (183). Even though it only shows 36 % sequence identity with PopZ from *C. crescentus*, the genomic context is conserved. Moreover, the N- and C-terminal regions, which were previously described to be required for ParAB interaction, oligomerization, and polar localization (189, 190) are largely conserved (see Figure 2-10).

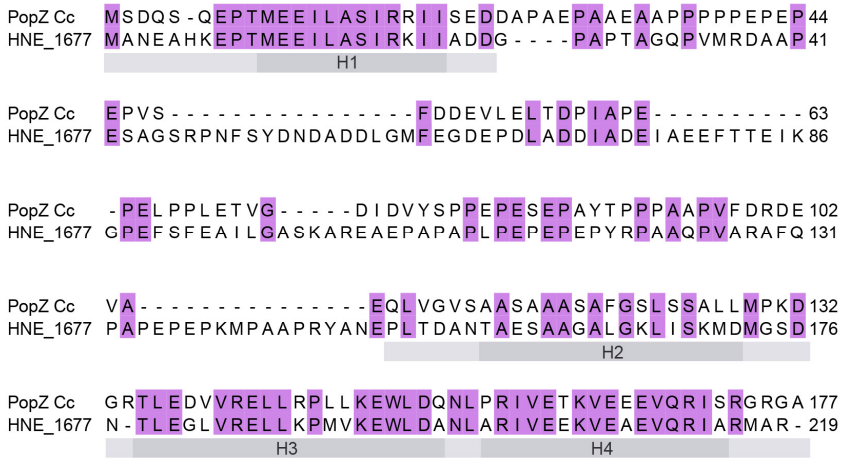

Figure 2-10: Alignment of the *C. crescentus* PopZ (CCNA_01380) and HNE_1677 primary sequences. Conserved residues are highlighted in purple. Bars in dark grey below the sequences indicate predicted α-helices of $PopZ_{Cc}$ (189, 190). Bars in light grey indicate the N- and C-terminal regions as described in (189, 190).

To analyze the function of PopZ in *H. neptunium*, we generated an inducible C-terminal Venus fusion of PopZ and analyzed its localization by snapshot and time-lapse microscopy. In swarmer cells, PopZ localized to the flagellated pole and remained at this pole also during stalk formation. At the onset of budding, it localized to the emerging bud (see Figure 2-11). In some cells, PopZ appeared to localize at the very tip of the stalk. It is likely that in these cells the budding process had already initiated but that the bud was not yet visible by microscopy (see Figure 2-11 A & B). In budding cells with a clearly visible bud, PopZ localized to the flagellated bud pole opposite the stalk. In some stalked and budding cells, we also could detect a bipolar localization pattern. However, the focus at the old cell pole (mother cell) disappeared when the cell proceeded through the cell cycle (see Figure 2-11 C). Furthermore, in a fraction of stalked cells, we only detected a diffuse signal (see Figure 2-11 B & E). Most likely, these stalked cells just finished cell division and were about to enter a new round of budding. However, immunoblot analysis revealed that the fusion construct is not completely stable since an additional signal of ~ 30 kDa was detected, which corresponds to the size of the cleaved Venus-tag. Hence, it is not possible to distinguish whether the diffuse signal observed in stalked cells results from PopZ-Venus or from the cleaved Venus-tag. PopZ-Venus migrates also slower than expected in SDS-PAGE (70 kDa instead of 54 kDa, see Figure 2-11 D). However, this was also observed for *C. crescentus* PopZ (74, 75). In order to verify the localization pattern of PopZ, we attempted to generate a PopZ-Venus fusion produced from its endogenous promoter. Attempts to integrate the corresponding plasmid at the native locus via single homologous recombination were not successful. Thus, further analysis will be required to validate the PopZ localization pattern. The observed pattern with PopZ localizing early to the emerging bud suggests that PopZ could anchor the segregated ParB/*parS* complex at the flagellated bud pole (new pole). To test this hypothesis and to further analyze the role of PopZ in *H. neptunium*, we generated an in-frame deletion and localized ParB in the absence of PopZ.

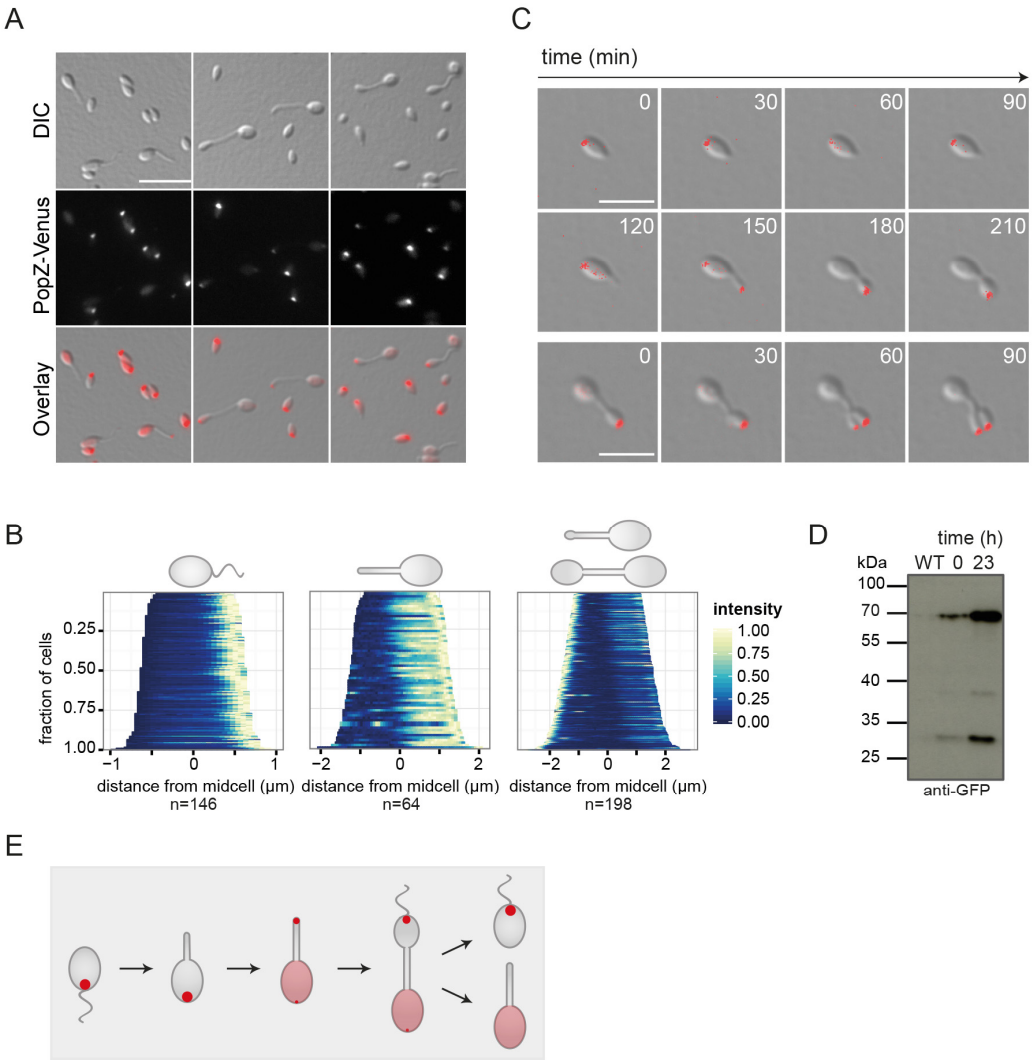

Figure 2-11: PopZ localization in *H. neptunium*. A) Cells of *H. neptunium* AJ34 (P_{Zn}::P_{Zn}-*popZ-venus*) were grown in MB medium, induced for 23 h with 0.5 mM $ZnSO_4$, and visualized by DIC and fluorescence microscopy. Bar 5 µm. B) Demographic representation of PopZ-Venus localization in swarmer (left), stalked (middle), and budding (right) cells. Cells of strain AJ34 were grown in MB medium, induced for 2.5 h with 0.5 mM $ZnSO_4$, and visualized by DIC and fluorescence microscopy. C) Time-lapse microscopy of AJ34. Cells of strain AJ34 were grown in MB medium to exponential phase, induced for ~ 2.5 h with 0.5 mM $ZnSO_4$, transferred to an MB agarose pad, and visualized at 30 min intervals by DIC and fluorescence microscopy. Overlays of DIC and fluorescence micrographs are shown. Bar 3 µm. D) PopZ-Venus levels of samples described in (A) were analyzed by immunoblot using an anti-GFP antibody. Expected molecular weight: 54 kDa. E) Schematic of dynamic PopZ-Venus localization (inducible fusion).

Deletion of *popZ* did not lead to any severe morphological changes (see Figure 2-12 A & Figure S6-1 C). Only ~2.8 % more cells showed morphological defects in the deletion strain compared to the wild-type population (data not shown). Moreover, ParB did not show any localization defect in the absence of PopZ in the majority of cells (see Figure 2-12 B). Only 13.7 % of cells showed aberrant ParB localization in the *popZ* deletion strain compared to 0.2 % in wild-type cells. As cells with aberrant ParB-Venus localization, we classified swarmer cells in which ParB did not show a polar localization or stalked/budding cells in which ParB did not localize to the old cell pole in the mother cell compartment (see Figure 2-12 C). For the second ParB focus that traverses the stalk and then localizes to the flagellated pole in the newly forming bud, it is difficult to assess whether the localization is aberrant or whether its movement has not been finished at the time of analysis. To address this issue, time-lapse analysis would be required. To determine whether PopZ interacts with ParB, further investigation is required in the future. The localization of PopZ

to the emerging bud is reminiscent of ParA localization (see Figure 1-5 C). To analyze if PopZ might be involved in capturing ParA, we tested if ParA localization depends on PopZ (especially in the bud). Preliminary data suggest that ParA still forms a focus in the (incipient) bud at the pole opposite the stalk in the absence of PopZ (data not shown), suggesting PopZ is not crucial for the polar localization of ParA. However, further analysis and quantification of the ParA localization pattern is required to confirm these observations.

Taken together, PopZ may be involved in the positioning of the ParB/*parS* complex at the flagellated bud pole. However, the loss of PopZ did not lead to severe morphological changes and the ParB/*parS* complex was only mislocalized in a subpopulation of cells, suggesting that PopZ is either partially redundant or that origin anchoring in the bud might not be a crucial process. Moreover, the PopZ localization pattern suggests that an additional factor might be required to capture monomeric ParA (and maybe also the ParB/*parS*) complex at the stalked mother cell pole.

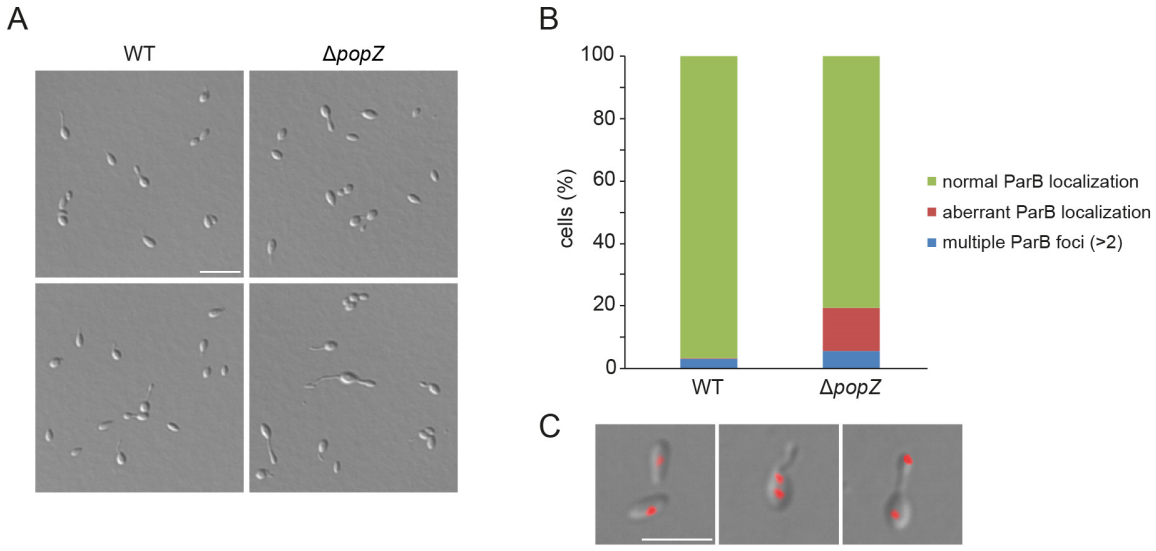

Figure 2-12: Effects of *popZ* deletion. A) Effects of *popZ* deletion on cell morphology. Cells of strain AJ38 (Δ*HNE_1677*) were grown in MB medium and visualized by DIC microscopy. Bar 5 µm. B) Comparison of ParB-YFP localization in wild-type and Δ*popZ (HNE_1677)* background strains. Cells of strains AR48 (*parB*::*parB-yfp*) and AJ89 (Δ*HNE_1677 parB*::*parB-yfp*) were grown in MB medium and analyzed by DIC and fluorescence microscopy. C) Exemplary micrographs of aberrant ParB foci localization. Overlays of DIC and fluorescence micrographs are shown. Bar 3 µm.

2.3 Analysis of SMC in *H. neptunium*

The bacterial SMC proteins are thought to be involved in chromosome organization, condensation, and segregation (reviewed in (3)). To analyze the function of SMC in *H. neptunium*, we generated an inducible C-terminal Venus fusion. A weak signal could already be detected by fluorescence microscopy without induction. In swarmer cells, SMC localized close to the flagellated pole. In some stalked cells, a bipolar localization pattern was observed in the mother cell. In some budding cells, two SMC foci could be detected at the poles opposite the stalk in the mother cell and in the bud. Interestingly, this localization pattern resembles the localization of ParB. This is consistent with observations in other bacteria, in which SMC is enriched and forms foci in the proximity to the origin regions (18, 97, 98, 129, 191). However, there were also budding cells with only one focus in the bud or stalked cells with up to three foci (see Figure 2-13 A). It is possible that due to the weak signal some foci were simply not detected. Furthermore, in most cases the foci were not very distinct. After induction of the fusion construct, the background signal was increased, so that in some cells only a diffuse signal was detected (data not shown). To better analyze the subcellular localization of SMC, we constructed a strain harboring an *smc-venus* fusion under

the control of the native promoter. This SMC fusion showed a similar localization pattern and thus confirmed the localization pattern observed for the inducible SMC fusion (see Figure 2-13 B). In general, the signal was weak and many cells did not show distinct foci. However, oftentimes we could detect a weak focus that clearly differed from a diffuse signal. Noteworthy, the strain harboring the *smc-venus* fusion under the control of the native promoter appeared to grow more slowly (24 % increased doubling time compared to wild type) but formed 140 % more biofilm than wild-type cells (data not shown). It is conceivable that the slower growth could be partially due to the increased biofilm formation. Commonly, the *H. neptunium* wild type forms a thick biofilm at the sidewall of the culture well. Increased biofilm formation could increase the number of cells stuck to the sidewall and hence exclude these cells from growth measurements. Why the SMC fusion produced from the native promoter leads to increased biofilm formation and if this indicates that the fusion protein might not be fully functional and thus, for instance, alter transcription due to aberrant chromosome condensation, requires further investigation in the future.

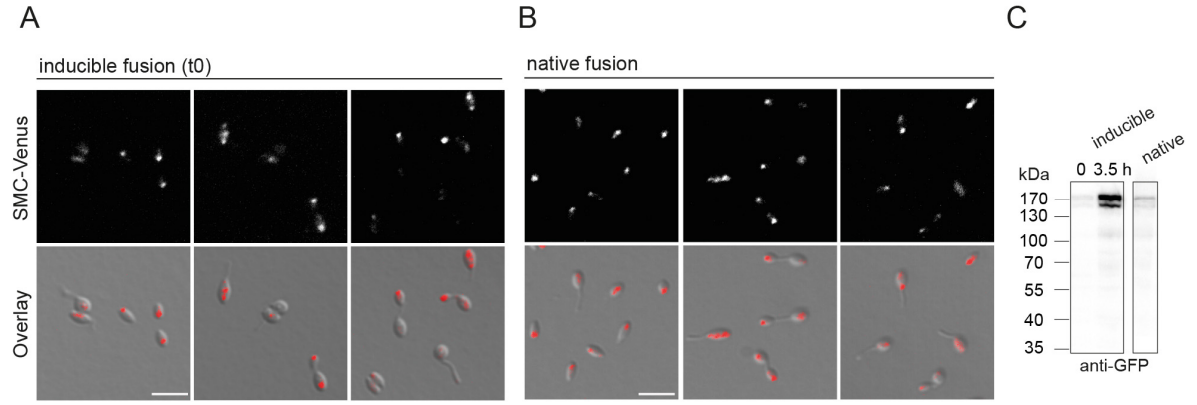

Figure 2-13: Analysis of SMC-Venus localization. A) Cells of strain AJ48 (P_{Zn}::P_{Zn}-*smc-venus*) were grown in MB medium in the absence of inducer to exponential phase and visualized by DIC and fluorescence microscopy. B) Cells of strain AJ85 (*smc-venus*) were grown in MB medium to exponential phase and visualized by DIC and fluorescence microscopy. Bar 3 µm. C) SMC-Venus levels were analyzed by immunoblot using an anti-GFP antibody. Expected molecular weight: ~153 kDa. Inducible SMC-Venus fusion: Cells of strain AJ48 were grown to exponential phase, induced with 0.3 mM $ZnSO_4$ for 3.5 h, and samples were taken at indicated time points. SMC-Venus fusion produced from native promoter: Immunoblot analysis of samples described in (B).

Furthermore, we attempted to generate an *smc* deletion strain. Under our standard growth conditions (rich medium, 28°C), SMC appears to be essential, which indicates that SMC might fulfill a crucial role in *H. neptunium*. However, in some bacteria, such as *B. subtilis* or *E. coli*, an *smc* null mutant is conditionally lethal, allowing growth only at low temperatures (3). To test whether this is also the case in *H. neptunium*, we will repeat the generation of the deletion strain at low temperatures and also try to generate an SMC depletion strain. In addition, it will be also highly interesting to perform co-localization studies with ParB and SMC in the future.

2.4 Localization studies of truncated versions of the ParA homolog HNE_0708

As mentioned in chapter 1.4.1, analyses of ParA homologs in *H. neptunium* drew our attention to the orphan ParA-like protein HNE_0708. Deletion of *HNE_0708* caused elongated stalks, and localization of ParB in the deletion background revealed multiple ParB foci in budding cells, indicating impaired origin segregation or initiation of replication (80). An inducible HNE_0708-Venus fusion showed a diffuse signal in the mother cell and bud and also sometimes a patchy pattern in the stalk (see Figure 1-6 B). However, similar to the deletion strain, cells carrying the fusion construct had elongated stalks in which DNA accumulated (80). This suggests that the fusion protein is either not functional and that its expression has

a dominant negative effect, or that its expression from the zinc-inducible promoter in addition to the wild-type copy leads to an overexpression phenotype. To further analyze the function of HNE_0708 in *H. neptunium*, we generated inducible C-terminal fusions of truncated versions of HNE_0708. By this, we wanted to test if the individual domains adopt a specific subcellular localization, and we furthermore hoped to avoid any adverse effects that were caused by the full length inducible C-terminal fusion. Assuming that HNE_0708 might play a role in chromosome replication or segregation, we would expect that it shows a specific localization pattern. However, localization studies of the TIR domain alone or a truncated version excluding the TIR domain, but containing the ParA-like ATPase domain, only revealed a diffuse localization (see Figure 2-14). Furthermore, cells producing the fluorescent fusion of the TIR domain appeared to have morphological alterations such as elongated stalks. However, this observation requires further quantification in future and it also needs to be tested if DNA accumulates in the stalk structure in these cells. Notably, the truncated version without the TIR domain showed only a very weak signal even after 5 h of induction. Up to now, no fluorescent fusion gives further evidence to a potential function of the protein. Currently, we are generating an N-terminal Venus fusion to test if this fusion might show a specific subcellular localization.

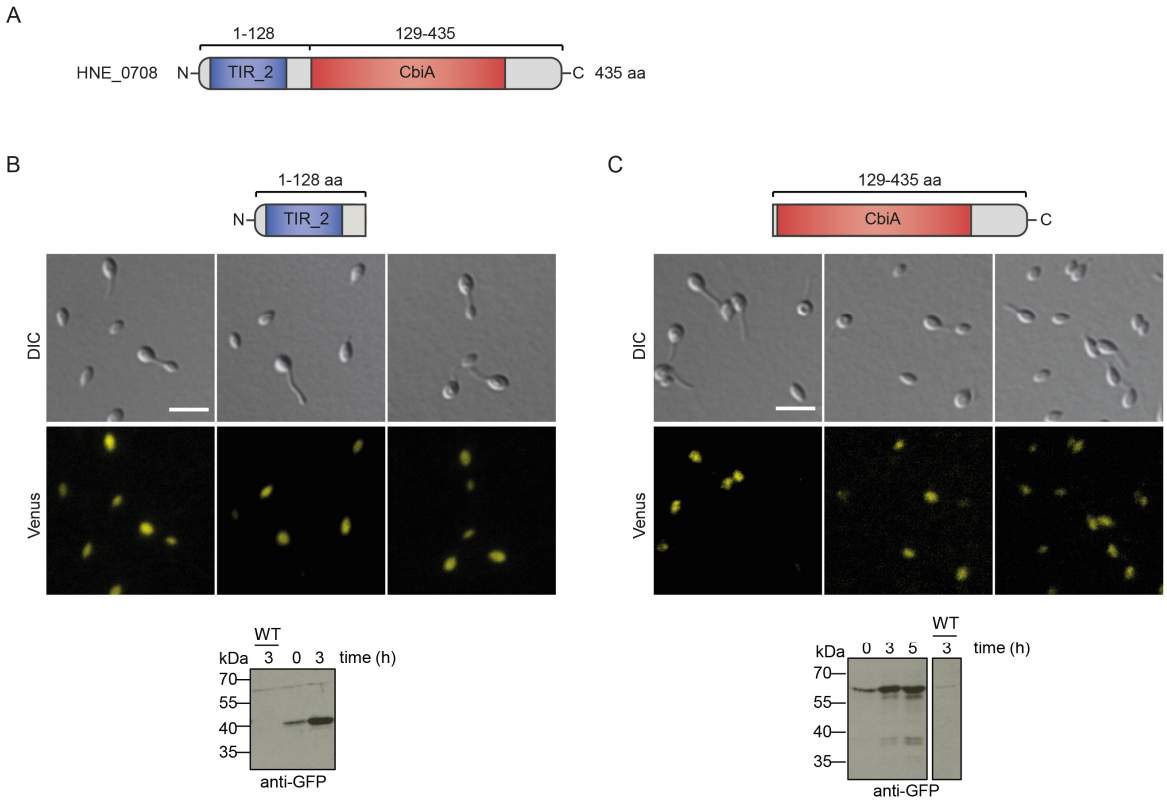

Figure 2-14: Localization studies of truncated versions of the ParA homolog HNE_0708. A) Schematic depicting the domain structure of HNE_0708. B) Localization of the HNE_0708 TIR domain. Cells of strain AJ55 (P_{Zn}::P_{Zn}-*HNE_0708*$_{AA1-128}$-*venus*) were grown in MB to exponential phase, induced with 0.5 mM $ZnSO_4$ for 3 h, and visualized by DIC and fluorescence microscopy (upper panel). HNE_0708$_{AA1-128}$-Venus levels of samples described above were analyzed by immunoblot using an anti-GFP antibody (lower panel). C) Localization of HNE_0708 lacking the TIR domain. Cells of strain AJ56 (P_{Zn}::P_{Zn}-*HNE_0708*$_{AA129-435}$-*venus*) were grown in MB to exponential phase, induced with 0.5 mM $ZnSO_4$ for 5 h, and visualized by DIC and fluorescence microscopy (upper panel). HNE_0708$_{AA129-435}$-Venus levels of samples described above were analyzed by immunoblot using an anti-GFP antibody (lower panel). Bar 3 µm.

2.5 Analysis of the organization and dynamics of the *H. neptunium* chromosome

Most bacteria studied so far possess circular chromosomes that mostly show a longitudinal or, in some cases, a transverse organization pattern or variations of these two themes (reviewed in (6)). For the close relative *C. crescentus*, it was shown that the chromosome has a longitudinal organization pattern with the origin present at the old cell pole, the terminus region located at the new cell pole, and the two chromosomal arms lying side by side in between them. Furthermore, it was shown that the chromosome has a conserved arrangement within the cell that is immediately restored after chromosome segregation. Each locus on the chromosome has a specific subcellular localization and this position correlates with the position on the genomic map (9).

2.5.1 The *H. neptunium* chromosome shows a longitudinal arrangement

In the next step, we analyzed the subcellular localization of the *H. neptunium* chromosome in more detail. A cryo-EM tomogram of a *H. neptunium* swarmer cell nicely shows the condensed nucleoid, which appears to occupy only part of the cell (see Figure 2-15 A).
To analyze the localization of specific chromosomal loci, we took advantage of the plasmid-encoded (pMT1) ParB-*parS* system of *Yersinia pestis*. To this end, a plasmid harboring *parS*$_{pMT1}$ sites was integrated at regions of interest in the *H. neptunium* chromosome (see Figure 2-15 B). N-terminally fluorescently tagged ParB of *Y. pestis* will then bind to *parS*$_{pMT1}$, allowing the visualization of chromosomal loci of interest within the cell. Importantly, it was shown previously that there is no crosstalk between ParB$_{pMT1}$ and the *parS* sites of *H. neptunium* (80). In addition, the strains harbor a fluorescently tagged ParB$_{Hne}$ (which binds to the *H. neptunium parS* sites) in order to label the origin region. In general, cells harboring ParB/*parS*$_{pMT1}$ system showed morphological defects, as reflected by elongated cells and stalks as well as amorphous cells in a subpopulation of cells (data not shown). However, many cells still exhibited wild-type morphology and ParB localization pattern and were analyzed further. We determined the localization of different chromosomal loci by fluorescence microscopy (see Figure 2-15 D-G) and quantified the position of each chromosomal locus within swarmer cells, cells that were at the transition to a stalked cell, and cells with very short stalks but only one ParB$_{Hne}$ focus (see Figure 2-15 C). We assume that these cells are all in non-replicative G1 phase meaning that each chromosomal locus is only present as a single copy in the cell.
As described before, the origin region (359°) localizes to the flagellated pole in swarmer cells (see Figure 2-15 C). Labeled regions close to the origin (357° and 5°) mostly or partially co-localized with ParB/*parS*$_{Hne}$ (see Figure 2-15 C & D). Loci that are at intermediate positions on the chromosomal arms (85° and 272°) localized close to midcell (see Figure 2-15 C & E). A locus labeled at 53° showed an intermediate localization between the flagellated pole and midcell (see Figure 2-15 C & G). Labeled regions close to the terminus (172° and 186°) localized to the future stalked pole (see Figure 2-15 C & F). However, when the stalk was formed and the bud was generated, we could observe the terminus region farther away from the stalked pole and closer to midcell in many cells (see Figure 2-15 F). In summary, the analysis of G1 cells revealed that the *H. neptunium* chromosome is orientated along the cellular long axis and suggests that the position of the analyzed chromosomal loci within the cell correlates with the position on the genomic map (see Figure 2-15 B & C). It should be noted that the majority of the cells lose the ParB/*parS*$_{pMT1}$ focus upon transport of the chromosome through the stalk, since we hardly observed a focus in the bud or in swarmer cells. This is a very interesting phenomenon, but it makes the quantification in swarmer cells rather difficult since only a minority of swarmer cells still possesses a measurable signal. The signal reappears upon progression of the swarmer cell through the cell cycle, with most of the stalked and budding cells showing a ParB/*parS*$_{pMT1}$ signal in the mother cell. Possibly, new mCherry-ParB$_{pMT1}$ is produced by the newly generated cell, which can then rebind to the *parS*$_{pMT1}$-sites. Why the signal (focus) is lost upon chromosome segregation through the stalk will be discussed in chapter 3.3.

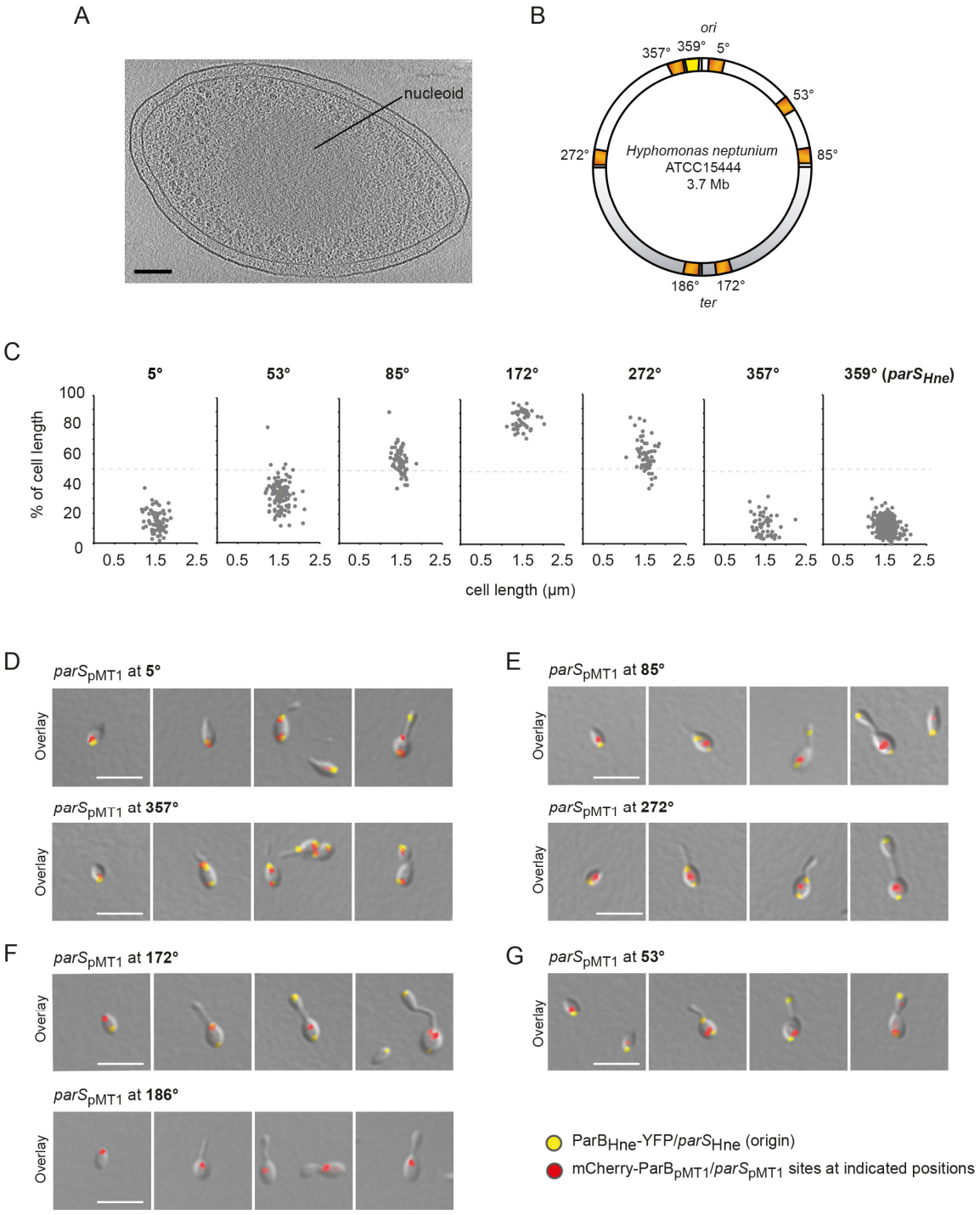

Figure 2-15: Arrangement of the *H. neptunium* chromosome. A) Cryo-electron tomogram of an *H. neptunium* swarmer cell. Bar 100 nm. Image taken by Yi-Wei Chang (CalTech, USA) B) Schematic of the regions (depicted in orange) on the *H. neptunium* chromosome that were visualized using the ParB/*parS*$_{pMT1}$ system of *Y. pestis* together with the origin region (ParB/*parS*$_{Hne}$, depicted in yellow). C) Subcellular localization of seven different chromosomal loci. Cells of strains AJ64-69 (*parB-yfp* P$_{Zn}$::P$_{Zn}$-*mCherry-ParB*$_{pMT1}$, *parS*$_{pMT1}$ inserted at indicated positions) and KH22 (*parB-yfp*) were grown in MB medium to exponential phase and visualized by phase contrast and fluorescence microscopy. Subcellular positions were quantified in swarmer cells, cells that are at the swarmer-to-stalked cell transition, and cells that already showed a small stalk but only one ParB focus. The old pole (flagellated pole) represents 0 % of cell length and the future stalked pole represents 100 % of cell length. n = 75 (5°), 52 (357°), 118 (53°), 53 (172°), 64 (272°), 60 (85°), 315 (359°). D)-G) Subcellular localization of six different chromosomal loci in relation to the origin region. Cells of strains AJ64-69 (*parB-yfp* P$_{Zn}$::P$_{Zn}$-*mCherry-ParB*$_{pMT1}$, *parS*$_{pMT1}$ inserted at indicated positions) were grown in MB medium to exponential phase and visualized by DIC and fluorescence microscopy. F) Lower panel: Subcellular localization of the terminus region. Cells of strain AJ49 (P$_{Zn}$::P$_{Zn}$-*mCherry-parB*$_{pMT1}$ *parS*$_{pMT1}$ at 186°) were grown in MB medium and visualized by DIC and fluorescence microscopy. Bar 3 µm.

2.5.2 Analysis of chromosome dynamics in *H. neptunium*

The observations made by snapshot fluorescence microscopy provide a first insight into how the chromosome is arranged in *H. neptunium*. In the next step, we intended to analyze the dynamics of the *H. neptunium* chromosome, since it will be highly interesting to analyze for instance the spatiotemporal pattern of terminus duplication and segregation. To further confirm that the origin region (359°) is the first region to be segregated through the stalk, it is required to co-localize the origin region with another origin-proximal region and analyze their segregation dynamics. We could show that origin-proximal regions (partially) co-localize with the origin (ParB/*parS*$_{Hne}$) in the cell (see Figure 2-15 C & D). By analyzing their distance to each other during transport through the stalk, we could gain insight into the condensation state of the chromosome during its segregation through the stalk.
For this purpose, we performed time-lapse microscopy with strains that are labeled at the terminus or an origin-proximal region, respectively, as well as the origin region itself. However, as described above, the ParB/*parS*$_{pMT1}$ system is not suitable for this purpose, since we "lose" the signal (focus) in most cases upon segregation of the chromosome through the stalk. Therefore, we took advantage of an alternative system and analyzed chromosome dynamics by using FROS. To this end, a *lacO* array is inserted at a region of interest on the chromosome and the fluorescently labeled LacI repressor that is produced from the zinc-inducible promoter then binds to the *lacO* array, thereby visualizing the region of interest on the chromosome. FROS was previously used to label chromosomal regions in *H. neptunium*, and it was shown that the origin region (ParB/*parS*) is segregated before the region close to *dnaA* (see Figure 1-7 B) (80). However, cells harboring FROS showed more severe morphological defects than cells harboring the ParB/*parS*$_{pMT1}$ system (see Figure 2-16 & data not shown). The phenotype caused by FROS has already been reported in a former study (80). However, a fraction of cells in the population showed wild-type morphology and was hence followed in the further analysis. Moreover, the results obtained were consistent with those obtained with the ParB/*parS*$_{pMT1}$ system.

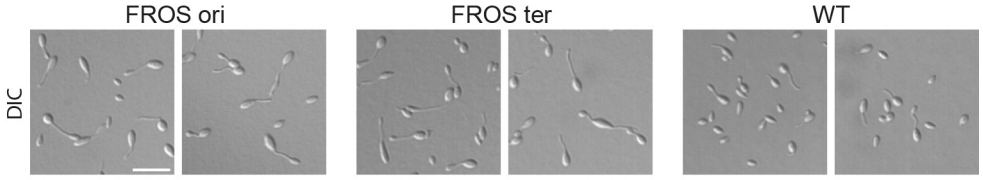

Figure 2-16: Effects of FROS labeling on cell morphology. Cells of strains labeled with FROS at origin- and terminus-proximal regions, respectively. AJ86: (*HNE_1729*::l*acO*$_n$, *parB-yfp* P$_{Zn}$::P$_{Zn}$-*lacI-mCherry*) and AJ87: (*HNE_3540*::l*acO*$_n$, *parB-yfp* P$_{Zn}$::P$_{Zn}$-*lacI-mCherry*) were grown to exponential phase in MB medium, induced with 0.3 mM $ZnSO_4$ for 3 h, and analyzed by DIC microscopy. The wild-type control was grown in MB medium to exponential phase and analyzed accordingly. Bar 5 µm.

Time-lapse microscopy of a strain labeled at an origin-proximal position (357°) in addition to the origin region (359°) revealed that the origin region is the first locus to be segregated within the mother cell and also through the stalk, even though both loci partially co-localize at the cell poles (see Figure 2-17 A) and are only 21 kb apart on the genomic map. In some cases, we could also observe a partial co-localization of both loci during segregation within the mother cell. If both loci can also be transported conjointly through the stalk requires further analysis. However, we never observed the FROS labeled region to be segregated first. This corroborates the notion that the origin region truly is the region that is segregated first.
Next, we performed time-lapse microscopy of a strain labeled at the terminus region to study the spatiotemporal pattern of terminus duplication and segregation. We could observe the typical terminus localization close to the stalked mother cell pole. In some cells, the terminus was displaced closer to midcell in the course of the cell cycle (see Figure 2-17 B). Interestingly, in some budding cells, we could observe two terminus foci in the mother cell, indicating that replication and separation of the terminus region occur in

the mother cell compartment. Furthermore, these cells mostly had mature buds, supporting the notion that terminus separation occurs at the final stage of the cell cycle shortly before cell division (see Figure 2-17 B lower panel, 3 min intervals). Remarkably, we did not observe segregation of the terminus region through the stalk, since we could not detect a signal in the generated bud (see Figure 2-17 B). The observation that we lose the signal for the labeled terminus region but not the origin-proximal region or the region labeled at 54° (80), indicates that the terminus region encounters different or special conditions compared to the other regions upon segregation through the stalk at this late stage of the cell cycle.

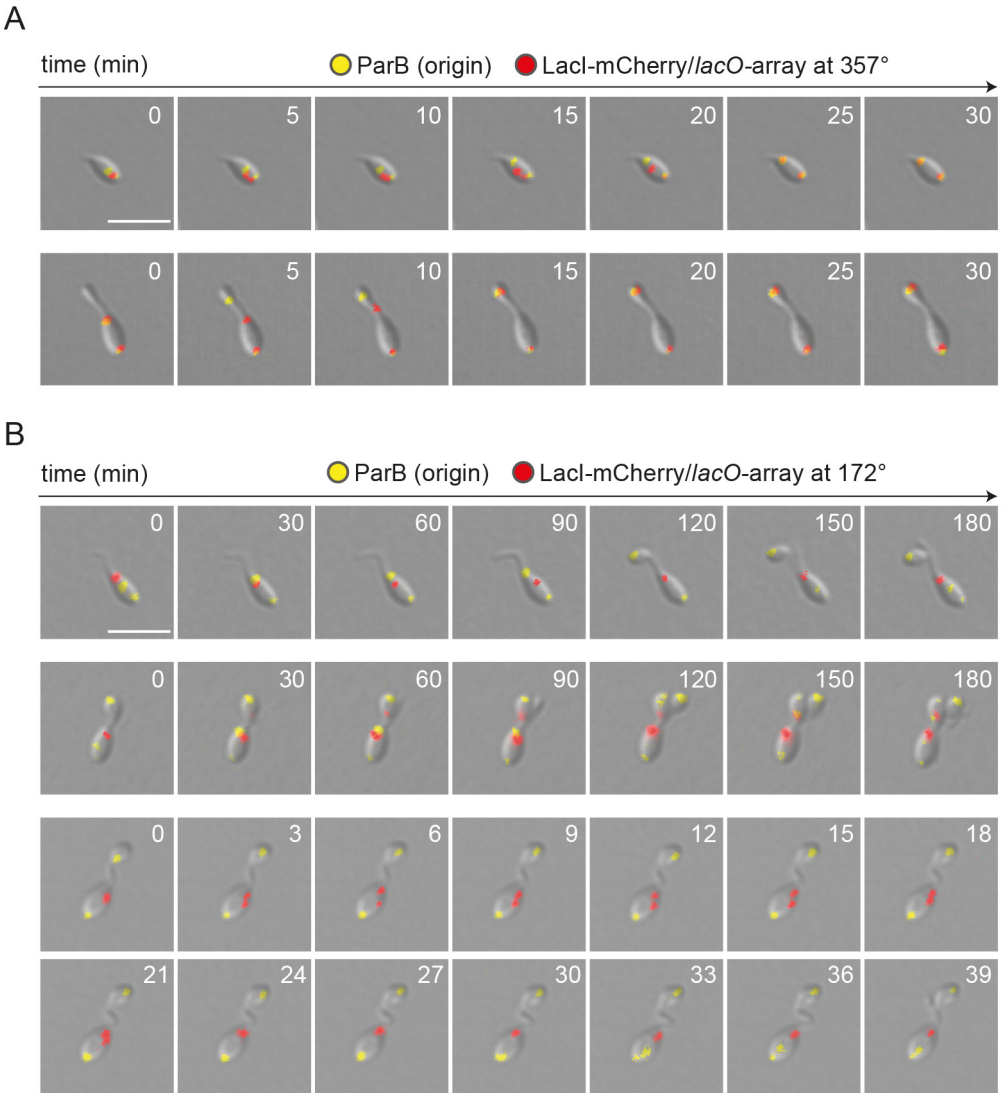

Figure 2-17: Analysis of chromosome dynamics by time-lapse microscopy. A) Analysis of the origin region. Cells of *H. neptunium* AJ87 (*HNE_3540*::l*acO*$_n$, *parB-yfp* P_{Zn}::P_{Zn}-*lacI-mCherry*) were grown in MB medium to exponential phase, induced with 0.3 mM $ZnSO_4$ for 2 h, transferred to an MB agarose pad, and visualized at 5 min intervals by DIC and fluorescence microscopy. Overlays of DIC and fluorescence micrographs are shown. Bar 3 µm. B) Analysis of the terminus region. Cells of *H. neptunium* AJ86 (*HNE_1729*::l*acO*$_n$, *parB-yfp* P_{Zn}::P_{Zn}-*lacI-mCherry*) were grown in MB medium to exponential phase, induced with 0.3 mM $ZnSO_4$ for 2.5-3 h, transferred to an MB agarose pad, and visualized at 3 and 30 min intervals by DIC and fluorescence microscopy. Overlays of DIC and fluorescence micrographs are shown. Bar 3 µm.

In agreement with the loss of the signal upon segregation through the stalk, we observed that 48 % of the swarmer cells did not have a signal for the terminus region (n_{total}= 145). On the other hand, half of the swarmer cells had a terminus signal (52 %, n_{total}= 145). This could indicate that the signal for terminus region is not lost upon segregation through the stalk in some cases, or that the signal is lost but reappears after a certain time. This could possibly be due to new LacI-mCherry produced by the newly generated

cell, which can than bind to the *lacO*-array. And indeed, this "reaccumulation" was observed in a few cells during time-lapse microscopy (see Figure 2-17 B, middle panel). This would also explain why stalked and budding cells show a terminus signal. It is important to mention that it is difficult to determine the exact time point of cell division in time-lapse series on agarose pads, since the newly formed daughter cells usually remain in close proximity of the mother cell. However, in order to state that the terminus signal is not segregated to the bud, we have to be sure that cell division already took place. Therefore, we considered the generation of a new bud and/or the duplication of the ParB-YFP focus (origin) as indicators for a new round of cell division.

2.6 Coordination of chromosome replication and segregation

In most bacteria, chromosome replication and segregation occur simultaneously. In contrast, in eukaryotes, these two processes are temporally uncoupled (reviewed in (41)). In *H. neptunium*, one of the newly replicated origin regions is segregated to the stalked pole of the mother cell and remains there until the stalk and bud are generated, before it is then transported through the stalk. Time-lapse microscopic analysis revealed that chromosome segregation within the mother cell took 30 ±13 min, with a "waiting time" of the duplicated origin at the stalked pole of 58±24 min (see chapter 2.1.2). Together, chromosome segregation within the mother cell and the "waiting time" of the duplicated origin at the stalked pole last for about 88±16 min. It is known from other organisms with non-overlapping replication cycles that DNA synthesis occurs at a rate of ~350-400 b/s (10, 192-194). Assuming that DNA synthesis occurs at a similar rate in *H. neptunium*, replication of the 3.7 Mb chromosome would take ~77-88 min. This would allow enough time for chromosome replication to be finished, at least largely, before chromosome segregation through the stalk occurs. This raises the question of whether chromosome replication and segregation through the stalk are temporally uncoupled in *H. neptunium*, reminiscent of mitosis in eukaryotes, or whether segregation and replication occur simultaneously, like in most bacteria.

2.6.1 Analysis of replisome dynamics in *H. neptunium*

To determine whether replication and segregation are temporally uncoupled, we set out to co-localize ParB with the replisome. The replication machinery assembles at the origin region upon initiation of DNA replication, moves along the chromosomal arms, and dissembles at replication termination at the terminus region. Tracking of the replisome by visualizing different components has already been successfully employed in diverse bacteria (10, 36, 38). To visualize the replication machinery in *H. neptunium*, we generated a HolC-Venus fusion produced from the native *holC* promoter and analyzed its localization by fluorescence microscopy. *HolC* encodes the chi-subunit of the DNA polymerase III and is part of the β-clamp loader complex (195). The fluorescent signal was generally very weak, but we could observe a dynamic localization in the mother cell. In many swarmer cells, we detected only a diffuse signal, indicating that chromosome replication has not been initiated yet. In a subpopulation of cells that are at the swarmer-to-stalked cell transition, HolC-Venus localized to the flagellated pole. In stalked cells, a signal close to midcell was observed, while in budding cells, HolC was observed between midcell and the stalked pole of the mother cell (see Figure 2-18 A & B). This localization pattern is in accordance with the localization of the origin and terminus region: at early stages in the cell cycle, HolC-Venus was observed at the pole where the origin region of the chromosome resides, whereas at late stages of the cell cycle (budding cells) it was observed at the subcellular region at which the terminus region of the chromosome localizes (see above).

In order to confirm the localization pattern of the replisome and to obtain a stronger signal, we tagged the single-stranded DNA binding protein Ssb, another component of the replisome. Ssb binds to single-

stranded DNA to prevent the formation of secondary structures as well as the degradation by nucleases. Hence, it participates in processes where single-stranded DNA occurs such as DNA replication, repair, and recombination (reviewed in (196)). The inducible Ssb-Venus fusion in *H. neptunium* exhibits a similar localization pattern as HolC-Venus (see Figure 2-18 C & D). However, the signal was not significantly stronger than that of HolC-Venus and the background fluorescence increased after longer induction times. Attempts to generate an Ssb-Venus fusion produced from the native *ssb* promoter were not successful. Despite the weak signal, we co-localized Ssb-Venus and HolC-Venus, respectively with ParB-Cerulean in *H. neptunium* to answer the question if the chromosome is first fully replicated and then segregated. In both cases, we could detect a replisome signal only in a minority of cells (data not shown). However, we noticed that in swarmer cells, which are at the transition to stalked cells, the replisome co-localized with the origin (ParB-Cerulean/*parS*). When the origin was duplicated and segregated within the mother cell, the replisome localized either to the midcell region or to the proximity of stalked cell pole. Later on, when ParB was already segregated through the stalk and cell division was about to take place or already took place, some cells showed again a replisome focus at the pole opposite the stalk in the mother cell (see Figure 2-19 A & Figure 2-18 D). This most likely indicates that a new round of chromosome replication has initiated.

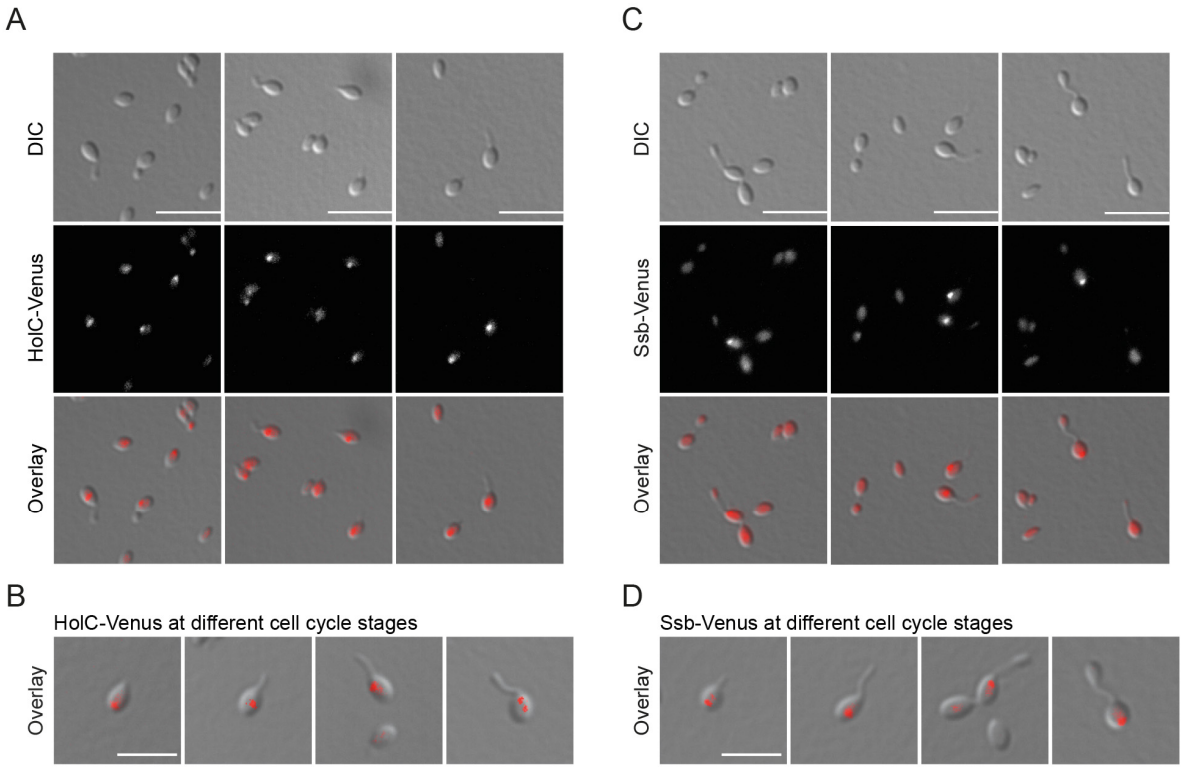

Figure 2-18: Dynamic localization of the replisome in the *H. neptunium* mother cell. A) Analysis of HolC-Venus localization. Cells of strain AJ32 (*holC::holC-venus*) were grown in MB medium and visualized by DIC and fluorescence microscopy. Bar 5 µm. B) Subcellular localization of HolC-Venus at different cell cycle stages. Micrographs are taken from the experiment described in (A). Bar 3 µm. C) Analysis of Ssb-Venus localization. Cells of strain AJ43 (P_{Zn}::P_{Zn}-*ssb-venus*) were grown in MB medium, induced with 0.5 mM $ZnSO_4$ for 4.5 h, and visualized by DIC and fluorescence microscopy. Bar 5 µm. D) Subcellular localization of Ssb-Venus at different cell cycle stages. Micrographs are taken from the experiment described in (C). Bar 3 µm.

To answer the question if chromosome replication and segregation are temporally uncoupled, we focused on two different localization patterns. First, we identified stalked or budding cells, in which ParB was segregated within the mother cell but that did not possess a replisome signal. This would indicate that replication was completed before chromosome translocation through the stalk occurred. However, due to the weak replisome signal, it was difficult to assess if there really was no replisome signal or if it was simply

too weak to detect. Moreover, we identified cells in which ParB was already transported to the daughter cell compartment but that still showed a replisome signal close to the stalked pole in the mother cell. This pattern indicates that transport of the origin region through the stalk occurred while replication was still ongoing. We detected the latter scenario only in very few cells (see Figure 2-19 right panels). In these cells, the replisome mostly localized between midcell and the stalked cell pole, where the terminus region is thought to localize. This suggests that at least a large part of the chromosome is replicated before segregation through the stalk occurs.

Overall, the replisome signals obtained with HolC or Ssb fluorescent fusions were too weak to quantify or analyze the exact timing of replication and segregation. In order to circumvent this problem and to obtain a stronger signal, we generated a DnaN-Venus fusion produced from the native *dnaN* promoter. DnaN encodes the β-sliding clamp subunit of DNA polymerase III, which positions the core polymerase onto the DNA. Fluorescently tagged DnaN was shown to give a strong signal in diverse bacteria (193, 194, 197, 198).

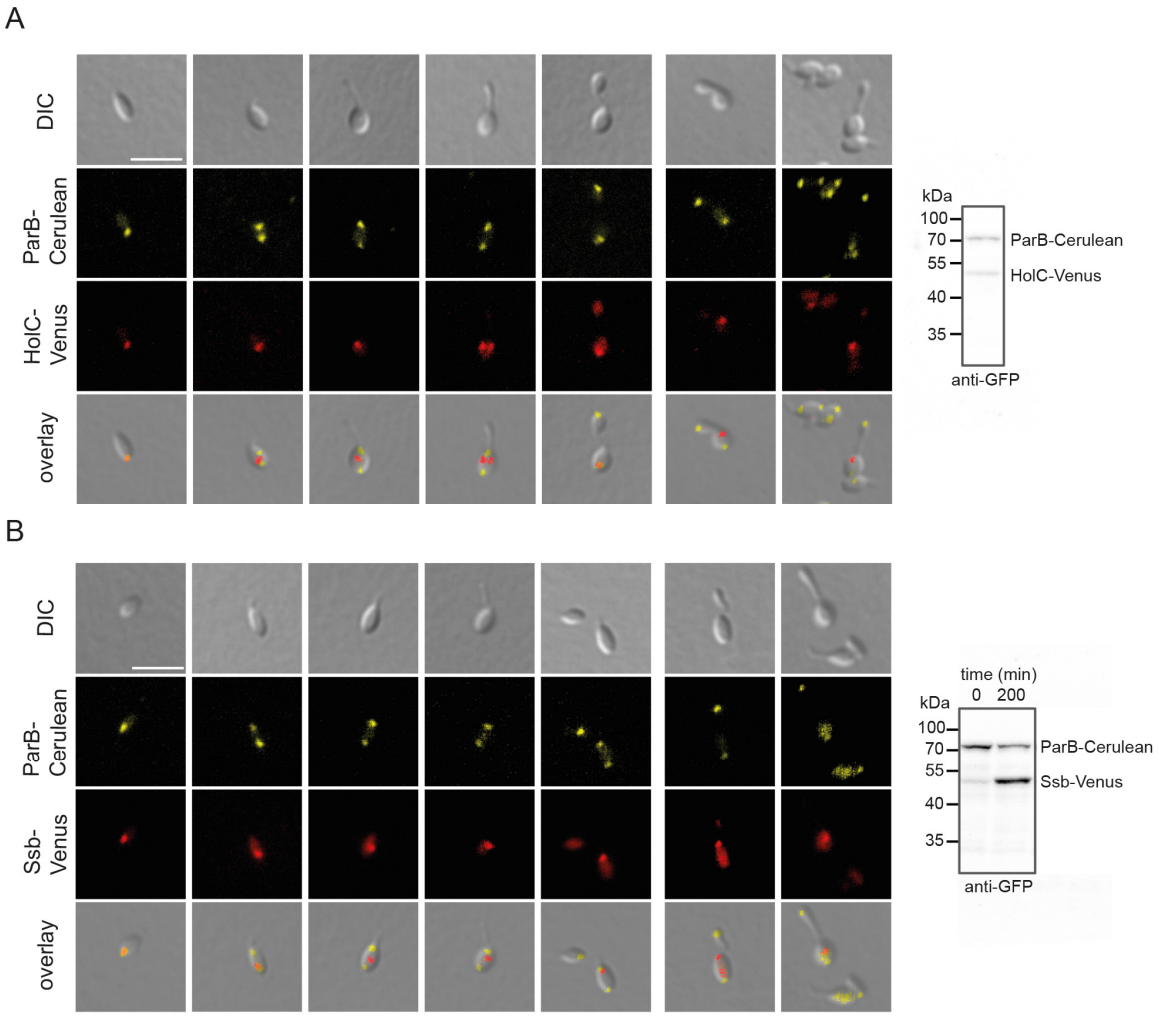

Figure 2-19: Co-localization of ParB with the replisome. A) Co-localization of ParB-Cerulean with HolC-Venus. Cells of strain AJ77 (*parB-cerulean holC::holC-venus*) were grown to exponential phase and visualized by DIC and fluorescence microscopy. HolC-Venus and ParB-Cerulean levels were analyzed by immunoblot analysis using an anti-GFP antibody (right panel). B) Co-localization of ParB-Cerulean and Ssb-Venus. Cells of strain AJ78 (*parB-cerulean* P_{Zn}::P_{Zn}-*ssb-venus*) were grown to exponential phase, induced with 0.5 mM $ZnSO_4$ for 3.5 h, and visualized by DIC and fluorescence microscopy. Ssb-Venus and ParB-Cerulean levels were analyzed by immunoblot using an anti-GFP antibody (right panel). Bar 3 µm.

Indeed, the DnaN-Venus fusion produced a strong signal in *H. neptunium* (see Figure 2-20 B). We observed that the majority (80 %) of swarmer cells or cells that were at the swarmer-to-stalked cell transition had no DnaN focus, consistent with the assumption that these cells are in G1-phase. In contrast, in the majority of stalked (87 %) and budding cells (89 %), a DnaN-Venus focus was observed, indicating that replication takes place in these cell types (see Figure 2-20 A). In budding cells with mature buds, DnaN-Venus was also detected at the pole opposite the stalk in the mother cell (instead of close to the stalked pole), marking the start of a new round of chromosome replication. Often, we also observed two DnaN-Venus foci in close proximity to each other, most likely reflecting the two independent replication forks that track along the two adjacent chromosome arms. Consistent with the localization patterns of Ssb-Venus and HolC-Venus, we also observed a dynamic localization of DnaN in the mother cell. Furthermore, many cells in which ParB was already transported through the stalk still showed a replisome signal close to the stalked pole in the mother cell (see Figure 2-20 B). This observation supports the notion that a large part of the chromosome appears to be replicated before segregation through the stalk starts, yet it also suggests that ParB is already transported through the stalk before replication is terminated.

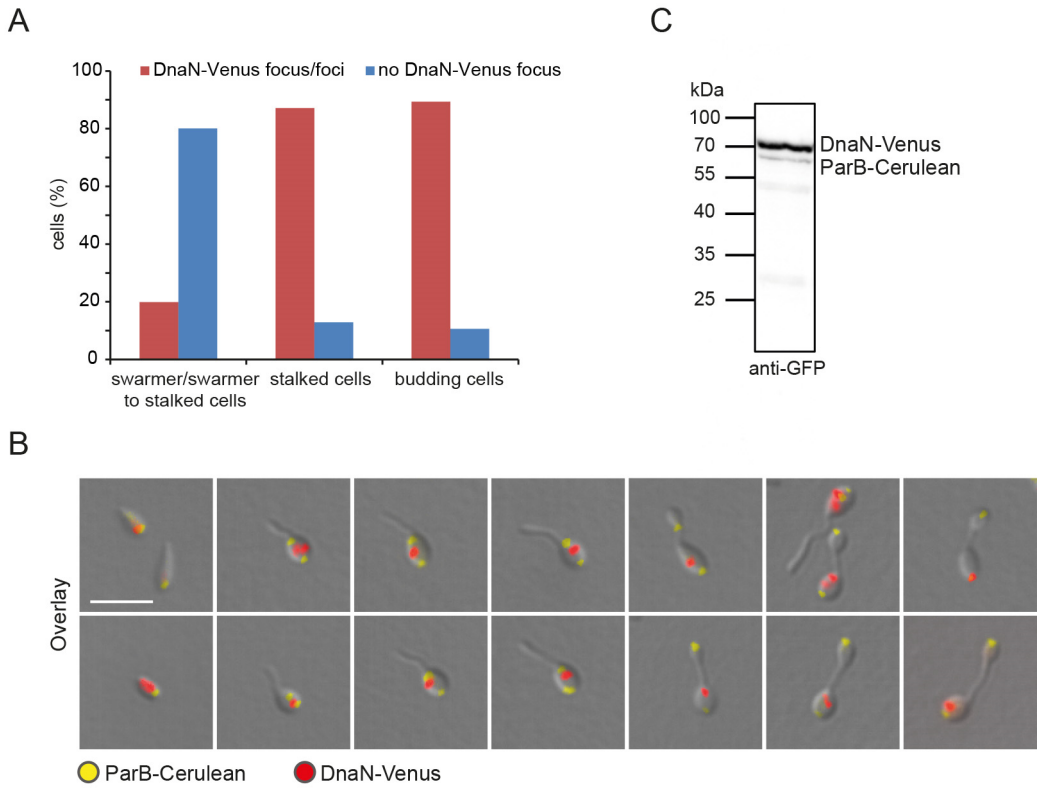

Figure 2-20: Co-localization of ParB and DnaN (replisome). A) Quantification of DnaN-Venus signal in different cell types: n= 342 (swarmer/swarmer-to-stalked cells), n= 233 (stalked cells), n= 216 (budding cells). Cells of strain AJ84 (*parB-cerulean dnaN::dnaN-venus*) were grown to exponential phase in MB and visualized by DIC and fluorescence microscopy. B) Overlays of DIC and fluorescence micrographs of samples described in A) showing cells at different cell cycle stages. Bar 3 µm. C) DnaN-Venus and ParB-Cerulean levels were analyzed by immunoblot using an anti-GFP antibody.

However, we cannot exclude a possible lag between the termination of replication and replisome disassembly. Moreover, the DnaN-Venus fusion caused morphological alterations, as reflected by elongated stalks and sometimes also elongated buds (see Figure 2-21 A). Quantification of cell length revealed an increased cell length compared to control strains, which became even more evident when quantifying cell length of long stalked, budding, and amorphous cells (see Figure 2-21 B). This indicates that the DnaN-Venus fusion might not be fully functional, which in turn could influence the timing or speed of replication and also consequently affect other cell cycle events such as budding and/or cell division. Possibly, the

dnaN-venus fusion, expressed from its native promoter, could also cause downstream effects since the entire plasmid encoding the fusion was integrated at the *dnaN* locus. Genes encoding an antibiotic biosynthesis monooxygenase domain protein (HNE_0562) and RecF, a protein implicated in DNA replication and repair in bacteria, are located ~ 100 bp downstream of *dnaN* (199, 200). However, operon prediction programs suggest that *dnaN* does not form a transcriptional unit with *HNE_0562* and *recF* (DOOR2, http://csbl.bmb.uga.edu/DOOR/ and ProOpDB, http://operons.ibt.unam.mx/OperonPredictor/), but transcriptome data of *H. neptunium* do not clearly exclude the possibility that these genes could be encoded in an operon (see 2.7 & Figure S6-2). We therefore plan to generate inducible N- and C-terminal fusions of DnaN to avoid potential downstream effects. Assuming that the C-terminal fluorescent fusion of DnaN was not fully functional, we will test the functionality of an N-terminal fusion. However, despite potential downstream effects or an adverse effect of the fluorescent label on the functionality of DnaN, there was always a subpopulation of cells showing wild-type morphology, which was used for further analysis (see below).

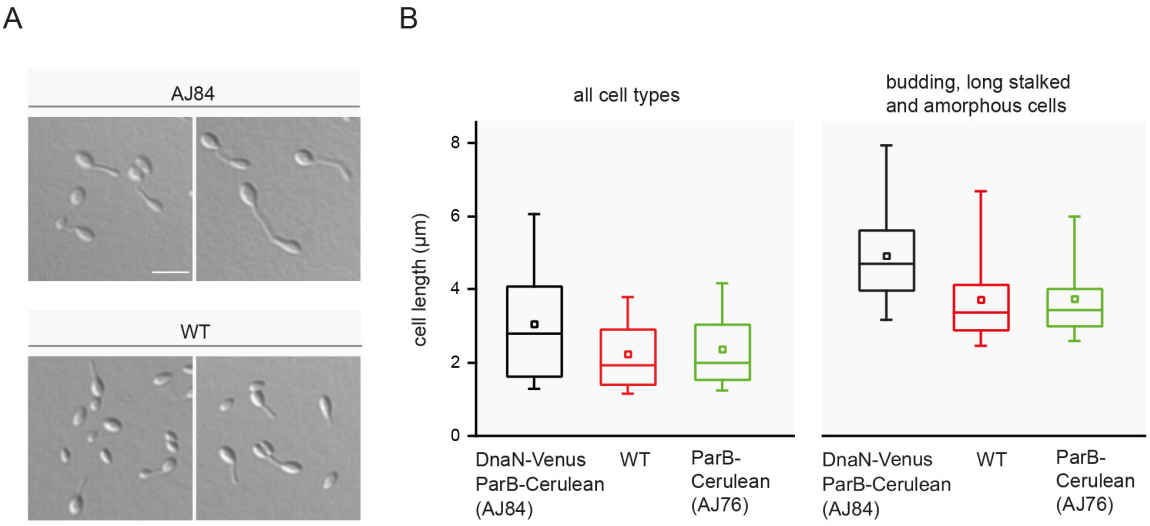

Figure 2-21: Effects of DnaN-Venus fusion on cell length. A) Example DIC micrographs of AJ84 (*parB-cerulean dnaN::dnaN-venus*) and *H. neptunium* wild type (WT) cells grown in MB to exponential phase. Bar 3 µm. B) Cells of *H. neptunium* wild type, AJ84, and AJ76 (*parB-cerulean*) were grown in MB to exponential phase and analyzed by DIC microscopy. Cell length was quantified in either all cell types (left panel) or only in budding, long stalked, and amorphous cells and is represented by box plots. The band within the box represents the median, the box boundaries indicate the 25th and the 75th percentile, and the whiskers continue to the 5th and 95th percentile of the data set. The square denotes the mean of the data. Left panel (all cell types): n= 878 (AJ84), n= 367 (WT), n= 703 (AJ76), Right panel (budding cells etc.): n= 341 (AJ84), n= 308 (WT), n=285 (AJ76).

In the next step, we intended to analyze replisome dynamics in more detail as well as the timing of origin segregation through the stalk and termination of replication. We therefore performed time-lapse microscopy at 15 min intervals of the strain in which ParB (origin) and DnaN (replisome) were fluorescently tagged. We could observe that many swarmer cells showed a diffuse DnaN-Venus signal. When the cells appeared to transit from the swarmer to the stalked stage, a DnaN-Venus focus became visible at the pole occupied by ParB-Cerulean (origin). Once the origin region was duplicated and segregated to the stalked mother cell pole, DnaN-Venus also translocated from the former flagellated pole via midcell to a region close to the stalked cell pole (see Figure 2-22). These results again confirm that the replisome shows a dynamic localization in the mother cell by following the two arms of the chromosome. Next, we followed budding cells that were about to start origin segregation through the stalk in order to analyze how long replication still continued once chromosome segregation through the stalk had initiated. In many cases, the replisome localized between midcell and the stalked cell pole when origin segregation through the stalk took place, which is also the region where the terminus is found in the cell (see Figure 2-22 B, Figure 2-15 C & F, and Figure 2-17 B). This suggests that even though replication and segregation are not com-

pletely uncoupled, a large part of the chromosome appears to be replicated before segregation through the stalk occurs. Subsequently, the replisome assembled again at the former flagellated pole in stalked cells, marking the re-initiation of replication. Most likely, cell division is just about to take place or already took place in these cells, but only became visible in the following frames (see Figure 2-22 B). The time period between ParB segregation through the stalk and disassembly of the replisome varied. In some cells it occurred within 15 minutes while in others it could take up to ≥ 45 min. However, due to the temporal resolution of only 15 min during time-lapse microscopy, it is possible the observed time periods are actually longer or shorter. As mentioned above, the DnaN-Venus fusion seems to be not fully functional, and it is possible that, for instance, the replication speed in general or the loading and/or unloading of DnaN (β-clamp) onto the DNA are impaired, which could impact the temporal coordination of chromosome replication and segregation through the stalk. Therefore, it will be of great importance to generate a fully functional fluorescently tagged DnaN. It is possible that this might reveal an even higher degree of uncoupling between chromosome replication and segregation. Furthermore, it is worth to mention that the experiments were performed on agarose pads containing 25 % instead of 100 % MB due to the strong autofluorescence of ParB-Cerulean on 100 % MB pads. Furthermore, we observed that the cells did not grow well on 100 % MB agarose pads. Currently, we cannot explain why this is the case. It will be of great importance to determine the length of cell cycle under these growth conditions (25 % MB agarose pads) and furthermore follow replisome assembly and disassembly over the whole cell cycle to identify the duration of DNA replication during the cell cycle.

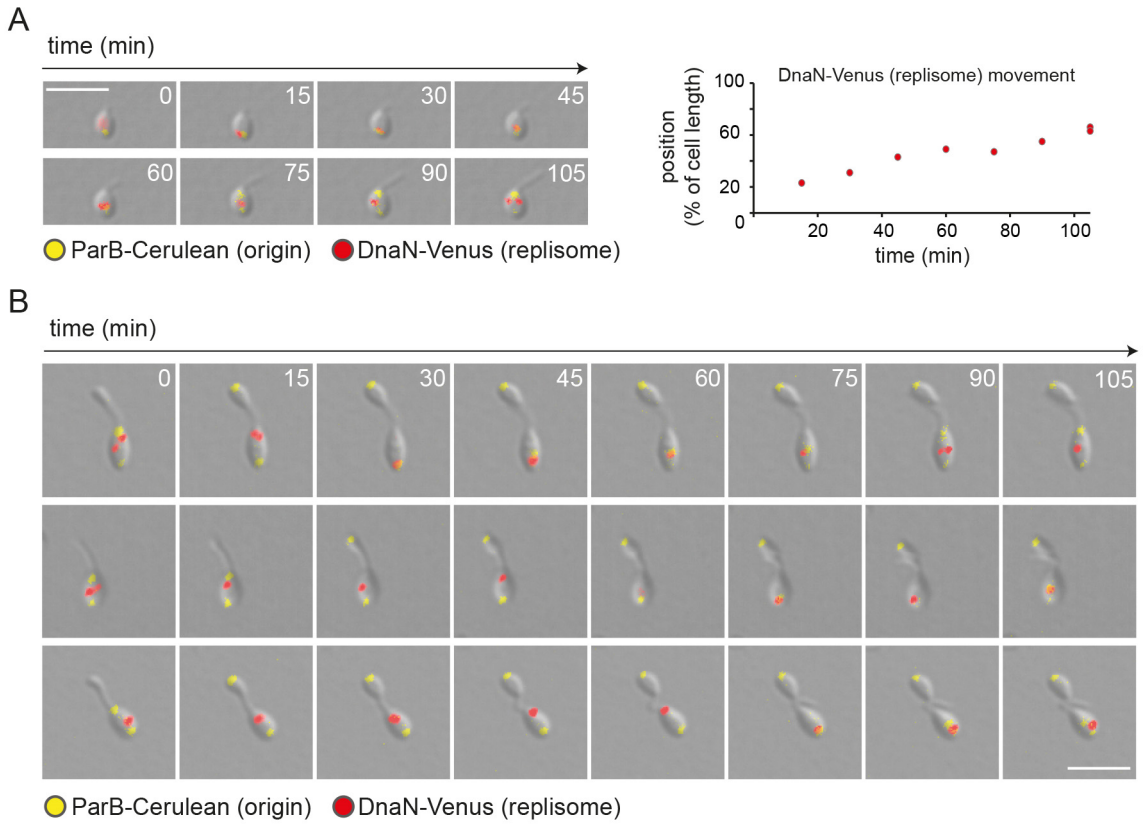

Figure 2-22: Replisome dynamics in *H. neptunium*. A) Replisome movement in the mother cell. Cells of *H. neptunium* AJ84 (*parB-cerulean dnaN::dnaN-venus*) were grown in MB medium to exponential phase, transferred to an 25 % MB agarose pad, and visualized at 15 min intervals by DIC and fluorescence microscopy. Overlays of DIC and fluorescence micrographs are shown. Bar 3 µm. Diagram on the right shows the subcellular position of DnaN-Venus over time. The (former) flagellated pole represents 0 % of cell length and the stalked pole represents 100 % of cell length. Please note that replication has not been finished at the time of analysis. B) Timing of chromosome replication and segregation through the stalk. Cells of *H. neptunium* AJ84 were analyzed by time-lapse microscopy as described in A). Overlays of DIC and fluorescence micrographs are shown. Bar 3 µm.

2.6.2 EdU labeling to mark newly replicated DNA in *H. neptunium*

In order to verify our results on the co-localization of ParB with the replisome with a different approach, we took advantage of EdU-Click labeling. This method can be used to fluorescently label newly replicated DNA in bacterial cells (201). In brief, cells are incubated with the modified thymidine analog EdU (5-ethynyl-2'-deoxyuridine), which is incorporated into the newly synthesized DNA and then labeled with a fluorescent Alexa dye in a so-called "click reaction" (Click-iT EdU Alexa Fluor Imaging Kit, Invitrogen). We first analyzed in which cell types active DNA replication takes place. We observed that the majority of swarmer cells or cells that are at the swarmer-to-stalked cell transition (92 %) had no EdU signal, whereas the majority of stalked cells (90 %) showed an EdU signal, indicating that active DNA replication takes place in this cell type. This is in agreement with the replisome localization pattern (DnaN-Venus) described above. However, for budding cells, the number of cells with or without an EdU signal was balanced (52 % and 48 %, respectively) (see Figure 2-23 A). This is different to what we observed for DnaN-Venus, where most budding cells (89 %) had a DnaN-Venus focus. In the case of EdU labeling, we only quantified the signal in 60 budding cells (compared to 216 in the case of DnaN-Venus). Interestingly, we detected many more budding cells in the strain carrying the DnaN-Venus fusion.

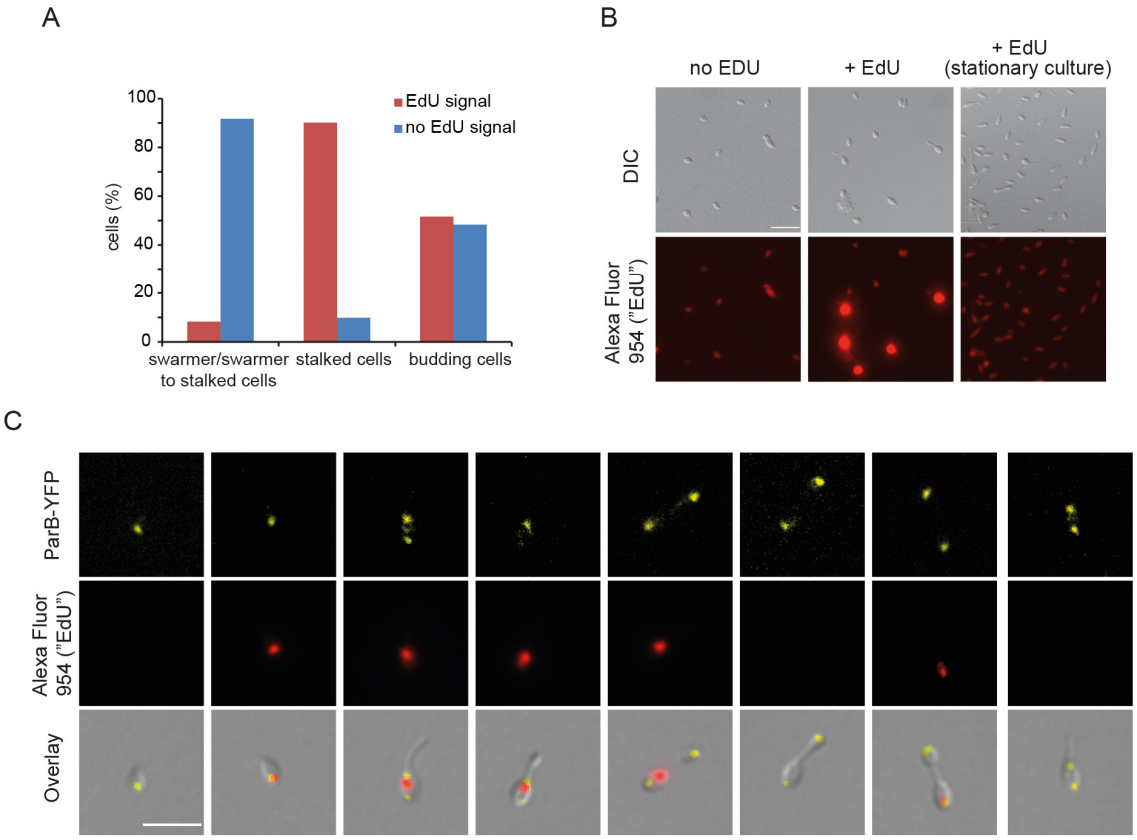

Figure 2-23: EdU-Alexa 954-Click labeling of newly replicated DNA in *H. neptunium*. A) Quantification of EdU-Alexa 954 signal in an exponentially growing cell culture: n= 314 (swarmer/ swarmer-to-stalked cells), n= 132 (stalked cells), n= 60 (budding cells). Cells of *H. neptunium* ATCC 15444 were grown in MB medium to exponential phase and treated with 0.06-0.24 mM EdU for 15 min. Subsequently, cells were fixed with methanol, click-labeled as described in (201), and visualized by DIC and fluorescence microscopy. B) Control cultures were grown to exponential (left and middle panel) or stationary phase (right panel) and treated as described in (A). Cells shown in the middle panel were fixed with ethanol instead of methanol. Bar 5 µm. C) Cells of strain KH22 (*parB-yfp*) were grown to exponential phase in MB medium and treated as described in (A) (0.12 mM EdU and fixed with ethanol). Bar 3 µm.

As mentioned above, the DnaN-Venus fusion, which might not be fully functional, caused morphological alterations such as elongated stalks. It is conceivable that besides the timing or speed of replication, other

cell cycle events such as budding and/or cell division might be altered in this strain. Hence, this could explain why we observe the different ratio of labeled and non-labeled budding cells in the two approaches (DnaN-Venus and EdU) and an increased number of budding cells in the strain carrying the DnaN-Venus fusion.
In order to verify that the observed EdU signal indeed indicated active DNA replication, we analyzed control cultures to which no EdU was added or which were in stationary phase. In both cases, we only detected a diffuse signal but no distinct EdU foci, indicating that the observed EdU foci reflect active replication (see Figure 2-23 B). We also performed EdU labeling in a strain in which ParB was tagged with YFP. We could observe that in cells that are at the swarmer-to-stalked cell transition the EdU signal co-localized with ParB. In stalked and budding cells that had an EdU signal, it was observed around midcell or close to the stalked pole of the mother cell (see Figure 2-23 C). In very few stalked cells in which ParB was already segregated within the mother cell, no EdU signal was detected. However, it requires further investigation to verify if this result is due to incomplete labeling or rather reflects an temporal uncoupling of chromosome replication and segregation through the stalk (i.e. that replication has finished before the initiation of chromosome segregation through the stalk). Moreover, we observed budding cells with fully segregated ParB and an EdU signal close to the stalked mother cell pole, suggesting that chromosome replication and segregation through the stalk are not completely temporally uncoupled. However, if this is the case is difficult to distinguish using this approach (see below). In some budding cells, we also observed re-initiation of DNA replication visible by an EdU signal at the pole opposite the stalk in the mother cell.

In summary, EdU labeling experiments confirmed the results of the replisome tagging. However, this method is not suitable to analyze the exact timing of replication and segregation, since the cells had been incubated with EdU for 15 min. This is quite a long time, considering that origin segregation through the stalk can occur within 3-4 min. Analyzing the exact timing of replication and segregation using EdU labeling would thus require a significant reduction of the incubation time of the cells with EdU. However, preliminary results show that incubation with EdU for 2-3 min is not sufficient for proper labeling.
Strikingly, we never observed two EdU foci in the mother cell or an EdU signal in the daughter cell. This would be expected upon segregation of newly replicated, labeled regions. In *C. crescentus*, BrdU labeling (a similar method to detect active DNA replication) revealed two BrdU foci in most stalked cells (38). The absence of two EdU foci in *H. neptunium* would suggest that the replicated chromosomal regions experience longer cohesion periods. However, this assumption needs further investigation.

2.7 Characterization of the transcriptome landscape of *H. neptunium*

In order to gain insight into the transcriptome landscape of *H. neptunium*, we started this side project to identify transcriptional start sites and operon structures. Additionally, these data can be helpful to identify wrongly annotated genes. Isolated total RNA of exponentially growing *H. neptunium* wild-type cells (two biological replicates) was send to Vertis (Germany) for RNA sequencing and bioinformatics analysis. The reads were mapped to the *H. neptunium* genome and can now be used for individual question. Table 2-1 shows the RPKM (Reads Per Kilobase per Million reads) values as a measure for normalized transcript abundance of the genes analyzed in this study. For instance, *smc* and *holC* have a low RPKM value (see Table 2-1) that might correlate with a low protein level. This could explain, for instance, the weak signal observed for the SMC-Venus and HolC-Venus fusions produced from their native promoters (see 2.3 & 2.6.1).

Table 2-1: RPKM values determined by RNA sequencing

Gene	RPKM 1	RPKM 2	**Mean value**
parA	246	301	**273,5**
parB	146	145	**145,5**
HNE_0708	117	115	**116**
HNE_1677 (popZ)	586	626	**606**
hup1	1559	2576	**2067,5**
hup2	1993	1023	**1507,5**
smc	51	66	**58,5**
ssb	1441	3601	**2520,5**
HNE_2272 (holC)	40	72	**56**
dnaN	472	712	**591,5**
HNE_3182	330	417	**373,5**
HNE_1048	102	95	**98,5**
HNE_3528	127	165	**146**
Lowest RPKM	0	0	0
Highest RPKM (*rplJ*)	40050	28858	34454
Mean value RPKM	331	321	326

3 Discussion

Faithful duplication and distribution of genetic material to its progeny is essential for the viability of every living cell. Until now, studies about bacterial chromosome segregation have mainly focused on a few well established model organisms that divide by binary fission (reviewed in (2)).
In this study, we analyzed chromosome organization, replication, and segregation in *H. neptunium*, which employs an unusual mechanism of reproduction. It divides by budding using its stalk as a reproductive structure (177, 178). This implies that the duplicated chromosome must transit the stalk before cell division. Several lines of evidence suggest that chromosome segregation is a two-step process and that segregation through the stalk may be driven by a novel segregation mechanism (80).

Here, we analyzed the role of the ParABS system and further proteins (PopZ, SMC, and HNE_0708) that might be implicated in chromosome segregation in *H. neptunium*. We could show that ParB binds to the two *parS* sites, which are located in close proximity to the origin region, and that the ParB/*parS* complex is the region to be at first segregated through the stalk. The ParABS system is essential in *H. neptunium* and impairment of ParA functioning resulted in morphological alterations, impaired origin segregation in the mother cell, and impaired chromosome segregation through the stalk. Localization and deletion studies of PopZ revealed that it might be involved in the positioning of the ParB/*parS* complex to the flagellated pole in the bud. However, deletion of *popZ* did not lead to severe morphological alterations. Interestingly, SMC appears to be essential under standard lab conditions, and its localization resembled in part the ParB localization pattern, consistent with observations in other bacteria that SMC is enriched and forms foci in the proximity to the origin regions (18, 97, 98, 129, 191). By analyzing the chromosome arrangement, we could show that the chromosome is arranged along the cellular long axis in non-replicative G1 cells. Moreover, we determined the spatiotemporal dynamics of chromosome replication and ParB/*parS* segregation through the stalk. The *H. neptunium* replisome showed a dynamic localization within the mother cell. It assembled at the pole opposite the stalk, possibly at the swarmer-to-stalked cell transition, and then gradually moved close to the stalked mother cell pole, where it disassembled again. Furthermore, we could show that terminus duplication occurs in the mother cell. Chromosome replication and segregation through the stalk appear to be partially temporally uncoupled. However, this observation requires further investigation in the future.

3.1 Chromosome segregation in *H. neptunium* is a two-step process

3.1.1 The role of the ParABS system in chromosome segregation within the mother cell

The majority of bacterial species sequenced to date harbor a chromosomally encoded ParABS system, which was shown to contribute to or mediate active origin segregation in several species (2, 43, 51). *H. neptunium* also encodes a ParABS partitioning system consisting of two *parS* sites in close proximity to one of the predicted origins of replication, the DNA binding protein ParB, and the ATPase ParA. In this study, we could show that ParB binds to the *parS* sites *in vitro*. The subcellular localization of ParB was already analyzed in previous studies, which showed that ParB localizes to the flagellated pole in swarmer cells. At the swarmer-to-stalked cell transition, the origin region is duplicated and one of the duplicated origins is translocated to the stalked mother cell pole. Interestingly, it remains there until the stalk and the bud are generated, and is then transported through the stalk to the newly generated bud and localized there again at the flagellated pole opposite the stalk (80, 182, 183).

Given that the generic ParABS system requires non-specific chromosomal DNA for function (58, 64, 65, 78) and taking into account that the stalk appears to be free of DNA before it is traversed by the ParB/*parS* complex, the transport of the chromosome through the stalk may be driven by a novel DNA segregation mechanism. At first, however, the chromosome and origin region, respectively, need to be segregated within the mother cell. Therefore, we analyzed how chromosome segregation within the mother cell is accomplished and determined the impact of the ParABS system in this step.

Analysis of the timing of the different segregation steps revealed that origin segregation in the mother cell took 10-55 min with an average speed of 0.05 μm/min. By comparison, in *C. crescentus*, origin segregation occurs within 10 min with an average speed of 0.27 μm/min (9). Interestingly, ParB/*parS* segregation in *M. xanthus* occurs at the same speed as in *H. neptunium* (10). Segregation in the gram-positive model organism *B. subtilis* lies in between with an average speed of 0.17 μm/min (202). Why the segregation time within the *H. neptunium* mother cell varied so much is not clear. In some cells, origin segregation occurred directedly within 10-15 min while in cells with longer segregation times ParB remained static at some point and segregation even reversed occasionally. One could speculate that segregation of the origin region does not start immediately after its replication. The replicated origins could then initially freely diffuse within the cell, and thus be detectable as two foci even before the actual segregation process has started. Interestingly, it was shown that origin translocation in *C. crescentus* occurs in distinct steps (79). At first, the origin is released from the pole and duplicated. Afterwards, one of the duplicated origins returns to the proximal pole, while the other one moves at first in a slow motion towards midcell followed by a final burst of fast motion towards the opposite cell pole (79). This final fast movement step is thought to be mediated by the ParABS segregation system (79). It is tempting to speculate that origin segregation in *H. neptunium* may occur in a similar manner and that the phase of slow motion might vary between individual cells.

Once one of the duplicated origins was segregated to the stalked mother cell pole, it "waited" there for a period of 25-105 min until a visible bud was generated. The "waiting" of the ParB/*parS* complex at the stalked mother cell pole might indicate that it is captured by a polar landmark complex. It will be of great importance to quantify the movement of the ParB focus once it reaches the stalked mother cell pole (e.g. by determination of the mean square displacement) to test this hypothesis.

In many bacteria, the ParABS partitioning system is dispensable. However, deletion of its components often leads to the formation of anucleate cells (20, 57, 87, 91, 95, 111-113, 119). Only in a few organism, it is essential for cell viability (e.g. *C. crescentus* and *M. xanthus*) (10, 66, 67, 106). Interestingly, the ParABS system also seems to be essential in *H. neptunium*. Since *parAB* could not be deleted from the genome, we tried to generate conditional mutants. We were not able to generate a conditional ParB mutant, but we succeeded in generating a conditional ParA mutant. Depletion of ParA resulted in amorphous and elongated cells, as well as impaired chromosome segregation through the stalk and the generation of DNA-free cells. Furthermore, production of a dominant negative ParA mutant (ParA K18R), which was shown to impair origin segregation in *C. crescentus* (68), resulted in incomplete origin segregation in the mother cell and impaired chromosome segregation through the stalk. Moreover, these cells showed similar morphological alterations as the ParA depletion strain. Remarkably, shortly after induction of the mutated ParA, the cells showed elongated stalks and a clubbed morphology. It appears that budding did not stop and that the buds continued to grow and extend into the stalk. These observations suggest that there may be a checkpoint linking chromosome segregation to budding and/or cell division, which in turn could explain the essentiality of the ParABS system in *H. neptunium*. Coupling of chromosome segregation with cell division (site selection) and/or cell growth has also been observed in other bacteria (10, 70, 116). For instance, in *C. crescentus*, origin segregation and cell division are tightly coordinated by the spatial regulator MipZ (70). *H. neptunium* also possesses a MipZ homolog but it does not appear to be involved in cell division or its coordination with chromosome segregation (80).

In summary, the ParABS system mediates origin segregation within the mother cell. The impairment of one component of the ParABS system, namely the ATPase ParA, resulted in morphological defects, in-

complete origin segregation within the mother cell, and consequently impaired chromosome segregation through the stalk. It is tempting to speculate that completion of the origin segregation in the mother cell might be required for the second step (transport through stalk) to start, indicating that origin segregation is a sequential process. One could envision that ParB or a stretch of DNA in the origin region is needed at the stalked mother cell pole for the second step to initiate. ParB or an origin-proximal chromosomal region could furthermore interact with a factor that is involved in or mediates the transport through the stalk. We cannot exclude the formal possibility that ParA itself is required for the transport of the origin through the stalk. However, given that the generic *parABS*-based partitioning system requires non-specific chromosomal DNA for function and that the stalk appears to be free of DNA before it is traversed by the ParB/*parS* complex, this scenario is rather unlikely (58, 64, 65, 78, 80).

The observed waiting period of the ParB/*parS* complex at the stalked mother cell pole raises the question whether the complex might be anchored at the stalked mother cell pole. Polar anchoring of origin regions has been described for different bacteria that show a longitudinal arrangement of the chromosome (74, 75, 85, 108, 115, 203, 204). These proteins oftentimes not only anchor the origin region to the cell poles, but act as pole organizing factors that additionally interact with proteins involved in diverse cellular functions. Moreover, different bacteria often employ distinct polar landmark proteins that share no homology among each other (205).
In *M. xanthus*, bactofilins are required to immobilize ParAB in the subpolar regions as well as the small GTPase SofG (108, 206). In sporulating *B. subtilis*, DivIVA anchors the origin region to the pole via an interaction with RacA, which in turn binds to the origin-proximal *ram* sites (203, 204, 207-209). In actinobacteria, DivIVA homologs were shown to be responsible for polar origin tethering as well as polar organization of the cell wall biosynthetic machinery (115, 210-212). DivIVA is a small peripheral membrane protein, which recognizes negative membrane curvature (208, 213). In *C. crescentus*, the pole organizing protein PopZ anchors the segregated origin to the new cell pole. Furthermore, PopZ is involved in capturing and regenerating monomeric ParA as well as in the recruitment of different cell cycle regulators to the pole (75-77). In *V. cholerae*, the non-polymer forming multifunctional polar hub, HubP, anchors the origin region to the cell pole via an interaction with ParA. Additionally, HubP is required for the polar recruitment of chemotaxis proteins and the flagellar apparatus (85).

H. neptunium possesses homologs of bactofilins (BacAB) and PopZ. However, both bactofilins and PopZ can be excluded as candidates to immobilize the ParB/*parS* complex at the stalked mother cell pole. PopZ does not localize to this pole but to the (former) flagellated pole, suggesting a potential function in positioning the origin region at the flagellated bud pole. The role of PopZ will be discussed in more detail in section 3.2. Moreover, bactofilins are not involved in origin segregation or positioning at the stalked mother pole, although they localize to both ends of the stalk. Even though deletion of *bacAB* results in highly asymmetric amorphous cells (E. Cserti, unpublished), ParB is segregated to the newly formed buds. Even more strikingly, ParB is still segregated to and "waits" at the junction where the new bud will be formed.

It is unclear if ParB is immobilized at the stalked mother cell pole. Since this pole is not the final destination of the ParB/*parS* complex, it is also possible that it is positioned there by the ParABS system and remains there without any anchoring until its translocation through the stalk is initiated. However, assuming that origin segregation occurs in a similar manner as proposed for *C. crescentus*, the presence of a factor that captures (monomeric) ParA would be crucial at the stalked mother cell pole. In *C. crescentus*, it was shown that the function of PopZ in capturing ParA is more important than its function in anchoring the *ori* region to the cell pole (via an interaction with ParB)(77). Defects in ParB-PopZ interaction cause "loose" tethering of the ParB/*parS* complex at the cell pole (77). In contrast, the ParA-PopZ interaction is

required for origin segregation and positioning. It was proposed that the capture of monomeric ParA by PopZ ensures the directionality of the segregation process by preventing the recovery of ParA-ATP behind the moving origin (77). In *H. neptunium*, the presence of a ParA capturing factor at this pole is further supported by the presence of a ParA focus at the stalked mother cell pole in a subpopulation of cells (80). Interestingly, in many investigated bacteria that anchor their origin at the cell pole by a polar landmark protein, this factor also, either directly or indirectly, interacts with ParA (77, 85, 108, 113). It is tempting to speculate that a factor that might capture ParA at the mother stalked pole could also anchor the ParB/*parS* region to the stalked mother cell pole and releases it upon origin segregation through the stalk.
How could such a potential landmark protein be localized (specifically) to the stalked mother cell pole? One possibility is that a geometric cue dictates its localization, such as positive membrane curvature, which can be found at this junction. Positive membrane curvature as a geometric cue was described for SpoVM of *B. subtilis*, which is involved in endospore formation, and it was also proposed as a potential mechanism to localize bactofilins in *C. crescentus* (213, 214). Another possibility could be that this potential landmark protein is inherited from the division site, like the polarity factor TipN in *C. crescentus*. TipN is essential for the correct placement of the flagellum and is involved in maintaining the directionality of origin segregation by interacting with ParA at the new cell pole (58, 78, 82, 83). It relocalizes to the division plane in predivisional cells, and it was shown that several divisome components are required for TipN localization to the division site (82, 83, 215). A similar scenario could be also envisioned for *H. neptunium*. However, the recruitment of the potential landmark protein to the division site would have to occur after translocation of ParB/*parS* through the stalk, since otherwise the ParB/*parS* complex would be also captured at the stalked bud pole, at which division occurs. Alternatively, the mechanism to recruit a potential polar landmark protein to the stalked mother cell pole could be linked to PG synthesis, since it was shown that stalk growth occurs from the stalk base (E. Cserti, unpublished). Moreover, it is conceivable that this potential polar localization factor might be also multifunctional, since both PG remodelling and divisome components are found to localize to the stalked mother cell pole (E. Cserti & S. Eisheuer, unpublished). On the other hand, it is also possible that the potential polar landmark protein that captures free ParA and might anchor the ParB/*parS* complex is not exclusively found at the stalked mother cell pole. It could also show a bipolar localization in the mother cell or a similar localization pattern like PopZ in *C. crescentus*. This would mean that it first localizes to the pole opposite the stalk and once one of the duplicated origins translocates to the stalked mother cell pole, it also accumulates there.

It is also currently not known what determines the "waiting time" of ParB at the stalked mother cell pole, and what triggers the initiation of ParB segregation though the stalk. One possibility is that ParB segregation through the stalk is coupled to the termination of chromosome replication, which would imply a temporal uncoupling of chromosome replication and segregation through the stalk. However, we could show that these two processes are not completely temporally uncoupled in *H. neptunium*, thereby excluding this possibility. Time-lapse microscopy revealed that a visible bud must be generated before ParB segregation through the stalk initiates, raising the question of whether bud size triggers chromosome segregation through the stalk. We observed that a critical minimal bud size is required for chromosome segregation through the stalk to start, since the bud was never smaller than 46 % of the mother cell width. However, there was no specific bud size at which ParB translocation occurred, since bud size varied from 46 % to 77 % of the mother cell width (0.45-0.82 μm). Nevertheless, it cannot be excluded that ParB translocation through the stalk is somehow coupled to budding (see above).
It will be of great importance to identify a potential capturing mechanism of ParA(B) at the stalked mother cell pole as well as the triggering signal for the translocation of origin region through the stalk.

3.1.2 Chromosome segregation through the stalk

It was shown that chromosome segregation within the mother cell is mediated by the ParABS partitioning system and it was further demonstrated that chromosome segregation within the mother cell and its translocation through the stalk are sequential processes. One of the most intriguing questions is how chromosome segregation through the stalk is accomplished. As described above, several lines of evidences suggest that chromosome translocation through the stalk is mediated by a novel mechanism: 1) The generic ParABS-based partitioning system requires non-specific chromosomal DNA for function, but the stalk appears to be free of DNA before it is traversed by the ParB/*parS* complex (58, 64, 65, 78, 80). This renders ParABS-mediated origin segregation through the stalk unlikely. 2) Consistently, even though ParA was detected at the tip of the stalk (before ParB) in some cells, we never observed ParA in the stalk structure (80). 3) Time-lapse analysis further showed that ParB segregation through the stalk can occur within 3-4 min, confirming that origin segregation through the stalk is rapid and directed, suggesting that chromosome segregation through the stalk is an active process.

To identify potential proteins mediating the translocation of the origin region through the stalk, we tried to identify interaction partners of ParB by pull-down analysis. The ParB/*parS* complex is the region that is at first segregated through the stalk and its presence at the stalked mother cell pole is required for chromosome segregation through the stalk. Therefore, we would assume that potential candidates that are involved in chromosome segregation through the stalk might also interact with ParB. However, pull-down analysis did not reveal any relevant ParB interaction partner. Therefore, it will be important to optimize and repeat the pull-down assay in the future.

As mentioned in 1.4.1, the DNA translocase FtsK is a potential candidate that might be involved in or even mediate chromosome segregation through the stalk. FtsK is a multifunctional protein that is widespread among bacteria. It is involved in processes such as dimer resolution, chromosome segregation, and cell division (reviewed in (160, 170, 216)). *In vivo* analyses showed that FtsK appears to localize throughout the whole stalk in *H. neptunium* instead of exclusively to the division site, as observed in other bacteria (S. Eisheuer, unpublished, (217)). Interestingly, the so-called KOPS (FtsK Orienting Polarized Sequence) sites, 8 bp conserved motifs that ensure the directionality of DNA pumping by FtsK towards the *dif* sites in the terminus region, are evenly distributed along the *H. neptunium* chromosome (80). In comparison, in *C. crescentus*, where FtsK mediates segregation of only the terminus region, the KOPS sites are enriched towards the terminus region (218). Hence, it is tempting to speculate that FtsK might pump the chromosome through the stalk. A potential role of FtsK in bulk chromosome segregation has been described for sporulating *B. subtilis*. Here, it was shown that the FtsK homolog SpoIIIE pumps ~75 % of the forespore chromosome from the mother cell into the forespore (173-175). Moreover, FtsK is essential in *H. neptunium*, and the additional production of an FtsK ATPase-deficient variant resulted in impaired chromosome segregation in a subpopulation of cells (S. Eisheuer, unpublished). The generation of an FtsK depletion strain is currently in progress and will be important for clarifying the role of FtsK in chromosome segregation in *H. neptunium*.

So far, we have only discussed chromosome segregation in *H. neptunium* as a two-step process. But what happens once the ParB/*parS* complex reaches the bud? It was observed by time-lapse microscopy that it localizes again to the pole opposite the stalk. How translocation of the ParB/*parS* complex from one pole to the other is accomplished in the bud and whether it might even represent a third step in the segregation process is currently not known and will be an interesting topic for future research. One could speculate that once part of the chromosome reaches the bud, ParA binds non-specifically to the DNA and origin segregation could then be mediated in ParABS-dependent manner. Interestingly, ParA localizes to the emerging bud in a fraction of cells, suggesting that ParA is already present in the newly generated bud

before the ParB/*parS* complex (80). As mentioned above, *H. neptunium* possesses a PopZ homolog, which localizes to the pole opposite the stalk in the bud. Its function in *H. neptunium* and a potential role in positioning of the ParB/*parS* complex at the flagellated bud pole will be discussed in the following chapter.

In the course of this study, we gained new insights into chromosome segregation in *H. neptunium*. However, there still remain many open questions: Is the ParB/*parS* complex (and also ParA) captured at the stalked mother cell pole and what determines its waiting period at this pole? What triggers the initiation of chromosome segregation through the stalk? And how is the ParB/*parS* complex traversed through the stalk and bud? To address these questions, a global approach will be required (e.g. transposon mutagenesis), which might identify for instance essential genes in *H. neptunium*. By this, new factors that are involved in chromosome segregation could be discovered.

3.2 Functional analysis of PopZ in *H. neptunium*

The cytoplasmic pole-organizing protein PopZ was first discovered in *C. crescentus* and has the ability to self-assemble into large polymeric networks in chromosome-free regions. PopZ is required to anchor the segregated origin region via an interaction with ParB to the cell pole (74, 75). It also captures monomeric ParA during origin segregation, which is required to ensure the directionality and correct positioning of the segregation machinery (77). Furthermore, it was shown to mediate the polar recruitment of several cell cycle regulators (75, 76). PopZ homologs are widely conserved among α-proteobacteria (75). However, apart from *C. crescentus*, the localization of PopZ homologs has only been investigated in the two polarly growing bacteria *Agrobacterium tumefaciens* and *Brucella abortus*. Interestingly, it was shown that PopZ exclusively localizes to the new pole (growth pole) in these organisms (219, 220).

H. neptunium also possesses a PopZ homolog and we could show that it exhibits a dynamic localization. In swarmer cells, it localizes to the flagellated pole and remains at this pole during stalk formation. At the onset of budding, it localizes to the bud at the pole opposite the stalk. In some cells, we also could detect a bipolar localization. However, the focus at the old cell pole disappears when the cell proceeds through the cell cycle. As described above, polar anchoring of origin regions appears to be a common feature of bacteria with longitudinally arranged chromosome. The observed localization pattern suggested that PopZ might position the ParB/*parS* complex at the flagellated pole in the bud after its segregation through the stalk. To test this and to further elucidate the role of PopZ in *H. neptunium*, we deleted *popZ* and analyzed ParB localization in the absence of PopZ. Deletion of *popZ* did not lead to severe morphological changes. Moreover, ParB localized normal in the majority of cells. Only 13.7 % of cells showed aberrant ParB localization in the *popZ* deletion background. This suggests that PopZ is either functionally redundant or that polar positioning of the ParB/*parS* complex in the bud might not be crucial for chromosome segregation. Similar to PopZ, ParA also localized to the emerging bud as well as to the flagellated pole in swarmer cells, indicating that PopZ might be involved in capturing free ParA. However, preliminary results showed that ParA still forms a focus in the emerging bud in the absence of PopZ, implying that another or an additional factor might capture ParA. Further investigations are required to analyze if PopZ interacts with ParA and/or ParB (e.g. analysis of interactions in a heterologous *E. coli* system that lacks ParAB and PopZ, co-localization of PopZ with ParAB, localization of $PopZ_{Hne}$ in *C. crescentus* Δ*popZ*). Moreover, the PopZ localization pattern raises the question if an additional factor might be required to capture monomeric ParA (and maybe also the ParB/*parS* complex) at the stalked mother cell pole (see above). It further suggests that the ParB/*parS* complex might not be anchored at the old mother cell pole in stalked cells, except for the first round of cell division, when the cell has to transit from a swarmer to a stalked cell. Most polar anchoring proteins analyzed to date, however, show a bipolar localization, at least before cell division, suggesting that the origin regions of the duplicated chromosomes are anchored at the

new and old cell pole, respectively (74, 75, 85, 108, 115). Interestingly, in *C. crescentus* it was shown that only the segregated origin region at the new cell pole is anchored by PopZ, while the origin region at the old cell pole remains unanchored after its release at the beginning of S-phase (76). It was suggested that anchoring of the translocating chromosome is sufficient to properly arrange the chromosome in the cell and that the bulkiness of the chromosome contributes to maintaining proper chromosome arrangement at the old cell pole. However, a transient interaction between PopZ and the released ParB/*parS* complex at the old pole could not be excluded (76).

The loss of polar landmarks that help to arrange the segregation machinery was shown to have different effects on chromosome segregation efficiency, cell morphology, and growth among bacteria in which ParAB are essential. In *M. xanthus*, the bactofilins BacNOP immobilize ParAB within the subpolar regions. Although loss of BacNOP resulted in aberrant ParAB localization and caused more compact nucleoids, their absence only led to mild chromosome segregation defects, suggesting that ParABS is still partially functional. Consistently, deletion of *bacNOP* had no effect on growth, cell length, and cell morphology (Lin *et al.*, submitted). As described above, deletion of *popZ* in *C. crescentus* resulted in aberrant ParAB localization, which in turn caused chromosome segregation and cell division defects (74, 75, 77). The latter is most likely due to the intimate coordination of chromosome segregation with cell division by the spatial regulator MipZ. Z-ring positioning in *C. crescentus* is established by a bipolar gradient of the FtsZ inhibitor MipZ, which interacts with ParB (70). In the absence of PopZ, ParB mislocalizes due to impaired origin segregation and positioning, which in turn also leads to an impaired MipZ localization that results in failure and wrong positioning of Z-ring assembly (74, 75, 77).
As mentioned above, *H. neptunium* also possesses a MipZ homolog. However, deletion of *mipZ* in *H. neptunium* did not cause any noticeable phenotype, and ParB and MipZ also showed a different localization pattern (80). This indicates that MipZ fulfills a different function in *H. neptunium*, which seems not to be essential for cell division or that MipZ is redundant. This could explain why deletion of *popZ* in *H. neptunium* has no impact on cell division. Remarkably, PopZ and MipZ showed a similar localization pattern in *H. neptunium* as well as the non-essential putative cell cycle regulators PodJ and PleD (80, 221, 222). To elucidate whether PopZ interacts with these proteins or whether it is involved in their polar recruitment will be a topic of future research.

3.3 Chromosome arrangement and dynamics

In this part of the study, we analyzed the subcellular arrangement and dynamics of the *H. neptunium* chromosome. Localization studies of seven genomic loci in non-replicative G1-like cells revealed that the chromosome is arranged along the long axis in the cell, with the origin region at the flagellated pole and the terminus region at the opposite pole. A longitudinal chromosome arrangement has been observed in many bacterial species such as *C. crescentus*, *M. xanthus*, and *V. cholerae* (9-11). Moreover, as also observed for *C. crescentus*, *M. xanthus*, and partially for *P. aeruginosa*, the subcellular localization of the different loci appears to be linearly correlated with their position on the genomic map (9, 10, 20). Analysis of chromosome dynamics of a strain, in which an origin-proximal region (357°) was labeled by FROS in addition to the ParB/*parS* complex (359°), revealed that the ParB/*parS* complex is the region to be first segregated within the mother cell and also through the stalk, emphasizing its central role in the segregation process. Interestingly, although both regions co-localized in the mother cell and bud, they are sequentially segregated through the stalk in some cells. Time-lapse analysis with shorter intervals is required to test whether the sequential segregation of these loci encoded in close proximity (21 kb) is an exception or the rule. However, labeling of the origin (359°) and an origin-distal region (51°) revealed a sequential segregation of these two loci, with the origin region being segregated first (80). Further analysis is required to determine the duration of chromosome segregation through the stalk and whether the sequential arrival of genes in

the bud might impact its development. Time-lapse analysis of the terminus region (172°) revealed that it is duplicated in the mother cell. Separation of the two terminus foci appears to occur quite late in the cell cycle, since the cells often had mature buds when two terminus foci were detected in the mother cell. This suggests that the segregation of the terminus region (through the stalk) might occur shortly before cell division, as also observed in other bacteria (72, 223, 224). We could not follow terminus segregation through the stalk due to the loss of the fluorescent signal. During time-lapse microscopy, we could observe that the terminus was duplicated and separated within the mother cell, but we never detected a terminus signal in the bud. However, the terminus signal reappeared in the newly generated daughter cells upon their progression through the cell cycle. This is possibly due to new LacI-mCherry produced by the newly generated cell, which can rebind to the *lacO* array. Interestingly, this loss of the fluorescence signal was not observed when terminus-distal regions (357° and 54°) were labeled by FROS, suggesting that the terminus region encounters different conditions than the other regions upon segregation through the stalk at this late stage in the cell cycle. It is tempting to speculate that LacI-mCherry might be, for instance, stripped off at the closing septum. This would also explain why the signal is not lost for the other FROS labeled regions, which are closer to the origin region and, hence, translocated earlier through the stalk, maybe even before divisome formation. A loss of signal of labeled terminus regions was not observed in other bacteria, in which also different regions of the chromosome were labeled (10, 20, 72, 223, 224). In *M. xanthus*, separation of the terminus regions was observed before visible constrictions are formed. For *C. crescentus* and *V. cholerae* chromosome I, it was reported that separation of the duplicated terminus regions occurs when deep constrictions are visible shortly before cell division but here the FROS signal is not lost (72, 224). One could speculate that the opening of the cell division septa at late stages of the cell cycle might differ in size between stalked budding bacteria and, for example, rod-shaped bacteria. In the future, it will be important to analyze (by e.g. short time frame time-lapse analysis) where exactly the terminus signal is lost. Is it really at the closing septum or already before, i.e. can we detect the FROS-labeled terminus region as a focus in the stalk? Alternatively, one could label different chromosomal regions that have increasing distances from the terminus and analyze whether the FROS signal is still lost upon translocation of the region through the stalk. Furthermore, it would be of great interest to determine how long chromosome segregation through the stalk generally takes. This could be done by analyzing how long a certain stretch of DNA needs for translocation through the stalk, e.g. by labeling two different regions on the chromosome. By determining the distance of the two regions and the time they need for translocation through the stalk, the average time for chromosome segregation through the stalk could be estimated.

The initial reason for analyzing chromosome dynamics by FROS instead of the $ParBS_{pMT1}$ labeling system was the apparent loss of the mCherry-$ParB_{pMT1}$ signal (focus) upon translocation of the labeled region through the stalk in most cases. We used the $ParBS_{pMT1}$ labeling system to analyze the subcellular localization of seven different genomic loci in non-replicative G1-cells (swarmer cells etc.). However, we observed that the majority of swarmer cells (especially the very small ones) did not have a mCherry-$ParB_{pMT1}$ focus. In contrast, most of the stalked and budding cells had mCherry-$ParB_{pMT1}$ focus/foci in the mother cell (but oftentimes not in the bud). This suggests that mCherry-$ParB_{pMT1}$ might be lost upon translocation of the labeled region through the stalk and that, once new mCherry-$ParB_{pMT1}$ is produced in the bud or in newly generated swarmer cell, it binds to the $parS_{pMT1}$ sites and the signal reappears. This could also explain why we could detect a signal in some swarmer cells.
The reason why we lose the mCherry-$ParB_{pMT1}$ signal upon translocation of the labeled region through the stalk is currently not known. However, it is known that ParB proteins bind to their corresponding *parS* sites and form large nucleoprotein complexes with adjacent DNA via a spreading mechanism that requires nearest-neighbor interactions and DNA bridging (52, 53, 55, 225, 226). Therefore, fluorescently labeled ParB is visible as a strong and distinct focus in the cell, even though some organisms only have a few *parS* sites in the origin region (51). Hence, one explanation for the loss of the mCherry-$ParB_{pMT1}$ signal could

be that the chromosome might change its condensation state upon translocation through the stalk, which might lead to the disturbance of the spreading and bridging capability of ParB. Consequently, this could result in the release of most ParB molecules from the complex so that the majority of released ParB proteins remain in the mother cell. Of note, an alternative model for the ParB/*parS* nucleoprotein complex formation has been recently proposed. In this model, termed "nucleation and caging model", complex formation is achieved by stochastic binding and caging of ParB proteins around ParB/*parS*-proximal DNA, thereby excluding the necessity of nearest-neighbor or bridging interactions (227). However, on the basis of this model, chromosome segregation could also result in the disturbance of the complex due to changes in the chromosome condensation/conformation state and, hence, lead to the loss of the mCherry-ParB$_{pMT1}$ signal.
Interestingly, when the labeled origin region of *H. neptunium* (i.e. ParB/*parS* complex) is segregated through the stalk the signal is not lost, suggesting that the origin region might represent a chromosomal domain that potentially does not change its condensation state upon translocation through the stalk.

Alternatively, assuming that FtsK could be involved in chromosome translocation through the stalk (see 1.4.1 & 3.1.2), one could speculate that it might strip certain proteins off the DNA, depending on their DNA binding affinity. It was shown previously that FtsK/SpoIIIE is capable of removing diverse DNA associated proteins *in vivo* and *in vitro* (228, 229). For FROS, it was described that the LacI repressor binds tightly to the *lacO* array (reviewed in (230)). Additionally, the *lacO* array is quite big (~9 kb) and contains more than 150 repeats of the operator site. Hence, the strong binding affinity of LacI for the *lacO* operator could be beneficial to keep the signal during translocation of the labeled DNA region through the stalk. As described above, the terminus region needs to be considered separately.

3.4 Coordination of chromosome replication and segregation in *H. neptunium*

In bacteria with circular chromosomes, chromosome replication starts at a single origin of replication and occurs bi-directionally along the chromosomal arms until the two replications forks meet in the terminus region. The process is mediated by a multiprotein complex called the replisome. Unlike in eukaryotes, chromosome replication and segregation occur concurrently in bacteria (1, 41).
The unique localization pattern of the ParB/*parS* complex in *H. neptunium* raised the question of whether these fundamental cellular events might be uncoupled in a way that the chromosome is first fully replicated in the mother cell before it is segregated through the stalk. We observed that ParB/*parS* complex segregation and its "waiting time" at the stalked mother cell pole took on average 88 ± 16 min. Assuming that chromosome replication occurs at the same speed as in other bacteria with non-overlapping replication cycles (~300-450 b/s), duplication of the 3.7 Mb chromosome would take ~77-88 min (10, 192-194). This would allow enough time for chromosome replication to be finished (or at least in large part) before segregation through the stalk starts.
By employing a dual reporter strain that expressed a tagged component of the replisome (HolC, Ssb or DnaN) and ParB-Cerulean (origin marker), we analyzed the temporal coupling of chromosome replication and segregation. We observed that the replisome shows a dynamic localization in the *H. neptunium* mother cell. It assembles, presumably at the swarmer-to-stalked cell transition, at the pole opposite the stalk and gradually moves through the cell to a position close to the stalked pole, where it disassembles again. This localization pattern is in agreement with the subcellular localization of the origin region at the pole opposite the stalk as well as the terminus region close to the stalked mother cell pole. After a short period, the replisome assembles again at the pole opposite the stalk in stalked cells, indicating a new round of replication initiation. Additionally, this localization pattern was confirmed by EdU labeling. Dynamic movement of the replisome from the origin region to the terminus was also observed in *E. coli*, *M. xanthus*, and *C. crescentus*, but differs from the stationary replisome observed at midcell in *P. aeruginosa* (10, 20, 36, 38).

Oftentimes, especially in the case of DnaN, we observed two replisome foci in close proximity to each other, most likely reflecting the two independent replication forks moving along the chromosomal arms. Independent movement of the two replisomes along the chromosomal arms was also observed in *E. coli*, *B. subtilis*, *M. xanthus*, and *M. smegmatis* and differs from the "moving DNA replication factory" model that was proposed for *C. crescentus* (10, 17, 36, 38, 194). Consistent with the above described localization pattern, quantification of the DnaN-Venus localization and EdU labeling revealed that DNA synthesis was absent in the majority of swarmer cells and cells that are at the swarmer-to-stalked cell transition. Only a small fraction of these cells showed a DnaN/EdU signal, suggesting that these cells just started DNA replication. Accordingly, DNA synthesis occurred in most stalked and budding cells. It is important to mention that it is oftentimes difficult to determine the exact cell type in which replication initiates, since it is possible that for instance the stalk is out of focus during image acquisition. Therefore, it is possible that cells that appear to be at the swarmer-to-stalked cell transition are in fact already at the stalked cell stage. In the future, it will be of great importance to exactly confirm in which cell type chromosome replication initiates. For instance, this could be done by using a marker for stalk growth. The histidine kinase PleC may be a suitable candidate, since it localizes to the flagellated pole in swarmer cells but switches to the stalked pole at the onset of stalk formation, and localizes to the tip of the stalk during stalk growth (221).

Analysis of the spatiotemporal dynamics of chromosome replication and segregation revealed that these two processes appear to be partially temporally uncoupled in *H. neptunium*. Time-lapse analysis showed that replication was still ongoing at the time the ParB/*parS* complex was segregated through the stalk. However, in many cases the replisome localized between midcell and the stalked pole (i.e. probably close to the terminus region), suggesting that a large part of the chromosome is replicated before segregation through the stalk initiates. The period between ParB segregation through the stalk and the disassembly of the replisome varied. In some cases it occurred within 15 min, but it could also take up to 45 min. However, the temporal resolution of 15 min during time-lapse microscopy does not allow an exact determination of the period. Therefore, we would like perform time-lapse microscopy with higher temporal resolution in the future. Generally, these timing experiments need to be considered with caution, considering that the DnaN-Venus fusion used in this study appears to be either not fully functional or might cause downstream effects (see 2.6.1). Many cells of the strain harboring the *dnaN-venus* fusion expressed from its native promoter showed morphological alterations, as reflected by elongated stalks and sometimes also elongated buds. Even though we focused on cells during time-lapse analysis that showed an morphology similar to wild type, we cannot exclude the possibility that the Venus tag negatively influences the function of the protein. DnaN encodes the β-sliding clamp, which is required to promote the processivity of the DNA polymerase and to recruit proteins involved in DNA repair, replication, and recombination (197, 231, 232). Hence, impairment of DnaN might alter the overall speed of DNA synthesis. Generation of a functional DnaN fusion construct that does not cause morphological alterations will be of great importance and might unravel an even higher degree of uncoupling of chromosome replication and segregation. Additionally, we cannot exclude that a gap exists between the end of replication and DnaN-Venus unloading from the DNA. However, a recent study in *E. coli*, which combined *in vivo* studies with simulations, showed that unloading of the β_2-sliding clamp presumably occurs within only 5 min (233).

HolC-Venus ("native" fusion) and Ssb-Venus (inducible fusion) were not suitable to analyze the timing of chromosome replication and segregation, since the fluorescent signals were too weak and thus rendered a quantitative or time-lapse analysis impossible. In the case of the inducible Ssb-Venus fusion, this was probably due to a mixture of tagged and untagged proteins in the replisome complex. In the case of HolC-Venus, transcriptome analysis revealed that *holC* has a low expression level that might correlate with a low protein level explaining the weak signal (see Table 2-1).

Generally, the partial uncoupling of chromosome replication in the mother cell and segregation through the stalk is reasonable in many ways. First of all, chromosome replication is initiated and one of the duplicated origins is already segregated to the stalked mother cell pole before a visible bud is generated. Segregation of the chromosome through the stalk before the daughter compartment is formed would possibly be detrimental for the cell. Furthermore, it has recently been discovered in bacteria that, in the course DNA double strand break repair by homologous recombination, an active search by the damaged DNA locus for the intact counterpart of the replicated chromosome occurs (234, 235). Assuming that this is also the case in *H. neptunium*, a (partial) temporal uncoupling of chromosome replication and segregation through the stalk would greatly facilitate this active search upon DNA double strand break repair. It is difficult to imagine that this active search would still occur once the duplicated chromosome has been segregated through the stalk. It is tempting to speculate that partial temporal uncoupling of chromosome replication and segregation might represent a common feature of stalked budding bacteria. However, this assumption requires further investigation in the future.

3.5 Potential sister chromosome cohesion within the mother cell

As mentioned above, unlike in eukaryotes, chromosome replication and segregation normally occur simultaneously in bacteria. Segregation can either occur immediately after replication, or replicated regions are sometimes held together for a certain time, a phenomenon called sister chromosome cohesion. However, the observed cohesion times mostly represent only a fraction of the S-phase (reviewed in (41)).
So far, we have only focused on the coordination of chromosome replication and segregation through the stalk. But what about the coupling of these two processes within the mother cell? Are duplicated sister regions immediately segregated within the mother cell (before segregation through the stalk) or do they experience longer cohesion times?
Strikingly, upon EdU labeling for 15 min in *H. neptunium*, we never observed cells with two EdU foci. However, this would be expected upon rapid segregation of newly replicated regions. In comparison, BrdU labeling for 15 min in *C. crescentus* revealed two BrdU foci in most stalked cells (38). Consistently, a very short gap of 2-4 min was observed between origin replication and the initiation of segregation in *C. crescentus* (72). The absence of two EdU foci in *H. neptunium* might indicate that duplicated sister loci experience longer cohesion times. To test this hypothesis, we would like to repeat the EdU labeling with longer incubation times and with *C. crescentus* as a control. By performing short interval time-lapse microscopy with the dual reporter strain in which DnaN and ParB are labeled, we can furthermore analyze how long the separation of the duplicated region takes after passage of the replication fork. Additionally, the chromosomal region labeled at 54° by FROS was not frequently observed to be segregated within the mother cell after replication. However, this is only a first observation and requires further validation and quantification in the future. By contrast, the duplicated origin and origin-proximal regions were at first segregated within the mother cell before the initiation of the second segregation step (through the stalk).
Taking into account the above observations, it is conceivable that chromosomal sister loci in *H. neptunium* might experience longer cohesion times. Consequently, only the origin and origin-proximal regions would be segregated within the mother cell (to the stalked cell pole) before segregation through the stalk starts, suggesting that chromosome replication and segregation are, to some degree, already temporally uncoupled within the mother cell. A close proximity of sister loci within the mother cell would most likely facilitate DNA double strand break repair by homologous recombination.
Prolonged sister cohesion of certain chromosomal loci other than the terminus has been only described for *E. coli* and *H. pylori* so far (134, 135, 236, 237). In *E. coli*, a protein called SeqA promotes extended cohesion of sister loci for ~ 10 min or even up to 20-30 min for some loci. The late-splitting sister loci, called snaps, have been shown to be required for efficient chromosome segregation (46, 134). It will be highly interesting to investigate in the future whether chromosome replication and segregation occur con-

currently or if sister loci experience extended cohesion periods within the *H. neptunium* mother cell and how this could contribute to efficient chromosome segregation.

3.6 Concluding remarks and future perspectives

In this work, we analyzed chromosome arrangement, replication, and segregation in the stalked budding bacterium *H. neptunium*. Like in most bacteria analyzed to date, the chromosome shows a longitudinal arrangement within the cell, with the ParB/*parS* complex ("origin") at the flagellated pole and the terminus at the opposite pole. It was shown previously that the chromosome is segregated in a two-step process in *H. neptunium* (80). At first, the duplicated ParB/*parS* complex is segregated within the mother cell to the stalked pole and remains there until the stalk and the bud are generated. Subsequently, the chromosome is segregated through the stalk and the ParB/*parS* complex localizes to the flagellated pole in the bud (see Figure 3-1) (80). We could show that the ParABS system is essential for origin segregation within the mother cell and cell viability. Chromosome segregation within the mother cell and through the stalk is sequential and the ParB/*parS* complex seems to be the region that is at first segregated through the stalk. However, several lines of evidence suggest that the ParABS system is not directly involved in chromosome segregation through the stalk and that this process is driven by a novel segregation mechanism.
We also showed in this study that the replisome exhibits a dynamic localization within the mother cell. It assembles, most likely at the swarmer-to-stalked cell transition, close to the former flagellated pole and gradually moves close to the stalked pole, where it disassembles again (see Figure 3-1). Microscopic analyzes suggest that chromosome replication and segregation through the stalk are partially temporally uncoupled. Furthermore, future research is required to analyze the temporal coordination of these two processes within the mother cell in order to elucidate whether they occur simultaneously or whether some of the duplicated sister loci might not be immediately segregated within the mother cell but experience longer cohesion times before segregation through the stalk.

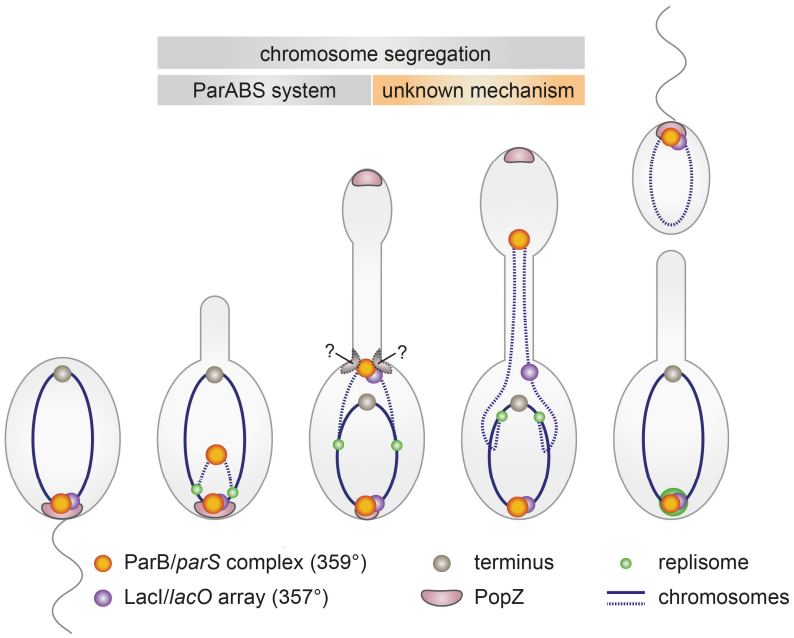

Figure 3-1: Model of chromosome arrangement and dynamics in *H. neptunium*. The *H. neptunium* chromosome is segregated in a two-step process (80). The model illustrates the chromosome arrangement and dynamics at different cell cycle stages. Grey protein with question mark depicts a potential ParB/*parS*-anchoring factor and/or ParA-capturing factor. Please refer to discussion for detailed description.

Analyses of PopZ revealed that it is to some extent involved in correct positioning of the origin region in the bud (see Figure 3-1). However, it might be partially redundant. It will be highly interesting to expand

our knowledge about the role of PopZ in *H. neptunium* and to identify whether other proteins are required for origin anchoring and/or ParA capturing at the flagellated bud pole. Assuming that origin segregation, mediated by the ParABS system, functions as proposed for *C. crescentus*, a ParA capturing factor might be required at the stalked mother cell pole (see Figure 3-1).

Unravelling the mechanism of chromosome segregation through the stalk in *H. neptunium* might identify a novel mode of chromosome segregation in bacteria. This would not only expand our understanding of how chromosome segregation is accomplished in stalked budding bacteria, but also illustrate the diversity of this crucial process in prokaryotes in order to adapt to the specific needs of the respective organism. Overall, the identification of the mechanism that mediates chromosome segregation in *H. neptunium* and its spatiotemporal coupling with cell division, budding, and other cell cycle events will greatly expand our knowledge about prokaryotic cell biology.

4 Material and Methods

4.1 Materials

4.1.1 Chemicals

All chemicals used in this study were obtained from Ambion (USA), Becton Dickinson (USA), Bioline (Germany), Carl-Roth (Germany), Difco (Spain), Fermentas (Germany), GE Healthcare (Germany), Invitrogen (Germany), Life Technologies (Germany), Merck (Germany), PerkinElmer (USA), peqlab (USA), Promega (USA), Sigma-Aldrich (Germany), Thermo Scientific (USA) or Qiagen (Germany).

4.1.2 Enzymes

Enzymes were obtained from New England Biolabs (NEB, USA) or Fermentas (Germany). KOD Hot Start Polymerase (Merck, Germany) or BioMix™Red (Bioline, Germany) were used for PCR reactions.

4.1.3 PCR primers

Oligonucleotides used in this study were synthesized by Eurofins MWG-Operon (Germany) or Sigma-Aldrich (Germany) and are listed in Table 6-4 (see appendix).

4.1.4 Plasmids and bacterial strains

All strains and plasmids used and generated in this study are listed in Table 6-1 and Table 6-2 (see appendix).

4.1.5 Kits

Table 4-1: Kits used in this study

Kit	Application
GenElute™ Gel Extraction Kit (Sigma, USA)	Elution of DNA from agarose gels
GenElute™ PCR Clean–Up Kit (Sigma,USA)	Purification of DNA
GenElute™ Plasmid Miniprep Kit (Sigma, USA)	Plasmid isolation
Western Lightening™ Chemiluminescence Reagent Plus kit (PerkinElmer, USA)	Detection of chemiluminescence
Turbo DNA-free Kit (Ambion, USA)	DNase digestion
Illustra bacteria genomicPrep Mini Spin Kit (GE Healthcare, Germany)	Isolation of chromosomal DNA
Roti®-Nanoquant (Carl-Roth, Germany)	Determination of protein concentrations
Click.iT® Plus EdU Imaging Kit (Molecular Probes, Germany)	*In vivo* labeling of newly synthesized DNA

4.1.6 Buffers and solutions

Standard buffers and solutions were prepared as described by Ausubel and Sambrook (238, 239). Special buffers and solutions are listed in the respective method section. All buffers were prepared with de-ionized water (Purelab Ultra water purification system, Elga).

4.1.7 Media

Complex media for *E. coli:*

LB (Luria-Bertani) medium (240):	Tryptone	10 g/L
	Yeast extract	5 g/L
	NaCl	10 g/L

All components were dissolved in de-ionized water. For preparation of LB agar plates, 1.5 % agar was added.

Complex medium for *H. neptunium*

MB (Marine Broth) medium:	Bacto peptone	5.00 g/L
	Bacto yeast extract	1.00 g/L
	Fe(III) citrate	0.10 g/L
	NaCl	19.45 g/L
	$MgCl_2$ (dried)	5.90 g/L
	Na_2SO_4	3.24 g/L
	$CaCl_2$	1.80 g/L
	KCl	0.55 g/L
	Na_2CO_3	0.16 g/L
	KBr	0.08 g/L
	$SrCl_2$	34.00 mg/L
	H_3BO_3	22.00 mg/L
	Na-silicate	4.00 mg/L
	NaF	2.40 mg/L
	$(NH_4)NO_3$	1.60 mg/L
	Na_2HPO_4	8.00 mg/L

All components were dissolved in de-ionized water and boiled for 1 min before autoclaving. Afterwards, the medium was filter-sterilized to remove the precipitate. For preparation of MB agar plates, 2 % agar was added

4.2 Microbiological , cell biological, and genetic methods

4.2.1 Cultivation of bacteria

Cultivation of *H. neptunium* ATCC 15444

H. neptunium ATCC15444 and its derivatives were grown in MB medium at 28°C under aerobic conditions (shaking at 210 rpm) in baffled flasks or on MB-agar plates. Media were supplemented with antibiotics

when appropriate: rifampicin was added to final concentrations of 2 μg/ml (agar plates) and 1 μg/ml (liquid media), and kanamycin was added to final concentrations of 200 μg/ml (agar plates) and 100 μg/ml (liquid media).

Cultivation of *E. coli*

E. coli was cultivated in LB medium (shaking at 210 rpm) or on LB-agar plates at 37°C. Kanamycin, rifampicin, and ampicillin, respectively, were added to the media when working with mutant strains. Kanamycin was added to final concentrations of 30 μg/ml (liquid media) and 50 μg/ml (agar plates). Rifampicin was added to final concentrations of 25 μg/ml (liquid media) and 50 μg/ml (agar plates). Ampicllin was added to final concentrations of 50 μg/ml (liquid media) and 200 μg/ml (agar plates).

4.2.2 Determination of the optical density of bacterial cultures

The optical density (OD) of bacterial cultures was determined photometrically by using an Ultrospec™ 10 Cell Density Meter or an Ultrospec™ 2100 pro UV/Visible spectrophotometer (GE Healthcare, Germany) at a wavelength of 600 nm. The corresponding culture medium was used as a blank.

4.2.3 Generation of growth curves and determination of doubling times of *H. neptunium*

To assess the growth of *H. neptunium* over time, cells were grown in MB to exponential phase and diluted to an OD_{600} of 0.05 in a 24-well plate (Becton Dickinson Labware, USA). Growth was then monitored at 31-33°C (shaking) in an EPOCH 2 microplate reader (BioTek, USA) for 26-30 h at a wavelength of 580 nm. Doubling times were calculated by fitting the linear part of the resulting growth curves (logarithmic scale) to a suitable model employing the Solver function of Microsoft Excel 2007 (241). A logarithmic plot was generated and the slope was determined to calculate the doubling time (doubling time =ln (2)/slope).

4.2.4 Quantification of *H. neptunium* biofilm formation

To quantify biofilm formation in *H. neptunium*, the biofilm was stained with crystal violet after growth assay in a 24-well plate (see above). To this end, 70 μl of a 0.5 % (w/v) crystal violet solution was added to each well and incubated for 10 min at room temperature. The liquid was then carefully removed and each well was washed twice with 1 ml ddH_2O. Subsequently, 1 ml 100 % (v/v) ethanol was added to each well and incubated at room temperature for 10 min. The absorbance of crystal violet was then measured at 580 nm in an EPOCH 2 microplate reader (BioTek, USA).

4.2.5 Preparation of Cryo-stocks

Permanent cultures for storage at -80°C (cryo-stocks) were prepared by adding 10 % DMSO to a bacterial culture with an OD_{600} of 0.8-1.0.

4.2.6 Preparation of competent *E. coli* cells

To generate chemically competent *E. coli* TOP10 cells, 10 ml LB medium was inoculated from an *E. coli* TOP10 cryo-stock and incubated at 37°C overnight. 250 ml LB medium were inoculated with 2.5 ml of

this pre-culture and incubated at 37°C until the cultures reached an OD_{600} of 0.6. The cells were transferred to pre-cooled GSA tubes, incubated on ice for 10 min, and harvested by centrifugation using a Sorvall GS3 rotor (Thermo Fisher, USA) at 3000 x g and 4°C for 10 min. The supernatant was discarded. The pellet was resuspended in 15 ml ice-cold 0.1 M $CaCl_2$ solution and transferred in pre-cooled SS34 tubes. Samples were then incubated on ice for 30 min and cells were collected by centrifugation with an SS34 rotor (Thermo Fisher, USA) at 3000 x g and 4°C for 10 min. Afterwards, the pellet was carefully resuspended in 4 ml pre-cooled 0.1 M $CaCl_2$ containing 15 % glycerol. Aliquots of 150 µl were transferred to Eppendorf tubes, snap-frozen in liquid nitrogen, and stored at -80°C.
For the generation of competent *E. coli* WM3064 cells, 300 µM diaminopimelic acid (DAP) was added to the LB medium.

4.2.7 Transformation of *E. coli*

E. coli TOP10

A 150 µl-aliquot of chemically competent *E. coli* TOP10 cells was thawed on ice and 10 µl (~100 ng/µl) of plasmid DNA were added. The mixture was kept on ice for 30 min. The cells were then heat-shocked at 42°C for 45 sec and incubated again on ice for 2 min. Subsequently, 500 µl LB medium were added, and the cells were incubated for 1 h at 37°C. 250 µl of the cell suspension was then spread onto an LB agar plate containing the corresponding antibiotic. The agar plate was then incubated at 37°C overnight.

E. coli WM3064

Competent *E. coli* WM3064 cells were thawed on ice and 5 µl plasmid DNA were added. The mixture was kept on ice for 30 min. The cells were then heat-shocked at 42°C for 90 sec. Afterwards, 500 µl LB medium supplemented with 300 µM DAP were added, and the cells were incubated for 1 h at 37°C. 400 µl of the cell suspension were then spread onto an LB agar plate containing the corresponding antibiotic and 300 µM DAP. The agar plates were then incubated at 37°C overnight.

E. coli Rosetta™ (DE3)pLysS

Competent *E. coli* Rosetta™ (DE3)pLysS were purchased from Merck Millipore (Germany). 100 µl of cells were mixed with 4 µl plasmid DNA and incubated on ice for 30 min. The cells were then heat-shocked at 42°C for 45 sec. Afterwards, 700 µl SOC medium were added and the cells were incubated for 1 h at 37°C. 250 µl of the cell suspension was then spread onto an LB agar plate containing 200 µg/ml ampicillin and 0.5 % glucose, and incubated at 37°C overnight.

4.2.8 Conjugation of *H. neptunium*

After transformation of *E. coli* WM3064 (donor strain) with the plasmid of interest, cells were grown to stationary phase in liquid LB medium supplemented with antibiotic and 300 µM DAP. *H. neptunium* (recipient strain) was grown to stationary phase in MB medium for two days. Afterwards, 1 ml of the *E. coli* WM3064 culture and 2 ml of the *H. neptunium* culture were harvested by centrifugation for 2 min at 7600 x g. Cell pellets were washed with MB medium (2 min, 7600 x g) and resuspended in 100 µl MB medium supplemented with 300 µM DAP. Both aliquots were mixed and spotted on an MB agar plate supplemented with 300 µM DAP. The cells were incubated overnight at 28°C, scraped from the MB agar plate, washed twice in 1 ml MB medium (without DAP) (2 min, 4600 x g), and finally resuspended in 1 ml MB medium. 200 µl of the cell suspension were plated on MB agar plates supplemented with the respective antibiotic and grown for at least five days at 28°C.

4.2.9 Synchronization of *H. neptunium*

In order to enrich an *H. neptunium* culture for swarmer cells, the culture was vacuum-filtered using nitrocellulose filter membranes with two different pore sizes (183, 242). Filtration equipment consisted of a vacuum filtering flask, a glass filter holder assembly with funnel, fritted base, stopper, support screen and clamp, and was assembled according to manufacturer's instructions (Millipore, Germany). During the course of the synchronization procedure, cells were constantly kept on ice and all equipment and buffers were pre-cooled to 4°C.
For synchronization, a culture of *H. neptunium* was diluted into 300 ml fresh MB medium and grown overnight to an OD_{600} of 0.6. Cells were then harvested by centrifugation (15 min, 3000 x g, 4°C) and resuspended in 100 ml 1x PBS. In a first filtration step, cells were filtered using a 1.2 µm nitrocellulose filter membrane (Millipore, Germany) and collected. Subsequently, a second filtration step was performed using a 0.8 µm nitrocellulose filter membrane (Millipore, Germany) and the cell suspension enriched for swarmer cells was harvested by centrifugation (15 min, 3000 x g, 4°C). The cell pellet was resuspended in 20 ml pre-warmed MB medium and growth was continued for 15 min at 28°C. Afterwards, cultures were pelleted by centrifugation (15 min, 3000 x g, 4°C), snap-frozen in liquid nitrogen, and stored at -80°C until further use.

10x PBS buffer: 1.4 M NaCl, 27 mM KCl, 100 mM Na_2HPO_4, 18 mM KH_2PO_4 (pH 7.4)

4.2.10 Flow cytometry

To analyze cell length and DNA content of a population, flow cytometry was performed at the SYNMIKRO Flow Cytometry Facility (Marburg). To this end, *H. neptunium* cells were grown to mid-exponential phase and the OD_{600} was adjusted to 0.1-0.2. DNA was then stained with 10 µM Vybrant® DyeCycle™ Orange (Invitrogen, Germany) at 28°C and 300 rpm for 25 min. Samples were analyzed using a BD Fortessa Flow Cytometer (excitation laser 488 nm and Blue 530/30 band pass filter, BD Biosciences). Flow cytometry data was acquired with FACSDiva™ 8.0 (BD Biosciences) and analyzed using FlowJo V10 (FlowJo LLC).

4.2.11 Microscopy and image processing

For DIC, phase contrast, and fluorescence microscopy, cells were immobilized on 1 % agarose pads. Microscopy was performed using a Zeiss Axio Imager.Z1 microscope (Zeiss, Germany) equipped with a Plan-Apochromat 100x/1.40 Oil DIC objective and a Plan-Apochromat 100x/1.40 Oil Ph3 M27 objective. Immersol® 518F was used as immersion oil. An X-Cite® 120 PC lamp (EXFO, Canada) was used for fluorescence microscopy in combination with ET-DAPI, ET-CFP, ET-YFP or ET-TexasRed filter cubes (Chroma, USA). Pictures were taken with a pco.edge sCMOS camera, recorded with VisiView 2.1.4 (Visitron, Germany), and processed with MetaMorph 7.7 (Universal Imaging, USA) and Adobe® Illustrator® (USA).

Time-lapse microscopy
To analyze bacterial growth and subcellular protein localization over time, cells were immobilized on 1 % agarose MB pads and the cover slide was sealed with VLAP (1:1:1 vaseline, lanolin, and paraffin) to prevent dehydration. In order to keep a constant temperature of 28°C, the microscope was additionally equipped with a climate chamber (Incubator XL-4). Pictures were taken at indicated time points.

DAPI staining

In order to stain the nucleoid of *H. neptunium*, the cell suspension was incubated with 4 µg/ml DAPI (4',6-diamidino-2-phenylindole) at 28°C and 400 rpm for 20 min. Samples were then analyzed by DIC and fluorescence microscopy.

EdU-Click labeling of newly synthesized DNA

In order to label newly synthesized DNA *in vivo*, EdU-Click labeling was performed as described previously by Ferullo *et al.* (201), using the Click-iT EdU Alexa Fluor Imaging Kit (Life Technologies, Germany). In brief, cells are incubated with the modified thymidine analog EdU (5-ethynyl-2'-deoxyuridine), which is incorporated in newly synthesized DNA and then labeled with a fluorescent Alexa dye in a so-called "click reaction". To this end, an exponentially growing culture was incubated with 0.06-0.24 mM EdU and incubated at 37°C and 28°C, respectively, for 5-15 min. The reaction was stopped by adding ethanol or methanol to a final concentration of 89 %. Cells were harvested by centrifugation (5000 x g, 4°C, 5 min) and washed two times with 1x PBS. The cell pellet was then resuspended in 200 µl Click-it reaction cocktail per 1 ml cell culture (see manufacturer's instructions) and incubated at room temperature for 30 min. Afterwards, the pellet was washed, resuspended in 1x PBS, and samples were analyzed by DIC and fluorescence microscopy.

Generation of demographs

For demographic representation of data, fluorescence intensity profiles were first generated with ImageJ (http://imagej.nih.gov/ij). Data were then processed and demographs were generated using R version 3.1.1 employing the Cell profiles script (https://github.com/ta-cameron/cell-profiles) (243).

4.3 Molecular biological techniques

4.3.1 Polymerase chain reaction (PCR) for cloning

To amplify template DNA for cloning purposes, KOD Hot Start DNA Polymerase (Merck, Germany) was used. All components (see Table 4-2) were mixed and subjected to the respective PCR program (see Table 4-3) in a thermo cycler. PCR products were purified using the PCR Clean-Up Kit (Sigma, USA).

Table 4-2: Composition of KOD PCR mix (100 µl)

Component	Volume
10x KOD Hot Start Polymerase buffer	10 µl
dNTPs (2 mM each)	10 µl
$MgSO_4$ (25 mM)	4 µl
DMSO	5 µl
forward primer (100 µM)	0.5 µl
reverse primer (100 µM)	0.5 µl
KOD Hot Start DNA Polymerase (1U/µl)	2 µl
template DNA	2 µl
H_2O	66 µl

Table 4-3: PCR cycle with KOD polymerase

Step	Temperature in °C	Duration in min
1. Initial denaturation	95	2
2. Denaturation	95	0.5
3. Primer annealing	depending on primer (standard 65)	0.5
4. Elongation	72	0.5 per 1 kb
Repetition of steps 2-4 for 25-30 cycles		
5. Final elongation	72	2x elongation time (step 4)
6. Pause	4	

4.3.2 Colony PCR

To perform PCR analyses on bacterial cells, a colony was picked and transferred to a 20 µl PCR reaction mixture. When using *H. neptunium* cells for colony PCR, the picked cells were first lysed in 50 µl ddH_2O for 10 min at 95°C, and 2 µl of the supernatant were used as template for the PCR reaction. BioMix Red™ (Bioline, Germany) was used for the colony PCR reactions. All components (see Table 4-4) were mixed and subjected to the respective PCR program (see Table 4-5) in a thermo cycler. PCR products were purified using the PCR Clean Up Kit (Sigma, USA).

Table 4-4: Composition of Colony PCR mixture (20 µl)

Component	Volume
BioMix Red™	10 µl
DMSO	2 µl
forward primer (100 µM)	0.1 µl
reverse primer (100 µM)	0.1 µl
template	2 µl
H_2O	5.8 µl

Table 4-5: Colony PCR Cycle

Step	Temperature in °C	Duration in min
1. Initial denaturation	95	4
2. Denaturation	95	0.5
3. Primer annealing	depending on primer (standard 65)	0.5
4. Elongation	72	0.5 per 1 kb
Repetition of steps 2-4 for 25-30 cycles		
5. Final elongation	72	2x elongation time (step 4)
6. Pause	4	

4.3.3 Determination of quantity and purity of nucleic acids

The concentration of DNA or RNA was measured with the NanoDrop® ND-1000 spectrophotometer. 1 µl of the nucleic acid solution was transferred to the NanoDrop, and the absorption was measured from

220-350 nm. Purity was determined by the 260 nm/280 nm ratio. A ratio of ~2 reflected a pure nucleic acid solution without protein contamination.

4.3.4 Agarose gel electrophoresis

Agarose gel electrophoresis was applied to separate DNA fragments according to their size, using 1 % (w/v) agarose gels. Agarose was dissolved in 0.5x TAE buffer and ethidium bromide was added (50 µl/L). Gels were immersed in 0.5x TAE running buffer and run at a constant voltage of 160 V. GeneRuler™ 1 kb ladder (Fermentas, Canada) was used as a size marker. PCR products obtained with BioMix Red™ were loaded directly onto the agarose gel. Other DNA samples were mixed with 6x DNA loading dye solution (Fermentas, Canada) prior to loading.

50x TAE buffer	242 g Tris, 57.1 ml glacial acetic acid, 18.6 g EDTA, adjusted to 1 L with deionized water

4.3.5 Digestion of DNA with restriction enzymes

Digestion of DNA was performed following the manufacturer's instructions using selected restriction enzymes (Fermentas, Canada; NEB, USA). BSA was only supplemented when using NEB restriction enzymes. Samples were incubated at 37°C for 1-12 h.

Table 4-6: Sample composition of restriction digests

Component	Digestion of vector DNA	Digestion of insert
10 x buffer	10 µl	10 µl
10 mg/ml BSA (NEB, USA)	1 µl	1 µl
template DNA	15 µl	50 µl
restriction enzyme(s)	0.5-1 µl each	0.5-1.5 µl each
FastAP (Thermo Scientific, USA)	2 µl	-
H_2O	ad 100 µl	ad 100 µl

After the restriction digest, the samples were purified using the PCR Clean-up Kit (Sigma, USA).

4.3.6 Ligation of linear DNA fragments into plasmid vectors

Ligation reactions were performed at room temperature for 30-60 min. T4 DNA Ligase (Fermentas, Canada) was used following the manufacturer's instructions.

Table 4-7: Ligation reaction mixture (20 µl)

5x Rapid Ligation Buffer (Fermentas, Canada)	4 µl
Plasmid DNA	1 µl
Insert DNA	3 µl
T4 DNA Ligase (5 U/µl) (Fermentas, Canada)	0.5 µl
H_2O	ad 20 µl

4.3.7 Construction of plasmids

All plasmids used in *H. neptunium* were first amplified in *E. coli* TOP10 cells. Colony PCR was performed to verify the presence of the insert. After plasmid preparation with the Plasmid Miniprep Kit (Sigma, USA), the plasmids were sent to Eurofins (Germany) for sequencing. The company's instructions for preparing DNA sequence samples were followed. The results were analyzed with Vector NTI Advance™ (Invitrogen, Germany) or Snapgene (GSL Biotech, USA).

4.3.8 Generation of markerless deletions or insertion mutants of *H. neptunium*

In-frame deletions were generated by double homologous recombination using the pNPTS138 suicide vector (M. R. K. Alley, unpublished) leaving 30-36 bp of the 5´and 3´end of the target gene in the genome. To this end, 500-1000 bp long flanks up- and downstream of the target region were cloned into the pNPTS138 vector. Derivatives of the pNPTS138 plasmid were used to transform *H. neptunium* by conjugation. Cells were plated on MB agar plates supplemented with kanamycin, which serves as the selection marker for the 1st homologous recombination. 16 clones were tested for the successful integration of the plasmid at one of the two flanks. Positive clones were inoculated in plain MB medium and grown to stationary phase (2nd homologous recombination). Subsequently, cells were plated in a 1:200 dilution on MB plates supplemented with 3 % sucrose to select for the 2nd homologous recombination event. Single colonies that arose from the 2nd homologous recombination were re-streaked in parallel on MB-kanamycin and MB-sucrose plates to check for kanamycin sensitive and sucrose resistant clones. Since the 2nd homologous recombination gives rise to either *H. neptunium* deletion mutants or wild type, deletion of the target region was verified by colony PCR.
In order to replace a gene with an allele encoding a C-terminal fluorescent protein fusion, a construct encoding a C-terminal fluorescent protein fusion was at first generated. Additionally, a 500 bp long downstream flanking region of the target gene was amplified and cloned together with the allele encoding the C-terminal fluorescent protein fusion in the pNPTS138 vector. Derivatives of the pNPTS138 plasmid were used to transform *H. neptunium* by conjugation and generation of markerless insertion mutants was carried out as described above.

4.3.9 Extraction of total RNA from *H. neptunium* for RNA-sequencing

Prior to RNA extraction, *H. neptunium* ATCC 15444 was grown in MB medium to exponential phase and 12.5 ml of the cell culture were mixed with 1.5 ml stop solution (95 % pure ethanol, 5 % phenol for RNA extraction), aliquoted, and cells were harvested by centrifugation (9300 x g, 10 min, 4°C). Subsequently, samples were frozen in liquid nitrogen and stored at -80°C until further use.
RNA was isolated using peqGold TriFast™ (Peqlab, Germany). To this end, cell pellets were thawed on ice and resuspended in 1 ml peqGold TriFast™ reagent (Peqlab, Germany) per 1 x 10^7 bacterial cells. Cells were lysed by repetitive up and down pipetting and incubation at 65°C for 10 min. Afterwards, RNA was extracted according to manufacturer's instructions (peqGold TriFast™, Peqlab, Germany) and subsequently dissolved in 50 µl of diethyl pyrocarbonate (DEPC)-treated water (Roth, Germany) Contaminating DNA was digested using the Turbo DNA-free Kit (Ambion). Additionally, RNasin (Promega) was added to inhibit RNases. The quality and quantity of RNA was determined by agarose gel electrophoresis and spectrophotometrically by NanoDrop measurements.

4.3.10 RNA sequencing

In order to gain insight into the transcriptome landscape of *H. neptunium*, RNA sequencing of exponentially growing wild-type cells was performed. Total RNA of two biological replicates was isolated and sent to Vertis (Germany) for further analysis. Library preparation, RNA sequencing, and bioinformatics analyses were performed by Vertis. In brief, rRNA was depleted from total RNA using the Ribo-Zero rRNA Removal Kit (Bacteria, Epicentre), random-primed cDNA libraries were generated, and Illumina HiSeq 2000 sequencing was performed (50 bp read length). Subsequently, bioinformatics analysis was performed and the reads were mapped to the *H. neptunium* genome and analyzed using the CLC Sequence Viewer (CLC bio). Furthermore, RPKM (Reads Per Kilobase per Million reads) were calculated as a measure for normalized transcript abundance.

4.4 Biochemical methods

4.4.1 SDS polyacrylamide gel electrophoresis (SDS-PAGE) of proteins

Protein samples were separated by SDS-PAGE as described by Laemmli (244). To this end, an 11 % resolving gel and a stacking gel were prepared, which had the following composition:

11 % Resolving gel:	1.9 ml de-ionized water, 1.25 ml 4x resolving gel buffer, 1.9 ml 30 % acrylamide, 40 µl 10 % APS, 3 µl TEMED
Stacking gel:	1.43 ml de-ionized water, 625 µl 4x stacking gel buffer, 417 µl 30 % acrylamide, 25 µl 10 % APS, 1.9 µl TEMED

To prepare samples for SDS-PAGE, bacterial cells were pelleted (9400 x g, 5 min), resuspended in 2x SDS sample buffer (100 µl per 1 OD_{600} unit), and incubated at 95°C for 10 min. Protein samples were then loaded onto the gel along with a molecular mass standard (PageRuler™ Prestained Protein ladder; Fermentas, Canada). Gels were run in 1x SDS electrophoresis buffer at a constant current of 30 mA per gel in Peqlab gel electrophoresis chambers (PerfectBlue™ Twin S system, Peqlab, USA). To visualize proteins separated by SDS-PAGE, they were stained with either Coomassie solution overnight or with Instant*Blue*™ (Expedeon, United Kingdom) for 60 min and destained with water.

2x SDS sample buffer:	0.125 M Tris base, 20 % (v/v) glycerol, 2 % (w/v) SDS, 200 mM DTT, 0.001 % (w/v) bromphenol blue, adjusted to pH 6.8 with 1 M HCl
10x SDS electrophoresis buffer:	0.25 M Tris base, 1.92 M glycine, 1 % (w/v) SDS
4x Stacking gel buffer:	0.5 M Tris base, 0.4 % (w/v) SDS, pH 6.8 (adjusted with 1M HCl)
4x Resolving gel buffer:	1.5 M Tris base, 0.4 % (w/v) SDS, pH 8.8 (adjusted with 1 M HCl)
Coomassie solution:	0.17 M H_3PO_4, 0.95 M NH_4Cl, 1.17 mM Coomassie Brilliant Blue G250

4.4.2 Immunodetection of proteins

After the separation of protein samples by SDS-PAGE, proteins were transferred onto PVDF membranes (Immobilon, Merck Millipore, Germany) for immunodetection. Western blotting was performed using the PerfectBlue™ semi-dry or tank electroblotter (Peqlab, USA). Please note, the tank electroblotter was used when proteins had a molecular weight > 150 kDa. The membrane was soaked in methanol for 15 sec, shortly washed in de-ionized water, and then equilibrated in Western transfer buffer (WTB) with 10 % methanol for 10 min. Blotting papers were equilibrated in WTB with 10 % methanol for 10-15 min, and stacked with the gel and membrane according to manufacturer's instructions. Blots were run at 2 mA/cm² membrane for 1.5 h (semi-dry blot) or 250 mA for 1 h 40 min (tank blot).

Subsequently, the membrane was blocked with 5 % (w/v) milk powder in Tris-Buffered Saline Tween-20 (TBST) buffer overnight. The next day, the membrane was incubated in primary antibody solution (consisting of 5 % milk-TBST and antibody in adequate dilution) for 1.5 h. Membranes were washed three times for 5-10 min in TBST before incubation with the secondary antibody solution (second antibody conjugated with horseradish peroxidase (HRP)) for another 1.5 h. The final wash lasted 25-50 min with five changes of TBST buffer. Afterwards, immuno complexes were visualized using the Western Lightening™ Chemiluminescence Reagent Plus kit (PerkinElmer, USA) according to the manufacturer's instructions. Chemiluniscence was detected on Amersham Hyperfilm ECL films (GE Healthcare, Germany) or with a ChemiDoc MP imaging system (Bio-Rad).

10x Western transfer buffer:	0.25 Tris base, 1.92 M glycine
10x TBST:	100 mM Tris, 1.5 M NaCl, adjusted to pH 7.5; 1 % (w/w) Tween 20

Table 4-8: Antibodies used in this study

Antibody	Dilution
anti-GFP (Sigma-Aldrich, Germany)	1:10 000
anti-mCherry (BioVision, USA)	1:10 000
anti-RFP (245)	1:10 000
HRP-labeld anti-rabbit IgG (goat) (PerkinElmer, USA)	1:20 000

4.4.3 Protein purification

In order to purify ParB (HNE_3560)-His_6, *E. coli* Rosetta™ (DE3)pLysS (Invitrogen) was transformed with pAJ40 and grown in LB supplemented with ampicillin (50 µg/ml) and chloramphenicol (20 µg/ml) to an OD_{600} of 1. ParB-His_6 production was induced with 0.5 mM IPTG and cells were harvested (4500 x g, 10 min, 4°C) after 3 h incubation at 37°C. Pellets were then washed twice with buffer B2 (4500 x g, 10 min, 4°C) and snap-frozen in liquid nitrogen.
Histidine-tagged ParB was purified by immobilized metal ion affinity chromatography with a HisTrap HP 5 ml column (GE Healthcare, Germany) using the ÄKTApurifier 10 system (GE Healthcare, Germany). To this end, cell pellets were resuspended in 10 ml Buffer B3 per 1 g cell pellet supplemented with 25 µg/ml DNaseI, 100 µg/ml PMSF (phenylmethyl sulfonyl fluoride) and 20 µg/ml lysozyme., and further lysed by two passages through a French press (16 000 psi). The cell suspension was then first centrifuged for 20 min at 4000 x g, followed by an ultracentrifugation step at 160 000 x g for 1 h (4°C) to remove cell debris. The supernatant was then loaded on a 5 ml HisTrap HP column (Ni sepharose). The column was equilibrated and washed with buffer B3, and the protein was eluted using a linear imidazole gradient (20 mM-400 mM imidazole, buffer B3-B4). Fractions containing the protein of interest were pooled and diluted 1:3 with buffer A to decrease the NaCl concentration of the sample. In order to in-

crease the purity of the eluted protein, anion exchange chromatography was performed. A 1 ml HiTrap Q FF column (GE Healthcare, Germany) was equilibrated and washed with buffer A and the protein was eluted using a linear NaCl gradient (0-1 M NaCl, buffer A-B). Fractions containing the protein were then dialyzed against buffer B6. The purified protein was aliquoted, snap-frozen in liquid nitrogen, and stored at -80°C.
Protein concentrations were determined spectrophotometrically by modified Bradford assay using Roti®-Nanoquant (Carl Roth, Germany) according to manufacturer´s instructions (246).

Buffer B2: 50 mM NaH_2PO_4, 300 mM NaCl, 10 mM imidazole; pH 8.0 (with NaOH)
Buffer B3: 50 mM HEPES, 150 mM NaCl, 20 mM imidazole; pH 8.0 (with NaOH)
Buffer B4: 50 mM HEPES, 150 mM NaCl, 400 mM imidazole; pH 8.0 (with NaOH)

Buffer A: 50 mM HEPES/NaOH, pH 8.0
Buffer B: 50 mM HEPES/NaOH, pH 8.0, 1 M NaCl

Buffer B6: 50 mM HEPES/NaOH, pH 7.2, 50 mM NaCl, 5 mM $MgCl_2$, 0.1 mM EDTA, 10 % Glycerol

4.4.4 Electrophoretic mobility shift assay (EMSA)

The ability of ParB-His_6 to bind to predicted *parS* sites was analyzed by an electrophoretic mobility shift assay (EMSA). 0.01 µM Cy3-labeled oligonucleotides containing either the wild-type (tgtttcacgtgaaaca) or a mutated *parS* (tgcctcacgtgaaaca) sequence were incubated with 0.05 µg/µl poly (dI-dC) (Sigma Aldrich, Germany) and varying ParB concentrations (0-0.6 µM) in buffer B6 (see 4.4.3, dialysis buffer used for protein purification) for 30 min at 28°C. 20 µl samples were mixed with 6x DNA loading dye (Fermentas, Germany) and loaded on a 6 % non-denaturing polyacrylamide gel, which was run for 50 min (120 V, 4°C) in 1x TBE buffer. Signals were detected with a Typhoon 8600 imager (GE Healthcare).

6 % Acrylamid gel: 1.5 ml 40 % Acrylamid/Bisacrylamid (19:1), 1 ml 10x TBE, 7.415 ml ddH_2O, 74 µl 10 % APS, 11 µl TEMED

10x TBE buffer: 1 M Tris base, 1 M Boric acid, 0.02 M EDTA

4.4.5 Pull-down assay

Pull-down assay was performed with ParB-His_6 as bait coupled to magnetic beads (His Mag Sepharose Ni, GE Healthcare, Germany). To this end, *H. neptunium* ATCC 15444 was grown in MB medium (250 ml) to exponential phase and cells were harvested by centrifugation at 6500 rpm for 10 min. Subsequently, the pellet was washed twice with buffer B3 (see 4.4.3) and snap-frozen in liquid nitrogen. To prepare cell lysates, cells were thawed on ice, resuspended in 5 ml buffer B3-1 supplemented with one tablet protease inhibitor without EDTA (Roche, Switzerland), 0.025 mg/ml DNaseI, and 0.02 mg/ml lysozyme, and further lysed by three passages through a French press (16 000 psi). The cell suspension was then first centrifuged for 10 min at 4000 x g followed by an ultracentrifugation step at 160 000 x g for 1 h (4°C) to remove cell debris. ParB-His_6 was coupled to the magnetic beads according to manufacturer's instructions. After the indicated washing steps with buffer B3-2, the cell lysate was incubated with ParB-His_6 coupled to the magnetic beads for 1.5 h at 4°C. Samples were washed thrice with buffer B3-2, and coupled proteins were eluted from the beads with 100 µl pull-down elution buffer. Subsequently, eluted proteins were

visualized by SDS-PAGE and were further analyzed by ESI mass spectrometry analysis at the Proteomics Facility (S. Baumeister, Biology department, Philipps-Universität, Marburg).

Buffer B3-1:	50 mM HEPES (pH 7.45), 150 mM NaCl, 20 mM imidazole (pH 8), 0.02 % Tween-20, 10 % Glycerol
Buffer B3-2:	50 mM HEPES (pH 7.45), 150 mM NaCl, 20 mM imidazole (pH 8), 0.02 % Tween-20,
Pull-down elution buffer:	50 mM HEPES (pH 7.45), 150 mM NaCl, 400 mM imidazole (pH 8),

4.5 Bioinformatics tools

All DNA and protein sequences were obtained from the NCBI (http://www.ncbi.nlm.nih.gov/) and JCVI CMR (http://cmr.jcvi.org/cgi-bin/CMR/CmrHomePage.cgi) databases. The molecular masses of proteins were calculated using the "Compute pI/Mw" tool (http://www.expasy.ch/tools/pi_tool.html).
Protein primary sequence alignments were generated with COBALT (http://www.ncbi.nlm.nih.gov/tools/cobalt/cobalt.cgi?LINK_LOC=BlastHomeLink) and edited with GeneDoc (247). Conserved domain prediction analyses were performed with SMART (http://smart.embl-heidelberg.de/). Box plots were generated using QTI plot (http://www.qtiplot.com/).

5 References

1. **Reyes-Lamothe R, Nicolas E, Sherratt DJ.** 2012. Chromosome replication and segregation in bacteria. Annu Rev Genet **46:**121-143.
2. **Badrinarayanan A, Le TB, Laub MT.** 2015. Bacterial chromosome organization and segregation. Annu Rev Cell Dev Biol **31:**171-199.
3. **Nolivos S, Sherratt D.** 2014. The bacterial chromosome: architecture and action of bacterial SMC and SMC-like complexes. FEMS Microbiol Rev **38:**380-392.
4. **Burmann F, Gruber S.** 2015. SMC condensin: promoting cohesion of replicon arms. Nat Struct Mol Biol **22:**653-655.
5. **Wilhelm L, Burmann F, Minnen A, Shin HC, Toseland CP, Oh BH, Gruber S.** 2015. SMC condensin entraps chromosomal DNA by an ATP hydrolysis dependent loading mechanism in *Bacillus subtilis*. Elife **4**.
6. **Wang X, Rudner DZ.** 2014. Spatial organization of bacterial chromosomes. Curr Opin Microbiol **22:**66-72.
7. **Wang X, Liu X, Possoz C, Sherratt DJ.** 2006. The two *Escherichia coli* chromosome arms locate to separate cell halves. Genes Dev **20:**1727-1731.
8. **Nielsen HJ, Ottesen JR, Youngren B, Austin SJ, Hansen FG.** 2006. The *Escherichia coli* chromosome is organized with the left and right chromosome arms in separate cell halves. Mol Microbiol **62:**331-338.
9. **Viollier PH, Thanbichler M, McGrath PT, West L, Meewan M, McAdams HH, Shapiro L.** 2004. Rapid and sequential movement of individual chromosomal loci to specific subcellular locations during bacterial DNA replication. Proc Natl Acad Sci U S A **101:**9257-9262.
10. **Harms A, Treuner-Lange A, Schumacher D, Sogaard-Andersen L.** 2013. Tracking of chromosome and replisome dynamics in *Myxococcus xanthus* reveals a novel chromosome arrangement. PLoS Genet **9:**e1003802.
11. **David A, Demarre G, Muresan L, Paly E, Barre FX, Possoz C.** 2014. The two cis-acting sites, *parS*1 and *oriC*1, contribute to the longitudinal organisation of *Vibrio cholerae* chromosome I. PLoS Genet **10:**e1004448.
12. **Youngren B, Nielsen HJ, Jun S, Austin S.** 2014. The multifork *Escherichia coli* chromosome is a self-duplicating and self-segregating thermodynamic ring polymer. Genes Dev **28:**71-84.
13. **Kleckner N, Fisher JK, Stouf M, White MA, Bates D, Witz G.** 2014. The bacterial nucleoid: nature, dynamics and sister segregation. Curr Opin Microbiol **22:**127-137.
14. **Glaser P, Sharpe ME, Raether B, Perego M, Ohlsen K, Errington J.** 1997. Dynamic, mitotic-like behavior of a bacterial protein required for accurate chromosome partitioning. Genes Dev **11:**1160-1168.

15. **Lin DC, Levin PA, Grossman AD.** 1997. Bipolar localization of a chromosome partition protein in *Bacillus subtilis*. Proc Natl Acad Sci U S A **94:**4721-4726.

16. **Webb CD, Teleman A, Gordon S, Straight A, Belmont A, Lin DC, Grossman AD, Wright A, Losick R.** 1997. Bipolar localization of the replication origin regions of chromosomes in vegetative and sporulating cells of *B. subtilis*. Cell **88:**667-674.

17. **Wang X, Montero Llopis P, Rudner DZ.** 2014. *Bacillus subtilis* chromosome organization o scillates between two distinct patterns. Proc Natl Acad Sci U S A **111:**12877-12882.

18. **Danilova O, Reyes-Lamothe R, Pinskaya M, Sherratt D, Possoz C.** 2007. MukB colocalizes with the *oriC* region and is required for organization of the two *Escherichia coli* chromosome arms into separate cell halves. Mol Microbiol **65:**1485-1492.

19. **Niki H, Yamaichi Y, Hiraga S.** 2000. Dynamic organization of chromosomal DNA in *Escherichia coli*. Genes Dev **14:**212-223.

20. **Vallet-Gely I, Boccard F.** 2013. Chromosomal organization and segregation in *Pseudomonas aeruginosa*. PLoS Genet **9:**e1003492.

21. **Jain IH, Vijayan V, O'Shea EK.** 2012. Spatial ordering of chromosomes enhances the fidelity of chromosome partitioning in cyanobacteria. Proc Natl Acad Sci U S A **109:**13638-13643.

22. **Valens M, Penaud S, Rossignol M, Cornet F, Boccard F.** 2004. Macrodomain organization of the *Escherichia coli* chromosome. EMBO J **23:**4330-4341.

23. **Mercier R, Petit MA, Schbath S, Robin S, El Karoui M, Boccard F, Espeli O.** 2008. The MatP/*matS* site-specific system organizes the terminus region of the *E. coli* chromosome into a macrodomain. Cell **135:**475-485.

24. **Dupaigne P, Tonthat NK, Espeli O, Whitfill T, Boccard F, Schumacher MA.** 2012. Molecular basis for a protein-mediated DNA-bridging mechanism that functions in condensation of the *E. coli* chromosome. Mol Cell **48:**560-571.

25. **Le TB, Imakaev MV, Mirny LA, Laub MT.** 2013. High-resolution mapping of the spatial organization of a bacterial chromosome. Science **342:**731-734.

26. **Wang X, Le TB, Lajoie BR, Dekker J, Laub MT, Rudner DZ.** 2015. Condensin promotes the juxtaposition of DNA flanking its loading site in *Bacillus subtilis*. Genes Dev **29:**1661-1675.

27. **Marbouty M, Le Gall A, Cattoni DI, Cournac A, Koh A, Fiche JB, Mozziconacci J, Murray H, Koszul R, Nollmann M.** 2015. Condensin- and replication-mediated bacterial chromosome folding and origin condensation revealed by Hi-C and super-resolution imaging. Mol Cell **59:**588-602.

28. **Postow L, Hardy CD, Arsuaga J, Cozzarelli NR.** 2004. Topological domain structure of the *Escherichia coli* chromosome. Genes Dev **18:**1766-1779.

29. **Wang X, Montero Llopis P, Rudner DZ.** 2013. Organization and segregation of bacterial chromosomes. Nat Rev Genet **14:**191-203.

30. **Stein RA, Deng S, Higgins NP.** 2005. Measuring chromosome dynamics on different time scales using resolvases with varying half-lives. Mol Microbiol **56:**1049-1061.
31. **Ptacin JL, Shapiro L.** 2013. Chromosome architecture is a key element of bacterial cellular organization. Cell Microbiol **15:**45-52.
32. **Magnan D, Bates D.** 2015. Regulation of DNA replication initiation by chromosome structure. J Bacteriol **197:**3370-3377.
33. **Mott ML, Berger JM.** 2007. DNA replication initiation: mechanisms and regulation in bacteria. Nat Rev Microbiol **5:**343-354.
34. **Donczew R, Zakrzewska-Czerwinska J, Zawilak-Pawlik A.** 2014. Beyond DnaA: the role of DNA topology and DNA methylation in bacterial replication initiation. J Mol Biol.
35. **Beattie TR, Reyes-Lamothe R.** 2015. A Replisome's journey through the bacterial chromosome. Front Microbiol **6:**562.
36. **Reyes-Lamothe R, Possoz C, Danilova O, Sherratt DJ.** 2008. Independent positioning and action of *Escherichia coli* replisomes in live cells. Cell **133:**90-102.
37. **Duderstadt KE, Reyes-Lamothe R, van Oijen AM, Sherratt DJ.** 2014. Replication-fork dynamics. Cold Spring Harb Perspect Biol **6**.
38. **Jensen RB, Wang SC, Shapiro L.** 2001. A moving DNA replication factory in *Caulobacter crescentus*. EMBO J **20:**4952-4963.
39. **Wolanski M, Donczew R, Zawilak-Pawlik A, Zakrzewska-Czerwinska J.** 2014. *oriC*-encoded instructions for the initiation of bacterial chromosome replication. Front Microbiol **5:**735.
40. **Skarstad K, Katayama T.** 2013. Regulating DNA replication in bacteria. Cold Spring Harb Perspect Biol **5:**a012922.
41. **Kuzminov A.** 2013. The chromosome cycle of prokaryotes. Mol Microbiol **90:**214-227.
42. **Kuzminov A.** 2014. The precarious prokaryotic chromosome. J Bacteriol **196:**1793-1806.
43. **Mierzejewska J, Jagura-Burdzy G.** 2012. Prokaryotic ParA-ParB-*parS* system links bacterial chromosome segregation with the cell cycle. Plasmid **67:**1-14.
44. **Jun S, Mulder B.** 2006. Entropy-driven spatial organization of highly confined polymers: lessons for the bacterial chromosome. Proc Natl Acad Sci U S A **103:**12388-12393.
45. **Jun S, Wright A.** 2010. Entropy as the driver of chromosome segregation. Nat Rev Microbiol **8:**600-607.
46. **Joshi MC, Magnan D, Montminy TP, Lies M, Stepankiw N, Bates D.** 2013. Regulation of sister chromosome cohesion by the replication fork tracking protein SeqA. PLoS Genet **9:**e1003673.
47. **Kjos M, Veening JW.** 2014. Tracking of chromosome dynamics in live *Streptococcus pneumoniae* reveals that transcription promotes chromosome segregation. Mol Microbiol **91:**1088-1105.
48. **Fisher JK, Bourniquel A, Witz G, Weiner B, Prentiss M, Kleckner N.** 2013. Four-dimensional imaging of *E. coli* nucleoid organization and dynamics in living cells. Cell **153:**882-895.

49. **Bouet JY, Stouf M, Lebailly E, Cornet F.** 2014. Mechanisms for chromosome segregation. Curr Opin Microbiol **22:**60-65.
50. **Gerdes K, Howard M, Szardenings F.** 2010. Pushing and pulling in prokaryotic DNA segregation. Cell **141:**927-942.
51. **Livny J, Yamaichi Y, Waldor MK.** 2007. Distribution of centromere-like *parS* sites in bacteria: insights from comparative genomics. J Bacteriol **189:**8693-8703.
52. **Graham TG, Wang X, Song D, Etson CM, van Oijen AM, Rudner DZ, Loparo JJ.** 2014. ParB spreading requires DNA bridging. Genes Dev **28:**1228-1238.
53. **Breier AM, Grossman AD.** 2007. Whole-genome analysis of the chromosome partitioning and sporulation protein Spo0J (ParB) reveals spreading and origin-distal sites on the *Bacillus subtilis* chromosome. Mol Microbiol **64:**703-718.
54. **Lin DC, Grossman AD.** 1998. Identification and characterization of a bacterial chromosome partitioning site. Cell **92:**675-685.
55. **Murray H, Ferreira H, Errington J.** 2006. The bacterial chromosome segregation protein Spo0J spreads along DNA from *parS* nucleation sites. Mol Microbiol **61:**1352-1361.
56. **Leonard TA, Butler PJ, Lowe J.** 2005. Bacterial chromosome segregation: structure and DNA binding of the Soj dimer--a conserved biological switch. EMBO J **24:**270-282.
57. **Fogel MA, Waldor MK.** 2006. A dynamic, mitotic-like mechanism for bacterial chromosome segregation. Genes Dev **20:**3269-3282.
58. **Ptacin JL, Lee SF, Garner EC, Toro E, Eckart M, Comolli LR, Moerner WE, Shapiro L.** 2010. A spindle-like apparatus guides bacterial chromosome segregation. Nat Cell Biol **12:**791-798.
59. **Banigan EJ, Gelbart MA, Gitai Z, Wingreen NS, Liu AJ.** 2011. Filament depolymerization can explain chromosome pulling during bacterial mitosis. Plos Comput Biol **7**.
60. **Ringgaard S, van Zon J, Howard M, Gerdes K.** 2009. Movement and equipositioning of plasmids by ParA filament disassembly. Proc Natl Acad Sci U S A **106:**19369-19374.
61. **Vecchiarelli AG, Neuman KC, Mizuuchi K.** 2014. A propagating ATPase gradient drives transport of surface-confined cellular cargo. Proc Natl Acad Sci U S A **111:**4880-4885.
62. **Vecchiarelli AG, Hwang LC, Mizuuchi K.** 2013. Cell-free study of F plasmid partition provides evidence for cargo transport by a diffusion-ratchet mechanism. Proc Natl Acad Sci U S A **110:**E1390-1397.
63. **Hwang LC, Vecchiarelli AG, Han YW, Mizuuchi M, Harada Y, Funnell BE, Mizuuchi K.** 2013. ParA-mediated plasmid partition driven by protein pattern self-organization. EMBO J **32:**1238-1249.
64. **Vecchiarelli AG, Han YW, Tan X, Mizuuchi M, Ghirlando R, Biertumpfel C, Funnell BE, Mizuuchi K.** 2010. ATP control of dynamic P1 ParA-DNA interactions: a key role for the nucleoid in plasmid partition. Mol Microbiol **78:**78-91.

65. **Lim HC, Surovtsev IV, Beltran BG, Huang F, Bewersdorf J, Jacobs-Wagner C.** 2014. Evidence for a DNA-relay mechanism in ParABS-mediated chromosome segregation. Elife **3:**e02758.

66. **Mohl DA, Easter J, Jr., Gober JW.** 2001. The chromosome partitioning protein, ParB, is required for cytokinesis in *Caulobacter crescentus*. Mol Microbiol **42:**741-755.

67. **Mohl DA, Gober JW.** 1997. Cell cycle-dependent polar localization of chromosome partitioning proteins in *Caulobacter crescentus*. Cell **88:**675-684.

68. **Toro E, Hong SH, McAdams HH, Shapiro L.** 2008. *Caulobacter* requires a dedicated mechanism to initiate chromosome segregation. Proc Natl Acad Sci U S A **105:**15435-15440.

69. **Umbarger MA, Toro E, Wright MA, Porreca GJ, Bau D, Hong SH, Fero MJ, Zhu LJ, Marti-Renom MA, McAdams HH, Shapiro L, Dekker J, Church GM.** 2011. The three-dimensional architecture of a bacterial genome and its alteration by genetic perturbation. Mol Cell **44:**252-264.

70. **Thanbichler M, Shapiro L.** 2006. MipZ, a spatial regulator coordinating chromosome segregation with cell division in *Caulobacter*. Cell **126:**147-162.

71. **Mera PE, Kalogeraki VS, Shapiro L.** 2014. Replication initiator DnaA binds at the *Caulobacter* centromere and enables chromosome segregation. Proc Natl Acad Sci U S A **111:**16100-16105.

72. **Jensen RB.** 2006. Coordination between chromosome replication, segregation, and cell division in *Caulobacter crescentus*. J Bacteriol **188:**2244-2253.

73. **Jensen RB, Shapiro L.** 1999. The *Caulobacter crescentus smc* gene is required for cell cycle progression and chromosome segregation. Proc Natl Acad Sci U S A **96:**10661-10666.

74. **Bowman GR, Comolli LR, Zhu J, Eckart M, Koenig M, Downing KH, Moerner WE, Earnest T, Shapiro L.** 2008. A polymeric protein anchors the chromosomal origin/ParB complex at a bacterial cell pole. Cell **134:**945-955.

75. **Ebersbach G, Briegel A, Jensen GJ, Jacobs-Wagner C.** 2008. A self-associating protein critical for chromosome attachment, division, and polar organization in *Caulobacter*. Cell **134:**956-968.

76. **Bowman GR, Comolli LR, Gaietta GM, Fero M, Hong SH, Jones Y, Lee JH, Downing KH, Ellisman MH, McAdams HH, Shapiro L.** 2010. *Caulobacter* PopZ forms a polar subdomain dictating sequential changes in pole composition and function. Mol Microbiol **76:**173-189.

77. **Ptacin JL, Gahlmann A, Bowman GR, Perez AM, von Diezmann AR, Eckart MR, Moerner WE, Shapiro L.** 2014. Bacterial scaffold directs pole-specific centromere segregation. Proc Natl Acad Sci U S A.

78. **Schofield WB, Lim HC, Jacobs-Wagner C.** 2010. Cell cycle coordination and regulation of bacterial chromosome segregation dynamics by polarly localized proteins. EMBO J **29:**3068-3081.

79. **Shebelut CW, Guberman JM, van Teeffelen S, Yakhnina AA, Gitai Z.** 2010. *Caulobacter* chromosome segregation is an ordered multistep process. Proc Natl Acad Sci U S A **107:**14194-14198.

80. **Raßbach A.** 2013. Chromosomensegregation in *Hyphomonas neptunium*: Das Kamel und das Nadelöhr. PhD Thesis. Philipps-Universität Marburg.

81. **Lutkenhaus J.** 2012. The ParA/MinD family puts things in their place. Trends Microbiol **20:**411-418.

82. **Huitema E, Pritchard S, Matteson D, Radhakrishnan SK, Viollier PH.** 2006. Bacterial birth scar proteins mark future flagellum assembly site. Cell **124:**1025-1037.

83. **Lam H, Schofield WB, Jacobs-Wagner C.** 2006. A landmark protein essential for establishing and perpetuating the polarity of a bacterial cell. Cell **124:**1011-1023.

84. **Ramachandran R, Jha J, Chattoraj DK.** 2014. Chromosome segregation in *Vibrio cholerae*. J Mol Microbiol Biotechnol **24:**360-370.

85. **Yamaichi Y, Bruckner R, Ringgaard S, Moll A, Cameron DE, Briegel A, Jensen GJ, Davis BM, Waldor MK.** 2012. A multidomain hub anchors the chromosome segregation and chemotactic machinery to the bacterial pole. Genes Dev **26:**2348-2360.

86. **Demarre G, Galli E, Muresan L, Paly E, David A, Possoz C, Barre FX.** 2014. Differential management of the replication terminus regions of the two *Vibrio cholerae* chromosomes during cell division. PLoS Genet **10:**e1004557.

87. **Yamaichi Y, Fogel MA, Waldor MK.** 2007. *par* genes and the pathology of chromosome loss in *Vibrio cholerae*. Proc Natl Acad Sci U S A **104:**630-635.

88. **Heidelberg JF, Eisen JA, Nelson WC, Clayton RA, Gwinn ML, Dodson RJ, Haft DH, Hickey EK, Peterson JD, Umayam L, Gill SR, Nelson KE, Read TD, Tettelin H, Richardson D, Ermolaeva MD, Vamathevan J, Bass S, Qin H, Dragoi I, Sellers P, McDonald L, Utterback T, Fleishmann RD, Nierman WC, White O, Salzberg SL, Smith HO, Colwell RR, Mekalanos JJ, Venter JC, Fraser CM.** 2000. DNA sequence of both chromosomes of the cholera pathogen *Vibrio cholerae*. Nature **406:**477-483.

89. **Gerdes K, Moller-Jensen J, Bugge Jensen R.** 2000. Plasmid and chromosome partitioning: surprises from phylogeny. Mol Microbiol **37:**455-466.

90. **Saint-Dic D, Frushour BP, Kehrl JH, Kahng LS.** 2006. A *parA* homolog selectively influences positioning of the large chromosome origin in *Vibrio cholerae*. J Bacteriol **188:**5626-5631.

91. **Kadoya R, Baek JH, Sarker A, Chattoraj DK.** 2011. Participation of chromosome segregation protein ParAI of *Vibrio cholerae* in chromosome replication. J Bacteriol **193:**1504-1514.

92. **Yamaichi Y, Gerding MA, Davis BM, Waldor MK.** 2011. Regulatory cross-talk links *Vibrio cholerae* chromosome II replication and segregation. PLoS Genet **7:**e1002189.

93. **Venkova-Canova T, Baek JH, Fitzgerald PC, Blokesch M, Chattoraj DK.** 2013. Evidence for two different regulatory mechanisms linking replication and segregation of *Vibrio cholerae* chromosome II. PLoS Genet **9:**e1003579.

94. **Ireton K, Gunther NWt, Grossman AD.** 1994. *spo0J* is required for normal chromosome segregation as well as the initiation of sporulation in *Bacillus subtilis*. J Bacteriol **176:**5320-5329.

95. **Lee PS, Grossman AD.** 2006. The chromosome partitioning proteins Soj (ParA) and Spo0J (ParB) contribute to accurate chromosome partitioning, separation of replicated sister origins, and regulation of replication initiation in *Bacillus subtilis*. Mol Microbiol **60:**853-869.

96. **Britton RA, Lin DC, Grossman AD.** 1998. Characterization of a prokaryotic SMC protein involved in chromosome partitioning. Genes Dev **12:**1254-1259.

97. **Gruber S, Errington J.** 2009. Recruitment of condensin to replication origin regions by ParB/SpoOJ promotes chromosome segregation in *B. subtilis*. Cell **137:**685-696.

98. **Sullivan NL, Marquis KA, Rudner DZ.** 2009. Recruitment of SMC by ParB-*parS* organizes the origin region and promotes efficient chromosome segregation. Cell **137:**697-707.

99. **Gruber S, Veening JW, Bach J, Blettinger M, Bramkamp M, Errington J.** 2014. Interlinked sister chromosomes arise in the absence of condensin during fast replication in *B. subtilis*. Curr Biol **24:**293-298.

100. **Wang X, Tang OW, Riley EP, Rudner DZ.** 2014. The SMC condensin complex is required for origin segregation in *Bacillus subtilis*. Curr Biol **24:**287-292.

101. **Murray H, Errington J.** 2008. Dynamic control of the DNA replication initiation protein DnaA by Soj/ParA. Cell **135:**74-84.

102. **Scholefield G, Errington J, Murray H.** 2012. Soj/ParA stalls DNA replication by inhibiting helix formation of the initiator protein DnaA. EMBO J **31:**1542-1555.

103. **Scholefield G, Whiting R, Errington J, Murray H.** 2011. Spo0J regulates the oligomeric state of Soj to trigger its switch from an activator to an inhibitor of DNA replication initiation. Mol Microbiol **79:**1089-1100.

104. **Burkholder WF, Kurtser I, Grossman AD.** 2001. Replication initiation proteins regulate a developmental checkpoint in *Bacillus subtilis*. Cell **104:**269-279.

105. **Veening JW, Murray H, Errington J.** 2009. A mechanism for cell cycle regulation of sporulation initiation in *Bacillus subtilis*. Genes Dev **23:**1959-1970.

106. **Iniesta AA.** 2014. ParABS system in chromosome partitioning in the bacterium *Myxococcus xanthus*. PLoS One **9:**e86897.

107. **Treuner-Lange A, Aguiluz K, van der Does C, Gomez-Santos N, Harms A, Schumacher D, Lenz P, Hoppert M, Kahnt J, Munoz-Dorado J, Sogaard-Andersen L.** 2013. PomZ, a ParA-like protein, regulates Z-ring formation and cell division in *Myxococcus xanthus*. Mol Microbiol **87:**235-253.

108. **Lin L.** 2013. Cytoskeletons as Polar Landmarks - Characterization of bactofilin homologs in *Myxococcus xanthus*. PhD thesis. Philipps-Universität Marburg

109. **Kysela DT, Brown PJ, Huang KC, Brun YV.** 2013. Biological consequences and advantages of asymmetric bacterial growth. Annu Rev Microbiol **67:**417-435.

110. **Sassetti CM, Boyd DH, Rubin EJ.** 2003. Genes required for mycobacterial growth defined by high density mutagenesis. Mol Microbiol **48:**77-84.

111. **Donovan C, Schwaiger A, Kramer R, Bramkamp M.** 2010. Subcellular localization and characterization of the ParAB system from *Corynebacterium glutamicum*. J Bacteriol **192:**3441-3451.

112. **Jakimowicz D, Brzostek A, Rumijowska-Galewicz A, Zydek P, Dolzblasz A, Smulczyk-Krawczyszyn A, Zimniak T, Wojtasz L, Zawilak-Pawlik A, Kois A, Dziadek J, Zakrzewska-Czerwinska J.** 2007. Characterization of the mycobacterial chromosome segregation protein ParB and identification of its target in *Mycobacterium smegmatis*. Microbiology **153:**4050-4060.

113. **Ginda K, Bezulska M, Ziolkiewicz M, Dziadek J, Zakrzewska-Czerwinska J, Jakimowicz D.** 2013. ParA of *Mycobacterium smegmatis* co-ordinates chromosome segregation with the cell cycle and interacts with the polar growth determinant DivIVA. Mol Microbiol **87:**998-1012.

114. **Jakimowicz D, van Wezel GP.** 2012. Cell division and DNA segregation in *Streptomyces*: how to build a septum in the middle of nowhere? Mol Microbiol **85:**393-404.

115. **Donovan C, Sieger B, Kramer R, Bramkamp M.** 2012. A synthetic *Escherichia coli* system identifies a conserved origin tethering factor in Actinobacteria. Mol Microbiol **84:**105-116.

116. **Donovan C, Schauss A, Kramer R, Bramkamp M.** 2013. Chromosome segregation impacts on cell growth and division site selection in *Corynebacterium glutamicum*. PLoS One **8:**e55078.

117. **Baronian G, Ginda K, Berry L, Cohen-Gonsaud M, Zakrzewska-Czerwinska J, Jakimowicz D, Molle V.** 2015. Phosphorylation of *Mycobacterium tuberculosis* ParB participates in regulating the ParABS chromosome segregation system. PLoS One **10:**e0119907.

118. **Jakimowicz D, Zydek P, Kois A, Zakrzewska-Czerwinska J, Chater KF.** 2007. Alignment of multiple chromosomes along helical ParA scaffolding in sporulating *Streptomyces* hyphae. Mol Microbiol **65:**625-641.

119. **Kim HJ, Calcutt MJ, Schmidt FJ, Chater KF.** 2000. Partitioning of the linear chromosome during sporulation of *Streptomyces coelicolor* A3(2) involves an *oriC*-linked *parAB* locus. J Bacteriol **182:**1313-1320.

120. **Flardh K, Buttner MJ.** 2009. *Streptomyces* morphogenetics: dissecting differentiation in a ilamentous bacterium. Nat Rev Microbiol **7:**36-49.

121. **Ditkowski B, Holmes N, Rydzak J, Donczew M, Bezulska M, Ginda K, Kedzierski P, Zakrzewska-Czerwinska J, Kelemen GH, Jakimowicz D.** 2013. Dynamic interplay of ParA with the polarity protein, Scy, coordinates the growth with chromosome segregation in *Streptomyces coelicolor*. Open Biol **3:**130006.

122. **Holmes NA, Walshaw J, Leggett RM, Thibessard A, Dalton KA, Gillespie MD, Hemmings AM, Gust B, Kelemen GH.** 2013. Coiled-coil protein Scy is a key component of a multiprotein assembly controlling polarized growth in *Streptomyces*. Proc Natl Acad Sci U S A **110:**E397-406.

123. **Ditkowski B, Troc P, Ginda K, Donczew M, Chater KF, Zakrzewska-Czerwinska J, Jakimowicz D.** 2010. The actinobacterial signature protein ParJ (SCO1662) regulates ParA polymerization and affects chromosome segregation and cell division during *Streptomyces* sporulation. Mol Microbiol **78:**1403-1415.

124. **Lasocki K, Bartosik AA, Mierzejewska J, Thomas CM, Jagura-Burdzy G.** 2007. Deletion of the *parA* (*soj*) homologue in *Pseudomonas aeruginosa* causes ParB instability and affects growth rate, chromosome segregation, and motility. J Bacteriol **189:**5762-5772.

125. **Bartosik AA, Mierzejewska J, Thomas CM, Jagura-Burdzy G.** 2009. ParB deficiency in *Pseudomonas aeruginosa* destabilizes the partner protein ParA and affects a variety of physiological parameters. Microbiology **155:**1080-1092.

126. **Bartosik AA, Glabski K, Jecz P, Mikulska S, Fogtman A, Koblowska M, Jagura-Burdzy G.** 2014. Transcriptional profiling of ParA and ParB mutants in actively dividing cells of an opportunistic human pathogen *Pseudomonas aeruginosa*. PLoS One **9:**e87276.

127. **Lin L, Thanbichler M.** 2013. Nucleotide-independent cytoskeletal scaffolds in bacteria. Cytoskeleton (Hoboken) **70:**409-423.

128. **Pinho MG, Kjos M, Veening JW.** 2013. How to get (a)round: mechanisms controlling growth and division of coccoid bacteria. Nat Rev Microbiol **11:**601-614.

129. **Minnen A, Attaiech L, Thon M, Gruber S, Veening JW.** 2011. SMC is recruited to *oriC* by ParB and promotes chromosome segregation in *Streptococcus pneumoniae*. Mol Microbiol **81:**676-688.

130. **Attaiech L, Minnen A, Kjos M, Gruber S, Veening JW.** 2015. The ParB-*parS* chromosome segregation system modulates competence development in *Streptococcus pneumoniae*. MBio **6:**e00662.

131. **Yamaichi Y, Niki H.** 2004. *migS*, a cis-acting site that affects bipolar positioning of *oriC* on the *Escherichia coli* chromosome. EMBO J **23:**221-233.

132. **Fekete RA, Chattoraj DK.** 2005. A cis-acting sequence involved in chromosome segregation in *Escherichia coli*. Mol Microbiol **55:**175-183.

133. **Wang X, Sherratt DJ.** 2010. Independent segregation of the two arms of the *Escherichia coli ori* region requires neither RNA synthesis nor MreB dynamics. J Bacteriol **192:**6143-6153.

134. **Joshi MC, Bourniquel A, Fisher J, Ho BT, Magnan D, Kleckner N, Bates D.** 2011. *Escherichia coli* sister chromosome separation includes an abrupt global transition with concomitant release of late-splitting intersister snaps. Proc Natl Acad Sci U S A **108:**2765-2770.

135. **Bates D, Kleckner N.** 2005. Chromosome and replisome dynamics in *E. coli*: loss of sister cohesion triggers global chromosome movement and mediates chromosome segregation. Cell **121:**899-911.

136. **Di Ventura B, Knecht B, Andreas H, Godinez WJ, Fritsche M, Rohr K, Nickel W, Heermann DW, Sourjik V.** 2013. Chromosome segregation by the *Escherichia coli* Min system. Mol Syst Biol **9:**686.

137. **Rybenkov VV, Herrera V, Petrushenko ZM, Zhao H.** 2014. MukBEF, a chromosomal organizer. J Mol Microbiol Biotechnol **24:**371-383.

138. **Nasmyth K, Haering CH.** 2005. The structure and function of SMC and kleisin complexes. Annu Rev Biochem **74:**595-648.

139. **Hirano T.** 2006. At the heart of the chromosome: SMC proteins in action. Nat Rev Mol Cell Biol **7:**311-322.

140. **Burmann F, Shin HC, Basquin J, Soh YM, Gimenez-Oya V, Kim YG, Oh BH, Gruber S.** 2013. An asymmetric SMC-kleisin bridge in prokaryotic condensin. Nat Struct Mol Biol **20:**371-379.

141. **Mascarenhas J, Soppa J, Strunnikov AV, Graumann PL.** 2002. Cell cycle-dependent localization of two novel prokaryotic chromosome segregation and condensation proteins in *Bacillus subtilis* that interact with SMC protein. EMBO J **21:**3108-3118.

142. **Volkov A, Mascarenhas J, Andrei-Selmer C, Ulrich HD, Graumann PL.** 2003. A prokaryotic condensin/cohesin-like complex can actively compact chromosomes from a single position on the nucleoid and binds to DNA as a ring-like structure. Mol Cell Biol **23:**5638-5650.

143. **Soh YM, Burmann F, Shin HC, Oda T, Jin KS, Toseland CP, Kim C, Lee H, Kim SJ, Kong MS, Durand-Diebold ML, Kim YG, Kim HM, Lee NK, Sato M, Oh BH, Gruber S.** 2015. Molecular basis for SMC rod formation and its dissolution upon DNA binding. Mol Cell **57:**290-303.

144. **Gruber S.** 2014. Multilayer chromosome organization through DNA bending, bridging and extrusion. Curr Opin Microbiol **22:**102-110.

145. **Moriya S, Tsujikawa E, Hassan AK, Asai K, Kodama T, Ogasawara N.** 1998. A *Bacillus subtilis* gene-encoding protein homologous to eukaryotic SMC motor protein is necessary for chromosome partition. Mol Microbiol **29:**179-187.

146. **Kleine Borgmann LA, Ries J, Ewers H, Ulbrich MH, Graumann PL.** 2013. The bacterial SMC complex displays two distinct modes of interaction with the chromosome. Cell Rep **3:**1483-1492.

147. **Kim H, Loparo JJ.** 2016. Multistep assembly of DNA condensation clusters by SMC. Nat Commun **7:**10200.

148. **Schwartz MA, Shapiro L.** 2011. An SMC ATPase mutant disrupts chromosome segregation in *Caulobacter*. Mol Microbiol **82:**1359-1374.

149. **Niki H, Jaffe A, Imamura R, Ogura T, Hiraga S.** 1991. The new gene *mukB* codes for a 177 kd protein with coiled-coil domains involved in chromosome partitioning of *E. coli*. EMBO J **10:**183-193.

150. **Zawadzki P, Stracy M, Ginda K, Zawadzka K, Lesterlin C, Kapanidis AN, Sherratt DJ.** 2015. The localization and action of topoisomerase IV in *Escherichia coli* chromosome segregation is coordinated by the SMC complex, MukBEF. Cell Rep **13:**2587-2596.

151. **Nicolas E, Upton AL, Uphoff S, Henry O, Badrinarayanan A, Sherratt D.** 2014. The SMC complex MukBEF recruits topoisomerase IV to the origin of replication region in live *Escherichia coli*. MBio **5:**e01001-01013.

152. **Vos SM, Stewart NK, Oakley MG, Berger JM.** 2013. Structural basis for the MukB-topoisomerase IV interaction and its functional implications *in vivo*. EMBO J **32:**2950-2962.

153. **Nolivos S, Upton AL, Badrinarayanan A, Muller J, Zawadzka K, Wiktor J, Gill A, Arciszewska L, Nicolas E, Sherratt D.** 2016. MatP regulates the coordinated action of topoisomerase IV and MukBEF in chromosome segregation. Nat Commun **7:**10466.

154. **Petrushenko ZM, She WF, Rybenkov VV.** 2011. A new family of bacterial condensins. Mol Microbiol **81:**881-896.

155. **Gruber S.** 2011. MukBEF on the march: taking over chromosome organization in bacteria? Mol Microbiol **81:**855-859.

156. **Bigot S, Sivanathan V, Possoz C, Barre FX, Cornet F.** 2007. FtsK, a literate chromosome segregation machine. Mol Microbiol **64:**1434-1441.

157. **Liu G, Draper GC, Donachie WD.** 1998. FtsK is a bifunctional protein involved in cell division and chromosome localization in *Escherichia coli*. Mol Microbiol **29:**893-903.

158. **Wang SC, West L, Shapiro L.** 2006. The bifunctional FtsK protein mediates chromosome partitioning and cell division in *Caulobacter*. J Bacteriol **188:**1497-1508.

159. **Stouf M, Meile JC, Cornet F.** 2013. FtsK actively segregates sister chromosomes in *Escherichia coli*. Proc Natl Acad Sci U S A **110:**11157-11162.

160. **Kaimer C, Graumann PL.** 2011. Players between the worlds: multifunctional DNA translocases. Curr Opin Microbiol **14:**719-725.

161. **Graham JE, Sherratt DJ, Szczelkun MD.** 2010. Sequence-specific assembly of FtsK hexamers establishes directional translocation on DNA. Proc Natl Acad Sci U S A **107:**20263-20268.

162. **Massey TH, Mercogliano CP, Yates J, Sherratt DJ, Lowe J.** 2006. Double-stranded DNA translocation: structure and mechanism of hexameric FtsK. Mol Cell **23:**457-469.

163. **Bigot S, Saleh OA, Lesterlin C, Pages C, El Karoui M, Dennis C, Grigoriev M, Allemand JF, Barre FX, Cornet F.** 2005. KOPS: DNA motifs that control *E. coli* chromosome segregation by orienting the FtsK translocase. EMBO J **24:**3770-3780.

164. **Levy O, Ptacin JL, Pease PJ, Gore J, Eisen MB, Bustamante C, Cozzarelli NR.** 2005. Identification of oligonucleotide sequences that direct the movement of the *Escherichia coli* FtsK translocase. Proc Natl Acad Sci U S A **102:**17618-17623.

165. **Lee JY, Finkelstein IJ, Crozat E, Sherratt DJ, Greene EC.** 2012. Single-molecule imaging of DNA curtains reveals mechanisms of KOPS sequence targeting by the DNA translocase FtsK. Proc Natl Acad Sci U S A **109:**6531-6536.

166. **Lesterlin C, Barre FX, Cornet F.** 2004. Genetic recombination and the cell cycle: what we have learned from chromosome dimers. Mol Microbiol **54:**1151-1160.

167. **Schvartzman JB, Stasiak A.** 2004. A topological view of the replicon. EMBO Rep **5:**256-261.

168. **Aussel L, Barre FX, Aroyo M, Stasiak A, Stasiak AZ, Sherratt D.** 2002. FtsK is a DNA motor protein that activates chromosome dimer resolution by switching the catalytic state of the XerC and XerD recombinases. Cell **108:**195-205.

169. **Steiner W, Liu G, Donachie WD, Kuempel P.** 1999. The cytoplasmic domain of FtsK protein is required for resolution of chromosome dimers. Mol Microbiol **31:**579-583.

170. **Grainge I.** 2013. Simple topology: FtsK-directed recombination at the *dif* site. Biochem Soc Trans **41:**595-600.

171. **Grainge I, Bregu M, Vazquez M, Sivanathan V, Ip SC, Sherratt DJ.** 2007. Unlinking chromosome catenanes *in vivo* by site-specific recombination. EMBO J **26:**4228-4238.

172. **Espeli O, Lee C, Marians KJ.** 2003. A physical and functional interaction between *Escherichia coli* FtsK and topoisomerase IV. J Biol Chem **278:**44639-44644.

173. **Bath J, Wu LJ, Errington J, Wang JC.** 2000. Role of *Bacillus subtilis* SpoIIIE in DNA transport across the mother cell-prespore division septum. Science **290:**995-997.

174. **Wu LJ, Errington J.** 1994. *Bacillus subtilis* SpoIIIE protein required for DNA segregation during asymmetric cell division. Science **264:**572-575.

175. **Wu LJ, Errington J.** 1998. Use of asymmetric cell division and *spoIIIE* mutants to probe chromosome orientation and organization in *Bacillus subtilis*. Mol Microbiol **27:**777-786.

176. **Jung A, Eisheuer S, Cserti E, Leicht O, Strobel W, Möll A, Schlimpert S, Kuhn J, Thanbichler M.** 2015. Molecular toolbox for genetic manipulation of the stalked budding bacterium *Hyphomonas neptunium*. Appl Environ Microbiol **81:**736-744.

177. **Leifson E.** 1964. *Hyphomicrobium Neptunium* Sp. N. Antonie van Leeuwenhoek **30:**249-256.

178. **Wali TM, Hudson GR, Danald DA, Weiner RM.** 1980. Timing of swarmer cell cycle morphogenesis and macromolecular synthesis by *Hyphomicrobium neptunium* in synchronous culture. J Bacteriol **144:**406-412.

179. **Garrity GM, Brenner DJ, Krieg NR, Staley JR.** 2005. Bergey's Manual of Systematic Bacteriology, Volume Two: The Proteobacteria, Parts A - C. Springer - Verlag, New York.

180. **Badger JH, Hoover TR, Brun YV, Weiner RM, Laub MT, Alexandre G, Mrazek J, Ren Q, Paulsen IT, Nelson KE, Khouri HM, Radune D, Sosa J, Dodson RJ, Sullivan SA, Rosovitz MJ, Madupu R, Brinkac LM, Durkin AS, Daugherty SC, Kothari SP, Giglio MG, Zhou L, Haft DH, Selengut JD, Davidsen TM, Yang Q, Zafar N, Ward NL.** 2006. Comparative genomic evidence for a close relationship between the dimorphic prosthecate bacteria *Hyphomonas neptunium* and *Caulobacter crescentus*. J Bacteriol **188:**6841-6850.

181. **Badger JH, Eisen JA, Ward NL.** 2005. Genomic analysis of *Hyphomonas neptunium* contradicts 16S rRNA gene-based phylogenetic analysis: implications for the taxonomy of the orders '*Rhodobacterales*' and *Caulobacterales*. Int J Syst Evol Microbiol **55:**1021-1026.

182. **Heinrich K.** 2011. Analyse der Chromosomensegregation in *Hyphomonas neptunium*. Bachelor Thesis. Philipps-Universität Marburg.

183. **Strobel W.** 2010. Etablierung von genetischen Methoden zur Analyse der Zellteilung in *Hyphomonas neptunium*. Bachelor Thesis. Philipps-Universität Marburg.

184. **Hirsch P.** 1974. Budding bacteria. Annu Rev Microbiol **28:**391-444.

185. **Spear AM, Loman NJ, Atkins HS, Pallen MJ.** 2009. Microbial TIR domains: not necessarily agents of subversion? Trends Microbiol **17:**393-398.

186. **Mackiewicz P, Zakrzewska-Czerwinska J, Zawilak A, Dudek MR, Cebrat S.** 2004. Where does bacterial replication start? Rules for predicting the *oriC* region. Nucleic Acids Res **32:**3781-3791.

187. **Eppinger M, Baar C, Raddatz G, Huson DH, Schuster SC.** 2004. Comparative analysis of four Campylobacterales. Nat Rev Microbiol **2:**872-885.

188. **Das D, Finn RD, Abdubek P, Astakhova T, Axelrod HL, Bakolitsa C, Cai X, Carlton D, Chen C, Chiu HJ, Chiu M, Clayton T, Deller MC, Duan L, Ellrott K, Farr CL, Feuerhelm J, Grant JC, Grzechnik A, Han GW, Jaroszewski L, Jin KK, Klock HE, Knuth MW, Kozbial P, Krishna SS, Kumar A, Lam WW, Marciano D, Miller MD, Morse AT, Nigoghossian E, Nopakun A, Okach L, Puckett C, Reyes R, Tien HJ, Trame CB, van den Bedem H, Weekes D, Wooten T, Xu Q, Yeh A, Zhou J, Hodgson KO, Wooley J, Elsliger MA, Deacon AM, Godzik A, Lesley SA, Wilson IA.** 2010. The crystal structure of a bacterial Sufu-like protein defines a novel group of bacterial proteins that are similar to the N-terminal domain of human Sufu. Protein Sci **19:**2131-2140.

189. **Bowman GR, Perez AM, Ptacin JL, Ighodaro E, Folta-Stogniew E, Comolli LR, Shapiro L.** 2013. Oligomerization and higher-order assembly contribute to sub-cellular localization of a bacterial scaffold. Mol Microbiol **90:**776-795.

190. **Laloux G, Jacobs-Wagner C.** 2013. Spatiotemporal control of PopZ localization through cell cycle-coupled multimerization. J Cell Biol **201:**827-841.

191. **Jensen RB, Shapiro L.** 2003. Cell-cycle-regulated expression and subcellular localization of the Caulobacter crescentus SMC chromosome structural protein. J Bacteriol **185:**3068-3075.

192. **Dingwall A, Shapiro L.** 1989. Rate, origin, and bidirectionality of *Caulobacter* chromosome replication as determined by pulsed-field gel electrophoresis. Proc Natl Acad Sci U S A **86:**119-123.

193. **Santi I, McKinney JD.** 2015. Chromosome organization and replisome dynamics in *Mycobacterium smegmatis*. MBio **6:**e01999-01914.

194. **Trojanowski D, Ginda K, Pioro M, Holowka J, Skut P, Jakimowicz D, Zakrzewska-Czerwinska J.** 2015. Choreography of the *Mycobacterium* replication machinery during the cell cycle. MBio **6:**e02125-02114.

195. **Kelman Z, Yuzhakov A, Andjelkovic J, O'Donnell M.** 1998. Devoted to the lagging strand-the subunit of DNA polymerase III holoenzyme contacts SSB to promote processive elongation and sliding clamp assembly. EMBO J **17:**2436-2449.

196. **Meyer RR, Laine PS.** 1990. The single-stranded DNA-binding protein of *Escherichia coli*. Microbiol Rev **54:**342-380.

197. **Fernandez-Fernandez C, Grosse K, Sourjik V, Collier J.** 2013. The beta-sliding clamp directs the localization of HdaA to the replisome in *Caulobacter crescentus*. Microbiology **159:**2237-2248.

198. **Su'etsugu M, Errington J.** 2011. The replicase sliding clamp dynamically accumulates behind progressing replication forks in *Bacillus subtilis* cells. Mol Cell **41:**720-732.

199. **Pages V.** 2016. Single-strand gap repair involves both RecF and RecBCD pathways. Curr Genet.

200. **Courcelle J.** 2005. Recs preventing wrecks. Mutat Res **577:**217-227.

201. **Ferullo DJ, Cooper DL, Moore HR, Lovett ST.** 2009. Cell cycle synchronization of *Escherichia coli* using the stringent response, with fluorescence labeling assays for DNA content and replication. Methods **48:**8-13.

202. **Webb CD, Graumann PL, Kahana JA, Teleman AA, Silver PA, Losick R.** 1998. Use of time-lapse microscopy to visualize rapid movement of the replication origin region of the chromosome during the cell cycle in *Bacillus subtilis*. Mol Microbiol **28:**883-892.

203. **Ben-Yehuda S, Rudner DZ, Losick R.** 2003. RacA, a bacterial protein that anchors chromosomes to the cell poles. Science **299:**532-536.

204. **Wu LJ, Errington J.** 2003. RacA and the Soj-Spo0J system combine to effect polar chromosome segregation in sporulating *Bacillus subtilis*. Mol Microbiol **49:**1463-1475.

205. **Treuner-Lange A, Sogaard-Andersen L.** 2014. Regulation of cell polarity in bacteria. J Cell Biol **206:**7-17.

206. **Bulyha I, Lindow S, Lin L, Bolte K, Wuichet K, Kahnt J, van der Does C, Thanbichler M, Sogaard-Andersen L.** 2013. Two small GTPases act in concert with the bactofilin cytoskeleton to regulate dynamic bacterial cell polarity. Dev Cell **25:**119-131.

207. **Ben-Yehuda S, Fujita M, Liu XS, Gorbatyuk B, Skoko D, Yan J, Marko JF, Liu JS, Eichenberger P, Rudner DZ, Losick R.** 2005. Defining a centromere-like element in *Bacillus subtilis* by identifying the binding sites for the chromosome-anchoring protein RacA. Mol Cell **17:**773-782.

208. **Lenarcic R, Halbedel S, Visser L, Shaw M, Wu LJ, Errington J, Marenduzzo D, Hamoen LW.** 2009. Localisation of DivIVA by targeting to negatively curved membranes. EMBO J **28:**2272-2282.

209. **Thomaides HB, Freeman M, El Karoui M, Errington J.** 2001. Division site selection protein DivIVA of *Bacillus subtilis* has a second distinct function in chromosome segregation during sporulation. Genes Dev **15:**1662-1673.

210. **Sieger B, Schubert K, Donovan C, Bramkamp M.** 2013. The lipid II flippase RodA determines morphology and growth in *Corynebacterium glutamicum*. Mol Microbiol **90:**966-982.

211. **Meniche X, Otten R, Siegrist MS, Baer CE, Murphy KC, Bertozzi CR, Sassetti CM.** 2014. Subpolar addition of new cell wall is directed by DivIVA in mycobacteria. Proc Natl Acad Sci U S A **111:**E3243-3251.

212. **Flardh K.** 2003. Essential role of DivIVA in polar growth and morphogenesis in *Streptomyces coelicolor* A3(2). Mol Microbiol **49:**1523-1536.

213. **Ramamurthi KS, Lecuyer S, Stone HA, Losick R.** 2009. Geometric cue for protein localization in a bacterium. Science **323:**1354-1357.

214. **Kuhn J, Briegel A, Morschel E, Kahnt J, Leser K, Wick S, Jensen GJ, Thanbichler M.** 2010. Bactofilins, a ubiquitous class of cytoskeletal proteins mediating polar localization of a cell wall synthase in *Caulobacter crescentus*. EMBO J **29:**327-339.

215. **Yeh Y-C, Comolli LR, Downing KH, Shapiro L, McAdams HH.** 2010. The *Caulobacter* Tol-Pal complex is essential for outer membrane integrity and the positioning of a polar localization factor. J Bacteriol **192:**4847-4858.

216. **Besprozvannaya M, Burton BM.** 2014. Do the same traffic rules apply? Directional chromosome segregation by SpoIIIE and FtsK. Mol Microbiol **93:**599-608.

217. **Typas A, Banzhaf M, Gross CA, Vollmer W.** 2012. From the regulation of peptidoglycan synthesis to bacterial growth and morphology. Nat Rev Microbiol **10:**123-136.

218. **Jensen RB.** 2006. Analysis of the terminus region of the *Caulobacter crescentus* chromosome and identification of the *dif* site. J Bacteriol **188:**6016-6019.

219. **Deghelt M, Mullier C, Sternon JF, Francis N, Laloux G, Dotreppe D, Van der Henst C, Jacobs-Wagner C, Letesson JJ, De Bolle X.** 2014. G1-arrested newborn cells are the predominant infectious form of the pathogen *Brucella abortus*. Nat Commun **5:**4366.

220. **Grangeon R, Zupan JR, Anderson-Furgeson J, Zambryski PC.** 2015. PopZ identifies the new pole, and PodJ identifies the old pole during polar growth in *Agrobacterium tumefaciens*. Proc Natl Acad Sci U S A **112:**11666-11671.

221. **Leicht O.** 2010. Etablierung eines genetischen Systems zur Analyse der Zellpolarität in *Hyphomonas neptunium*. Bachelor Thesis. Philipps-Universität Marburg.

222. **Leicht O.** 2012. Charakterisierung von Zellzyklusregulatoren in *Hyphomonas neptunium*. Master Thesis. Philipps-Universität Marburg.

223. **Li Y, Sergueev K, Austin S.** 2002. The segregation of the *Escherichia coli* origin and terminus of replication. Mol Microbiol **46:**985-996.

224. **Srivastava P, Fekete RA, Chattoraj DK.** 2006. Segregation of the replication terminus of the two *Vibrio cholerae* chromosomes. J Bacteriol **188:**1060-1070.

225. **Broedersz CP, Wang X, Meir Y, Loparo JJ, Rudner DZ, Wingreen NS.** 2014. Condensation and localization of the partitioning protein ParB on the bacterial chromosome. Proc Natl Acad Sci U S A **111:**8809-8814.

226. **Chen B-W, Lin M-H, Chu C-H, Hsu C-E, Sun Y-J.** 2015. Insights into ParB spreading from the complex structure of Spo0J and *parS*. Proc Natl Acad Sci U S A **112:**6613-6618.

227. **Sanchez A, Cattoni Diego I, Walter J-C, Rech J, Parmeggiani A, Nollmann M, Bouet J-Y.** Stochastic self-assembly of ParB proteins builds the bacterial DNA segregation apparatus. Cell Syst **1:**163-173.

228. **Lee JY, Finkelstein IJ, Arciszewska LK, Sherratt DJ, Greene EC.** 2014. Single-molecule imaging of FtsK translocation reveals mechanistic features of protein-protein collisions on DNA. Mol Cell **54:**832-843.

229. **Marquis KA, Burton BM, Nollmann M, Ptacin JL, Bustamante C, Ben-Yehuda S, Rudner DZ.** 2008. SpoIIIE strips proteins off the DNA during chromosome translocation. Genes Dev **22:**1786-1795.

230. **Le TB, Laub MT.** 2014. New approaches to understanding the spatial organization of bacterial genomes. Curr Opin Microbiol **22:**15-21.

231. **Georgescu R, Langston L, O'Donnell M.** 2015. A proposal: Evolution of PCNA's role as a marker of newly replicated DNA. DNA Repair **29:**4-15.

232. **Lenhart JS, Sharma A, Hingorani MM, Simmons LA.** 2013. DnaN clamp zones provide a platform for spatiotemporal coupling of mismatch detection to DNA replication. Mol Microbiol **87:**553-568.

233. **Moolman MC, Krishnan ST, Kerssemakers JW, van den Berg A, Tulinski P, Depken M, Reyes-Lamothe R, Sherratt DJ, Dekker NH.** 2014. Slow unloading leads to DNA-bound beta2-sliding clamp accumulation in live *Escherichia coli* cells. Nat Commun **5:**5820.

234. **Badrinarayanan A, Le TB, Laub MT.** 2015. Rapid pairing and resegregation of distant homologous loci enables double-strand break repair in bacteria. J Cell Biol **210:**385-400.

235. **Lesterlin C, Ball G, Schermelleh L, Sherratt DJ.** 2014. RecA bundles mediate homology pairing between distant sisters during DNA break repair. Nature **506:**249-253.

236. **Sharma A, Kamran M, Verma V, Dasgupta S, Dhar SK.** 2014. Intracellular locations of replication proteins and the origin of replication during chromosome duplication in the slowly growing human pathogen *Helicobacter pylori*. J Bacteriol **196:**999-1011.

237. **Lesterlin C, Gigant E, Boccard F, Espeli O.** 2012. Sister chromatid interactions in bacteria revealed by a site-specific recombination assay. EMBO J **31:**3468-3479.

238. **Ausubel FM.** 1988. Current protocols in molecular biology, Greene Pub. Associates ; Wiley-Interscience, New York.

239. **Sambrook J, Fritsch EF, Maniatis T.** 1989. Molecular cloning: a laboratory manual., Cold Spring Harbor Laboratory Press, Cold Spring Harbor, N.Y.

240. **Miller JH.** 1972. Experiments in molecular genetics, Cold Spring Harbour Laboratory, Cold Spring Harbour, New York.

241. **Huang L.** 2011. A new mechanistic growth model for simultaneous determination of lag phase duration and exponential growth rate and a new Belehdradek-type model for evaluating the effect of temperature on growth rate. Food Microbiol **28:**770-776.

242. **Moore RL, Hirsch P.** 1973. First generation synchrony of isolated *Hyphomicrobium* swarmer populations. J Bacteriol **116:**418-423.

243. **Cameron TA, Anderson-Furgeson J, Zupan JR, Zik JJ, Zambryski PC.** 2014. Peptidoglycan synthesis machinery in *Agrobacterium tumefaciens* during unipolar growth and cell division. MBio **5:**e01219-01214.

244. **Laemmli UK.** 1970. Cleavage of structural proteins during the assembly of the head of bacteriophage T4. Nature **227:**680-685.

245. **Chen JC, Viollier PH, Shapiro L.** 2005. A membrane metalloprotease participates in the sequential degradation of a *Caulobacter* polarity determinant. Mol Microbiol **55:**1085-1103.

246. **Bradford MM.** 1976. A rapid and sensitive method for the quantitation of microgram quantities of protein utilizing the principle of protein-dye binding. Anal Biochem **72:**248-254.

247. **Nicholas KB, Nicholas HBJ.** 1997. GeneDoc: a tool for editing and annotating multiple sequence alignments. Distributed by the author.

248. **Lau IF, Filipe SR, Soballe B, Okstad OA, Barre FX, Sherratt DJ.** 2003. Spatial and temporal organization of replicating *Escherichia coli* chromosomes. Mol Microbiol **49:**731-743.

249. **Eisheuer S.** 2011. Analyse der Zellteilung in *Hyphomonas neptunium*. Master Thesis. Philipps-Universität Marburg.

250. **Thanbichler M, Iniesta AA, Shapiro L.** 2007. A comprehensive set of plasmids for vanillate- and xylose-inducible gene expression in *Caulobacter crescentus*. Nucleic Acids Res **35:**e137.

6 Appendix

Table 6-1: Strains used in this study

Strain	Genotype	Construction/Reference
H. neptunium		
LE670	wild type (*aka* ATCC 15444)	(177)
KH22	*parB-yfp*	(182)
KH23	*parB-yfp* P_{Zn}::P_{Zn}-*lacI-mCherry*	(182)
EC33	Δ*bacAB*	E. Cserti, unpublished
AR33	P_{Zn}::P_{Zn} (RBS-3*)-parA-venus*	(80)
AR48	*parB*::*parB-yfp*	(80)
AR58	P_{Zn}::P_{Zn}-*mcherry-parB*$_{pMT1}$	(80)
AJ32	*HNE_2272*::*HNE_2272(holC)-venus*	Transformation of ATCC 15444 with pAJ32
AJ34	P_{Zn}::P_{Zn}-*HNE_1677 (popZ)-venus*	Transformation of ATCC 15444 with pAJ34
AJ38	Δ*HNE_1677 (popZ)*	Deletion of *HNE_1677* in ATCC 15444 using pNPTS138 derivative pAJ38
AJ43	P_{Zn}::P_{Zn}-*ssb-venus*	Transformation of ATCC 15444 with pAJ43
AJ44	Δ*HNE_1677 (popZ)* P_{Zn}::P_{Zn}-*parA-venus*	Transformation of AJ38 with pAR25
AJ46	Δ*parA* P_{Zn}::P_{Zn}-*parA-venus*	Deletion of *parA* in AJ73 using pNPTS138 derivative pAJ46
AJ48	P_{Zn}::P_{Zn}-*smc-venus*	Transformation of ATCC 15444 with pAJ55
AJ49	P_{Zn}::P_{Zn}-*mCherry-parB*$_{pMT1}$ *parS*$_{pMT1}$ at 186°	Transformation of AR58 with pAJ36
AJ55	P_{Zn}::P_{Zn}-*HNE_0708*$_{AA1-128}$-*venus*	Transformation of ATCC 15444 with pAR62
AJ56	P_{Zn}::P_{Zn}-*HNE_0708*$_{AA129-435}$-*venus*	Transformation of ATCC 15444 with pAR63
AJ57	*parB-yfp parS*$_{pMT1}$ at 172°	Transformation of KH22 with pAJ62
AJ58	*parB-yfp parS*$_{pMT1}$ at 272°	Transformation of KH22 with pAJ63
AJ59	*parB-yfp parS*$_{pMT1}$ at 85°	Transformation of KH22 with pAJ64
AJ60	*parB-yfp parS*$_{pMT1}$ at 53°	Transformation of KH22 with pAJ65
AJ61	*parB-yfp parS*$_{pMT1}$ at 357°	Transformation of KH22 with pAJ66
AJ62	*parB-yfp parS*$_{pMT1}$ at 5°	Transformation of KH22 with pAJ67
AJ64	*parB-yfp* P_{Zn}::P_{Zn}-*mCherry-parB*$_{pMT1}$, *parS*$_{pMT1}$ at 172°	Transformation of AJ57 with pAJ70
AJ65	*parB-yfp* P_{Zn}::P_{Zn}-*mCherry-parB*$_{pMT1}$, *parS*$_{pMT1}$ at 272°	Transformation of AJ58 with pAJ70
AJ66	*parB-yfp* P_{Zn}::P_{Zn}-*mCherry-parB*$_{pMT1}$, *parS*$_{pMT1}$ at 85°	Transformation of AJ59 with pAJ70
AJ67	*parB-yfp* P_{Zn}::P_{Zn}-*mCherry-parB*$_{pMT1}$, *parS*$_{pMT1}$ at 53°	Transformation of AJ60 with pAJ70
AJ68	*parB-yfp* P_{Zn}::P_{Zn}-*mCherry-parB*$_{pMT1}$, *parS*$_{pMT1}$ at 357°	Transformation of AJ61 with pAJ70
AJ69	*parB-yfp* P_{Zn}::P_{Zn}-*mCherry-parB*$_{pMT1}$, *parS*$_{pMT1}$ at 5°	Transformation of AJ62 with pAJ70
AJ73	P_{Zn}::P_{Zn}-*parA-venus*	Transformation of ATCC 15444 with pAJ45
AJ74	Δ*bacAB parB*::*parB-yfp*	Transformation of EC33 with pSW55
AJ76	*parB-cerulean*	Replacement of *parB* with *parB-cerulean* in ATCC 15444 using pNPTS138 derivative pAJ74
AJ77	*parB-cerulean HNE_2272:: HNE_2272(holC)-venus*	Transformation of AJ76 with pAJ32
AJ78	*parB-cerulean* P_{Zn}::P_{Zn}-*ssb-venus*	Transformation of AJ76 with pAJ43
AJ79	*parB-cerulean* P_{Cu}::P_{Cu}-*parA(K18R)-venus*	Transformation of AJ76 with pAJ75
AJ80	*parB-cerulean* P_{cu}::P_{cu}-*parA-venus*	Transformation of AJ76 with pAJ78

Table 6-1: Strains used in this study (continued)

Strain	Genotype	Construction/Reference
AJ81	P_{Zn}::P_{Zn}-*HNE_3182-venus*	Transformation of ATCC 15444 with pAJ49
AJ82	*HNE_3528*::*HNE_3528-venus*	Transformation of ATCC 15444 with pAJ53
AJ83	*HNE_1048*::*HNE_1048-venus*	Transformation of ATCC 15444 with pAJ51
AJ84	*parB-cerulean dnaN*::*dnaN-venus*	Transformation of AJ76 with pAJ81
AJ85	*smc-venus*	Replacement of *smc* with *smc-venus* in ATCC 15444 using pNPTS138 derivative pAJ73
AJ86	*HNE_1729*::l*acO*$_n$, *parB-yfp* P_{Zn}::P_{Zn}-*lacI-mCherry*	Transformation of KH23 with pAJ79
AJ87	*HNE_3540*::l*acO*$_n$, *parB-yfp* P_{Zn}::P_{Zn}-*lacI-mCherry*	Transformation of KH23 with pAJ80
AJ89	Δ*HNE_1677* (*popZ*) *parB*::*parB-yfp*	Transformation of AJ38 with pSW55
E. coli		
TOP10	cloning strain	Invitrogen
WM3064	Donor strain for conjugation: *thrB1*004 *pro thi rpsL hsdS lacZ*⊿M15 RP4–1360 Δ(*araBAD)567* ⊿*dapA*1341::[*erm pir*(wt)]	W. Metcalf (unpublished)
Rosetta™ (DE3) pLysS	Protein overproduction strain: F^- *ompT* $hsdS_B$(r_{B-} m_{B-}) *gal dcm* (DE3) pLysSRARE (Cam^R)	Merck Millipore

Table 6-2: Plasmids used in this study

Plasmid	Description	Reference
pAJ32	pVENC-2 carrying *holC* (*HNE_2272*), Kan^R	This study
pAJ34	pZVENC-2 carrying *popZ* (*HNE_1677*), Kan^R	This study
pAJ36	pAR46 (contains $parS_{pMT1}$) carrying part of *HNE_1854*, Rif^R	This study
pAJ38	pNPTS138 derivative for in-frame deletion in *popZ* (*HNE_1677*), Kan^R	This study
pAJ40	pET21a+ carrying *parB* (*HNE_3560*), Amp^R	This study
pAJ43	pZVENC-2 carrying *ssb* (*HNE_2764*), Kan^R	This study
pAJ45	pSE31 derivative carrying *parA* (*HNE_3561*), Rif^R	This study
pAJ46	pNPTS138 derivative for in-frame deletion in *parA* (*HNE_3561*), Kan^R	This study
pAJ49	pZVENC-2 carrying *HNE_3182*, Kan^R	This study
pAJ51	pVENC-2 carrying *HNE_1048,* Kan^R	This study
pAJ54	pCERC-2 carrying *parB* (*HNE_3560*)	This study
pAJ53	pVENC-2 carrying *HNE_3528,* Kan^R	This study
pAJ55	pZVENC-2 carrying *smc* (*HNE_1917*), Kan^R	This study
pAJ56	pMCS-3 carrying $parS_{pMT1}$ and part of *HNE_1729*, Rif^R	This study
pAJ57	pMCS-3 carrying $parS_{pMT1}$ and part of *HNE_2644*, Rif^R	This study
pAJ58	pMCS-3 carrying $parS_{pMT1}$ and part of *HNE_0857*, Rif^R	This study
pAJ59	pMCS-3 carrying $parS_{pMT1}$ and part of *HNE_0550*, Rif^R	This study
pAJ60	pMCS-3 carrying $parS_{pMT1}$ and part of *HNE_3540*, Rif^R	This study
pAJ61	pMCS-3 carrying $parS_{pMT1}$ and part of *HNE_0063*, Rif^R	This study
pAJ62	pMCS-2 carrying $parS_{pMT1}$ and part of *HNE_1729*, Kan^R	This study
pAJ63	pMCS-2 carrying $parS_{pMT1}$ and part of *HNE_2644*, Kan^R	This study
pAJ64	pMCS-2 carrying $parS_{pMT1}$ and part of *HNE_0857*, Kan^R	This study
pAJ65	pMCS-2 carrying $parS_{pMT1}$ and part of *HNE_0550*, Kan^R	This study
pAJ66	pMCS-2 carrying $parS_{pMT1}$ and part of *HNE_3540*, Kan^R	This study
pAJ67	pMCS-2 carrying $parS_{pMT1}$ and part of *HNE_0063*, Kan^R	This study
pAJ70	pZCHYN-3 carrying $parB_{pMT1}$, Rif^R	This study
pAJ73	pNPTS138 derivative to replace *smc* with *smc-venus*, Kan^R	This study
pAJ74	pNPTS138 derivative to replace *parB* with *parB-cerulean*, Kan^R	This study
pAJ75	pCVENC-2 carrying *parA* (*K18R*), Kan^R	This study
pAJ78	pCVENC-2 carrying *parA* (*HNE_3561*), Kan^R	This study
pAJ79	pKH3 (containing $lacO_n$) carrying part of *HNE_1729*, Kan^R, Amp^R	This study
pAJ80	pKH3 (containing $lacO_n$) carrying part of *HNE_3540,* Kan^R, Amp^R	This study
pAJ81	pVENC-2 carrying C-terminal part of *dnaN* (*HNE_0563*), Kan^R	This study
pKH3	pLAU43 (containing $lacO_n$) carrying *oriT,* Kan^R, Amp^R	(182, 248)
pSW55	pYFPC carrying *parB* (*HNE_3560*), Kan^R	S. Wick, unpublished

Table 6-2: Plasmids used in this study (continued)

Plasmid	Description	Reference
pAR25	pSE31 carrying *parA* (*HNE_3561*), Kan^R	(80)
pAR46	pMCS-3 carrying $parS_{pMT1}$-sites, Rif^R	(80)
pAR51	pZCHYN-2 carrying $parB_{pMT1}$, Kan^R	(80)
pAR62	pSE31 carrying $HNE\_0708_{AA1\text{-}128}$, Kan^R	A. Raßbach, unpublished
pAR63	pSE31 carrying $HNE\_0708_{AA129\text{-}435}$, Kan^R	A. Raßbach, unpublished
pCVENC-2 (pEC111)	Integrating plasmid for generation of C-terminal Venus fusion under control of P_{Cu}, Kan^R	(176)
pZVENC-2 (pSE50)	Integrating plasmid for generation of C-terminal Venus fusion under control of P_{Zn}, Kan^R	(176)
pSE31	Integrating plasmid for generation of C-terminal Venus fusion under control of P_{Zn} (RBS-3), Kan^R	(249)
pZCHYN-3	Integrating plasmid for generation of N-terminal mCherry fusion under control of P_{Zn}, Rif^R	(176)
pMCS-2	Integrating plasmid containing multiple cloning site, Kan^R	(250)
pMCS-3	Integrating plasmid containing multiple cloning site, Rif^R	(250)
pVENC-2	Integrating plasmid for generation of C-terminal Venus fusion at site of interest, Kan^R	(250)
pCERC-2	Integrating plasmid for generation of C-terminal Cerulean fusion at site of interest, Kan^R	(250)
pCYFP-2	Integrating plasmid for generation of C-terminal YFP fusion at site of interest, Kan^R	(250)
pNPTS138	*sacB*-containing suicide vector used for double homologous recombination, Kan^R	M. R. K. Alley, unpublished
pET21a+	Plasmid for overexpression of C-terminally His_6-tagged proteins, Amp^R	Novagen

Table 6-3: Plasmid construction

Plasmid	Construction
pAJ32	a) digestion of pSW84 (pVENC-2 with insert, S. Wick unpublished) with *Nde*I and *Kpn*I to cut out insert, b) amplification of *HNE_2272* with primer 144 (adding *Nde*I site) and primer 145 (adding *Kpn*I site), c) ligation of vector backbone and insert via *Nde*I and *Kpn*I sites
pAJ34	a) digestion of pZVENC-2 (pSE50) with *Nde*I and *Kpn*I, b) amplification of *HNE_1677* with primer 146 (adding *Nde*I site) and primer 147 (adding *Kpn*I site), c) ligation of vector backbone and insert via *Nde*I and *Kpn*I sites
pAJ36	a) digestion of pAR46 with *Sac*I and *Kpn*I, (pAR46 contains *parS* sites of *Y. pestis*), b) amplification of part of *HNE_1854* with primer 173 (adding *Kpn*I site) and primer 174 (adding *Sac*I site), c) ligation of vector backbone and insert via *Sac*I and *Kpn*I sites
pAJ38	a) digestion of pNPTS138 with *Hind*III and *Eco*RI, b) amplification of 547 bp 5´flanking region of *HNE_1677* with primer 177 (adding *Hind*III restriction site) and primer 178 (*Kpn*I site), c) amplification of 507 bp 3`flanking region of *HNE_1677* with primer 179 (adding *Kpn*I site) and primer 180 (adding *Eco*RI restriction site), d) three fragment ligation of vector backbone and two inserts via *Hind*III, *Kpn*I, and *Eco*RI sites
pAJ40	a) digestion of pET21a+ with *Nde*I and *Eco*RI, (pET21a: T7 promoter, His-tag for C-term fusion), b) amplification of *HNE_3560* with primer 148 (adding *Nde*I site) and primer 186 (adding *Eco*RI site), c) ligation of vector backbone and insert via *Nde*I and *Eco*RI sites
pAJ43	a) digestion of pZVENC-2 (pSE50) with *Nde*I and *Kpn*I, b) amplification of *ssb (HNE_2764)* with primer 142 (adding *Nde*I site) and primer 143 (adding *Kpn*I site), c) ligation of vector backbone and insert via *Nde*I and *Kpn*I sites
pAJ45	a) sequential digestion of pAR25 with first *Nhe*I and then *Sfi*I, elution of vector backbone (cut out kanamycin resistance), b) sequential digestion of pEC45 with first *Nhe*I and then *Sfi*I, elution of rifampicin backbone, c) ligation of pAR25 backbone and rifampicin backbone via *Nhe*I and *Sfi*I
pAJ46	a) digestion of pNPTS138 with *Hind*III and *Nhe*I, b) amplification of 677 bp 5´flanking region of HNE_3561 with primer 216 (adding *Hind*III restriction site) and primer 217 (adding *Kpn*I restriction site), c) amplification of 758 bp 3`flanking region of *HNE_3561* with primer 218 (adding *Kpn*I restriction site) and primer 219 (adding *Nhe*I restriction site), d) three fragment ligation of vector backbone and two inserts via *Hind*III, *Nhe*I, and *Kpn*I sites
pAJ49	a) digestion of pZVENC-2 (pSE50) with *Nde*I and *Kpn*I, b) amplification of *HNE_3182* with primer 211 (adding *Nde*I site) and primer 212 (adding *Kpn*I site), c) ligation of vector backbone and insert via *Nde*I and *Kpn*I sites
pAJ51	a) digestion of pVENC-2 with *Nde*I and *Kpn*I, b) amplification of *HNE_1048* with primer 209 (adding *Nde*I site) and primer 210 (adding *Kpn*I site), c) ligation of vector backbone and insert via *Nde*I and *Kpn*I sites
pAJ53	a) digestion of pVENC-2 with *NdeI* and *Kpn*I, b) amplification of *HNE_3528* with primer 213 (add *Nde*I site) and primer 214 (add *Kpn*I site), c) ligation of vector backbone and insert via *Nde*I and *Kpn*I
pAJ54	a) digestion of pCERC-2 with *Nde*I and *Eco*RI, b) digestion of pSW55 (pYFPC-2+*HNE_3560*) with *Nde*I and *Eco*RI, c) ligation of vector backbone and insert via *Nde*I and *Eco*RI sites

Table 6-3: Plasmid construction (continued)

Plasmid	Construction
pAJ55	a) digestion of pZVENC-2 (pSE50) with *Nde*I and *Kpn*I, b) amplification of *smc* with primer 227 (adding *Nde*I site) and primer 228 (adding *Kpn*I site), c) ligation of vector backbone and insert via *Nde*I and *Kpn*I sites
pAJ56	a) digestion of pAR46 with *Nhe*I and *Kpn*I, (pAR46 contains *parS* sites of *Y. pestis*), b) amplification of part of *HNE_1729* with primer 238 (adding *Kpn*I site) and primer 239 (adding *Nhe*I site), c) ligation of vector backbone and insert via *Nhe*I and *Kpn*I sites
pAJ57	a) digestion of pAR46 with *Nhe*I and *Kpn*I, (pAR46 contains *parS* sites of *Y. pestis*), b) amplification of part of *HNE_2644* with primer 240 (adding *Kpn*I site) and primer 241 (adding *Nhe*I site), c) ligation of vector backbone and insert via *Nhe*I and *Kpn*I sites
pAJ58	a) digestion of pAR46 with *Sac*I and *Kpn*I, (pAR46 contains *parS* sites of *Y. pestis*), b) amplification of part of *HNE_0857* with primer 242 (adding *KpnI* site) and primer 243 (adding *Sac*I site), c) ligation of vector backbone and insert via *Sac*I and *Kpn*I sites
pAJ59	a) digestion of pAR46 with *Sac*I and *Kpn*I, (pAR46 contains *parS* sites of *Y. pestis*), b) amplification of part of *HNE_0550* with primer 244 (adding *Kpn*I site) and primer 245 (adding *Sac*I site), c) ligation of vector backbone and insert via *Sac*I and *Kpn*I sites
pAJ60	a) digestion of pAR46 with *Sac*I and *Kpn*I, (pAR46 contains *parS* sites of *Y. pestis*), b) amplification of part of *HNE_3540* with primer 246 (adding *Kpn*I site) and primer 247 (adding *Sac*I site), c) ligation of vector backbone and insert via *Sac*I and *Kpn*I sites
pAJ61	a) digestion of pAR46 with *Sac*I and *Kpn*I, (pAR46 contains *parS* sites of *Y. pestis*), b) amplification of part of *HNE_0063* with primer 248 (adding *Kpn*I site) and primer 249 (adding *Sac*I site), c) ligation of vector backbone and insert via *Sac*I and *Kpn*I sites
pAJ62	a) digestion of pMCS-2 with *Hinc*II and *Nhe*I and elution of vector backbone, b) digestion of pAJ56 with *Hinc*II and *Nhe*I, elution of insert, c) ligation of vector backbone and insert via *Nhe*I and *Hinc*II sites
pAJ63	a) digestion of pMCS-2 with *Sfi*I and *Nhe*I and elution of vector backbone, b) digestion of pAJ57 with *Sfi*I and *Nhe*I, elution of insert, c) ligation of vector backbone and insert via *Nhe*I and *Sfi*I sites
pAJ64	a) digestion of pMCS-2 with *Hinc*II and *Nhe*I and elution of vector backbone, b) digestion of pAJ58 with *Hinc*II and *Nhe*I, elution of insert, c) ligation of vector backbone and insert via *Nhe*I and *Hinc*II sites
pAJ65	a) digestion of pMCS-2 with *Sfi*I and *Nhe*I and elution of vector backbone, b) digestion of pAJ59 with *Sfi*I and *Nhe*I, elution of insert, c) ligation of vector backbone and insert via *Nhe*I and *Sfi*I sites
pAJ66	a) digestion of pMCS-2 with *Sfi*I and *Nhe*I and elution of vector backbone, b) digestion of pAJ60 with *Sfi*I and *Nhe*I, elution of insert, c) ligation of vector backbone and insert via *Nhe*I and *Sfi*I sites
pAJ67	a) digestion of pMCS-2 with *Hinc*II and *Nhe*I and elution of vector backbone, b) digestion of pAJ61 with *Hinc*II and *Nhe*I, elution of insert, c) ligation of vector backbone and insert via *Nhe*I and *Hinc*II sites

Table 6-3: Plasmid construction (continued)

Plasmid	Construction
pAJ70	a) sequential digestion of pAR51 with first *Nhe*I and then *Sfi*I, elution of vector backbone (cut out kanamycin resistance), b) sequential digestion of pEC45 with first *Nhe*I and then *Sfi*I, elution of rifampicin backbone, c) ligation of pAR51 backbone and rifampicin backbone via *Nhe*I and *Sfi*I
pAJ73	a) digestion of pNPTS138 with *Hind*III and *Nhe*I, b) amplification of *smc* fused to *venus* with primer 297 (adding *Hind*III site) and 269 (adding *Bam*HI site) using pAJ55 as template, c) amplification of 3´flanking region of *smc* with primer 298 (adding *Bam*HI site) and 280 (adding *Nhe*I site), d) 3 fragment ligation via *Hind*III, *Nhe*I, and *Bam*HI
pAJ74	a) digestion of pNPTS138 with *Hind*III and *Nhe*I, b) amplification of part of *parB* fused to *cerulean* with primer 299 (adding *Hind*III site) and 257 (adding *Kpn*I site) using pAJ54 as template, c) amplification of 838 bp of 3´flanking region of *parB* with primer 300 (adding *Kpn*I site) and 301 (adding *Nhe*I site), d) 3 fragment ligation via *Hind*III, *Kpn*I, and *Nhe*I
pAJ75	a) digestion of pCVENC-2 (pEC111) with *Nde*I and *Kpn*I, b) mutagenesis PCR with primer 307 and 308 using pAR25 (P_{Zn}-*parA-venus*) as template to amplify whole plasmid and subsequent *Dpn*I digest, c) digestion of pAR25* (P_{Zn}-*parA (K18R)-venus*) with *Nde*I and *Kpn*I, d) ligation of vector backbone of pEC111 and insert (*parA K18R*) via *Nde*I and *Kpn*I
pAJ78	a) digestion of pCVENC-2 (pEC111) with *Nde*I and *Kpn*I, b) digestion of pAJ45 with *Nde*I and *Kpn*I to cut out *parA* (without stop codon), c) ligation of vector backbone of pEC111 and insert (*parA*) via *Nde*I and *Kpn*I
pAJ79	a) digestion of pKH3 (*oriT*, *lacO* array) with *Eco*RI and *Nhe*I, b) amplification of part of *HNE_1729* + downstream region with primer 311 (adding *Eco*RI site) and primer 312 (adding *Nhe*I site), c) ligation of vector backbone and insert via *Eco*RI and *Nhe*I site
pAJ80	a) digestion of pKH3 (*oriT*, *lacO* array) with *Eco*RI and *Nhe*I, b) amplification of part of *HNE_3540* + downstream region with primer 313 (adding *Eco*RI site) and primer 314 (adding *Nhe*I site), c) ligation of vector backbone and insert via *Eco*RI and *Nhe*I sites
pAJ81	a) digestion of pVENC-2 with *Nde*I and *Kpn*I, b) amplification of C-terminal part of *dnaN* with primer 317 (adding *Nde*I site) and primer 318 (adding *Kpn*I site), c) ligation of vector backbone and insert via *Nde*I and *Kpn*I sites

Table 6-4: Oligonucleotides used in this study

Name	Description	Sequence (5´-3´)
General oligonucleotides (for sequencing and colony PCR)		
M13for		gccagggttttcccagtcacga
M13rev		gagcggataacaatttcacacagg
IntSpec-1		atgccgtttgtgatggcttccatgtcg
REV-uni		ggggatgtgctgcaaggcgattaagttg
eGYC-up		cttgccgtaggtggcatcgccctcg
eGYC-down		gctgctgcccgacaaccactacctgag
mCherry-up		ctcgccctcgccctcgatctcgaac
mCherry-down		ggcgcctacaacgtcaacatcaagttgg
RecZn-2		aggcaaccagcacgaacgccagc
2372_prom_out_for		cgcgggcgatgttgaggaagttctg
pCop1486_out_for		cgaagtccgccgtggccgag
pCop1486_check_for		ccccttatcatccagaccagctacg
pCop1486_check_rev		ggcttttgatttttgacgtcgag
oKH21		tttacactttatgcttccggctcgt
Oligonucleotides used for gene amplification, integration/deletion check, and sequencing		
142	ssb for	atatCATatggcgggatcggtaaacaaggtcatt
143	ssb rev fusion 2	atatGGTACCgaacgggatctcgtcgtcgagatcctg
144	holC for	atatCATatgcagccagcagcccccgaatg
145	holC rev fusion	atatGGTACCaacccccgcctctttccagccgc
146	HNE_1677 (PopZ) fw	atatCATatggccaacgaagcgcataaagaaccg
147	HNE_1677 (PopZ) rv fusion	atatGGTACCgcgcgccatgcgggcaatcc
148	ParB fw	atatCATatgagtgatccggcagaggacaatcgc
165	pAJ32(holC) intergration check	ggcgagaaatcccccaccgaccc
173	part HNE_1854 fw	atatGGTACCaagctctttcccgatcccccgccc
174	HNE_1854 rv	atGAGCTCtcagtccgggacatccggagacca
177	HNE_1677 F1fw	atatAAGCTTgatgccaaccagcgggacaccag
178	HNE_1677 F1rv	atatGGTACCcgtcggttctttatgcgcttcgttgg
179	HNE_1677 F2fw	atatGGTACCgtacagcggattgcccgcatggc
180	HNE_1677 F2rv	atGAATTCgctgaccaacaattgcgccgccg
186	ParB rv fusion for pET	atGAATTCgattccgcagtccggcgcttagcg
187	HNE_1677 genom up	tccgccagaacaatgtgaccgtgacc
188	HNE_1677 genom down	cggatcccagttcacgaggcgcttg
191	pAJ36 integration check fw	tcaaggccgcacatctccaccgacg

Table 6-4: Oligonucleotides used in this study (continued)

Name	Description	Sequence (5´-3´)
196	Cy3 parS wt	ggtccaatgtttcacgtgaaacatcattggtttttccaatgatgtttcacgtgaaacattggacc
197	Cy3 parSmut	ggtccaatgcctcacgtgaaacatcattggtttttccaatgatgtttcacgtgaggcattggacc
209	HNE_1048 fw	atatCATatgagccaggccacagctgaaca
210	HNE_1048 rv	atatGGTACCcaccaccggcgcgcgcagcagatc
211	HNE_3182 fw	atatCATatgaaatgccctgtcgataatgag
212	HNE_3182 rv	atatGGTACCgaagtcgaacaggtcgctgagaaag
213	HNE_3528 fw	atatCATatgcgcctgcccctgcttctgatc
214	HNE_3528 rv	atatGGTACCgcccggaccctggcaggcgcccg
215	parA genom up	gggtcaggccgggcggatcgaag
216	parA F1 fw	atatAAGCTTccgcgtccggaaagctgggtgac
217	parA F1 rv	atatGGTACCttgattcaccacggcaaatattc
218	parA F2 fw	atatGGTACCgaagtgttgcagcgtgaaagggc
219	parA F2 rv	atataGCTAGCggcttcgacctcccggacgctga
220	parA genom down	agcggcggcagacttcatcgagc
222	parB F1 fw	atatAAGCTTacattgtgccgggcgacgagaa
227	HNE_1917 (SMC) fw	atatCATatgcagataactgaactccgcat
228	HNE_1917 (SMC) rv ohne stop	atatGGTACCctccgccgcaacaagctcctcgg
229	smc intern for seq. fw	cgaagccaatctccagcgcctcg
230	smc intern for seq. Rv	cgcggccttcggcgttgagggctt
231	smc intern for seq.2 fw	ccctcaacgacgccgaacgcacc
232	smc intern for seq. 2 Rv	gttgtcgatgtcacgcgcgagcgc
233	pAJ51 int check (HNE_1048)	gccagcagcgcaatgacacgatcc
235	pAJ53 int check (HNE_3528)	cggcccggtagagctggaattcg
238	part HNE_1729 fw	atatGGTACCgcccggatcgctgatgagctgctc
239	HNE_1729 rv	atataGCTAGCtcatggagctgcaaatctcatcacttctgc
240	part of HNE_2644	atatGGTACCacggtcaccaacggcatcatctccg
241	HNE_2644 rv	atataGCTAGCtcaggtgcgcactgtgcctcgc
242	part of HNE_0857 fw	atatGGTACCaaggacatcggcgcggtgatctgc
243	HNE_0857 rv	atGAGCTCtcagcccacccgctccaccacaac
244	part of HNE_0550 fw	atatGGTACCgcccgcccctaaagcgcctcc
245	HNE_0550 rv	atGAGCTCtcatcgagcggggcggggagggc
246	part of HNE_3540 fw	atatGGTACCcgggcgctggatgaaaaccaaggac
247	HNE_3540 rv	atGAGCTCtcaccccatcggatagagaatttcccg
248	part of HNE_0063 fw	atatGGTACCcggaccgcgaatggatggatgcct

Table 6-4: Oligonucleotides used in this study (continued)

Name	Description	Sequence (5´-3´)
249	HNE_0063 rv	atGAGCTCtcacatttctttcgggggcttcaggc
250	int check pAJ56	cggcgcctagaagctcggacgatg
251	int check pAJ57	gctgctcgcggctgccttcctcg
252	int check pAJ58	accccgatatcatgaccccgcgc
253	int check pAJ59	gcccttcacctcccatcgctttgc
254	int check pAJ60	ggatcaacttttttcgacacggccg
255	int check pAJ61	gccgcaatcagcaccaagtcgcc
257	cerulian rv F2	atatGGTACCttacttgtacagctcgtccatgccg
269	venus rv F2 (BamHI)	atatGGATCCttacttgtacagctcgtccatgccg
280	down rv F4	atataGCTAGCtgccgatgaggtttgcgaacagg
297	smc int fw F1 (2)	atatAAGCTTacgtccgaagcccgcctcgtcgag
298	down fw F3 (2)	atatGGATCCtagcgcaccgtgttcgtcatttt
299	parB fw HindIII	atatAAGCTTatgagtgatccggcagaggacaatcgc
300	part of holA fw F3	atatGGTACCtaatccgttaacgaacgttttcag
301	part of holA rv F4	atataGCTAGCggcggcccgatccggaagtctgg
304	smc int fw	cgcgtgacatcgacaactggaccg
305	genom down smc	agggcgccggtgacgatgatgtg
306	parB genom down 3	gatgctgcacaaggggcgcgcgg
307	parA K18R mut fw	caaaagggcggggtcggaagaaccacgacctcgatcaatc
308	parA K18R mut rv	gattgatcgaggtcgtggttcttccgaccccgccctttg
311	part of HNE_1729 FROS fw	atGAATTCttttgacgatgccaacaaaatgcc
312	inter HNE_1729 FROS rv	atataGCTAGCagtggtacgtgccccgcctgctac
313	part of HNE_3540 FROS fw	atGAATTCcgggcgctggatgaaaaccaaggac
314	inter HNE_3540 FROS rv	atataGCTAGCgccctcccttggctcccggtctag
317	dnaN int fw	atatCATATGaagctgccctccggcgctgagg
318	dnaN no stop rv	atatGGTACCcacccgcagcggcatcacgacaa
319	int. Check dnaN fusion	aacccagggcgcgctgaagctc
320	downstr HNE_1729 for seq	tagcgaactgactggcgcgcgcg
321	downstr HNE_3540 for seq	gcaaggcgaggtctgcggcgagg
322	int. Check pAJ79 (FROS ter)	tcgggctcttcggaacggcatcg
323	int. Check pAJ80 (FROS ori)	cggcggtggcagcgatgatgatg
330	genom up smc	cgcagacacctacgccacctccg
331	genom down dnaN	gccgtacatgcccgtctccctgg
332	int. Check pAJ79 (FROS ter)-2	tggcattttggttctggcgcacg
333	int. Check pAJ80 (FROS ori)-2	ccatgccggcaaacgcgaagtcc

Table 6-5: Percentage of anucleate cells in different *H. neptunium* strains (DAPI staining)

Strain	Description	Anucleate cells (%)	n (total)
ATCC 15444	Wild type	0.3	879
AJ46	Depletion ParA, grown in presence of inducer (0.3 mM $ZnSO_4$)	0.5	848
	Depletion ParA, grown in absence of inducer	12	454
AJ79	ParA(K18R)-Venus induced for 4.5 h with 0.3 mM $CuSO_4$	10.8	663
	ParA(K18R)-Venus not induced	1.5	1012
AJ80	ParA-Venus induced for 4.5 h with 0.3 mM $CuSO_4$	0.6	889
	ParA-Venus not induced	0.3	1307

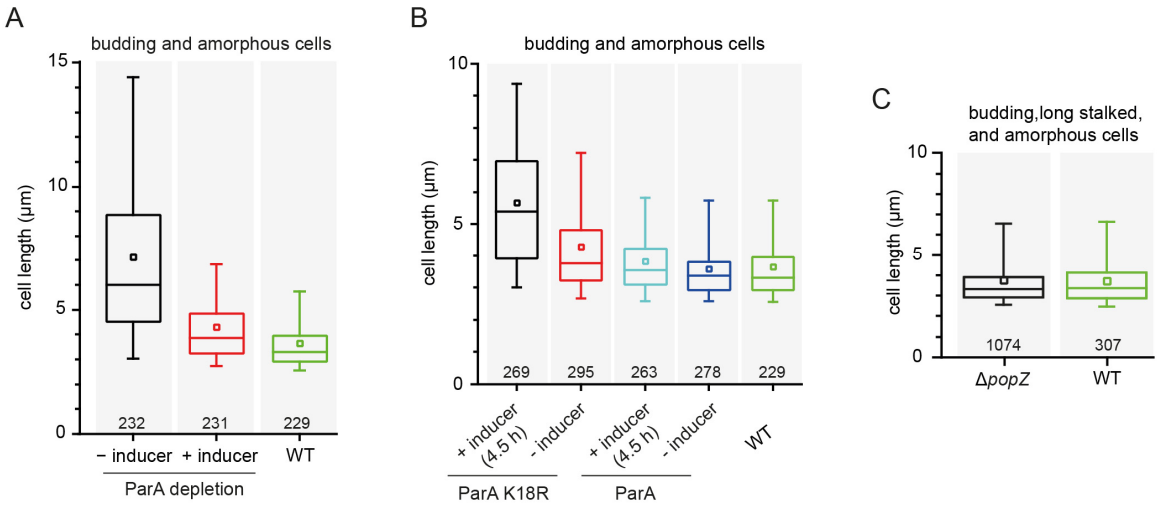

Figure S6-1: Effects of impairment of ParA function and deletion of *popZ* on cell length. A) Effects of ParA depletion on cell length. Cells of strain AJ46 were grown in MB with or without 0.3 mM $ZnSO_4$ and *H. neptunium* wild-type cells were grown in MB to exponential phase, stained with DAPI for 20 min, and visualized by DIC and fluorescence microscopy. Cell length of budding and amorphous cells was quantified and is represented by box plots. The band within the box represents the median, the box boundaries indicate the 25th and the 75th percentile, and the whiskers continue to the 5th and 95th percentile of the data set. The square denotes the mean of the data. The number of cells analyzed is indicated in each panel. B) Effects of ParA K18R production on cell length. Cells of strain AJ79 (*parB-cerulean* P_{Cu}::P_{Cu}-*parA(K18R)-venus*) and AJ80 (*parB-cerulean* P_{Cu}::P_{Cu}-*parA-venus*) were grown in MB medium with or without 0.3 mM $CuSO_4$ for 4.5 h and *H. neptunium* wild-type cells were grown in MB to exponential phase, stained with DAPI for 25 min, and visualized by DIC and fluorescence microscopy. Cell length of budding and amorphous cells was quantified and is represented by box plots as described in (A). C) Effects of *popZ* deletion on cell length. Cells of strain AJ38 (Δ*HNE_1677*) and and *H. neptunium* wild type were grown in MB medium to exponential phase and visualized by DIC microscopy. Cell length of budding, long stalked, and amorphous cells was quantified and is represented by box plots as described in (A).

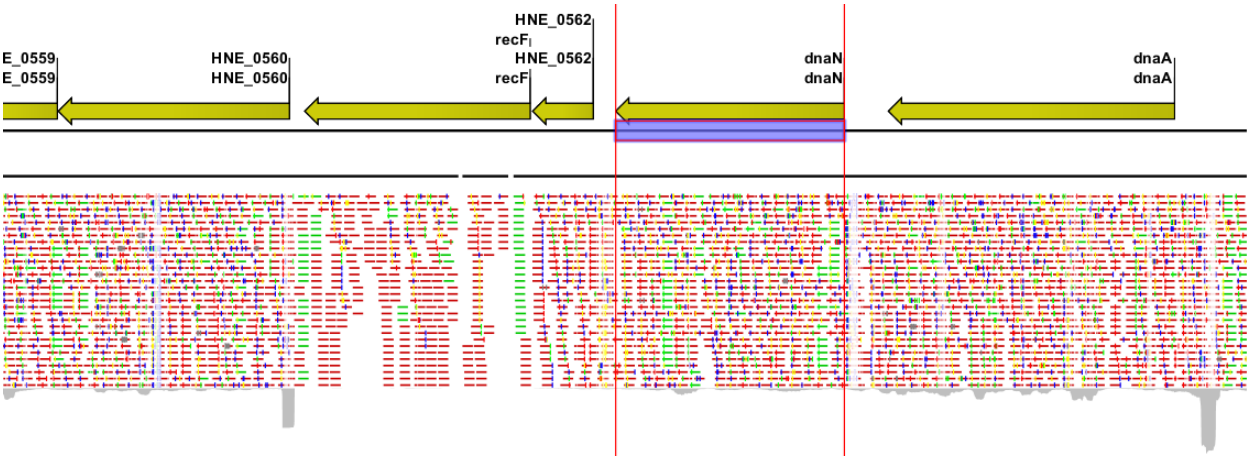

Figure S6-2: Screenshot of mapping of RNA-sequencing reads against *H. neptunium* genome. Shown is the *dnaN* genomic locus with up- and downstream regions (yellow arrows). Green and red lines denote sense and antisense reads, respectively. The remainder of the reads is shown in a compressed form below in grey. Grey peak upstream of gene indicates potential transcriptional start site.

Acknowledgements

[redacted]

CURRICULUM VITAE

Erklärung

Ich versichere, dass ich meine Dissertation:

„Chromosome arrangement and dynamics in the budding bacterium *Hyphomonas neptunium*“

selbstständig, ohne unerlaubte Hilfe angefertigt und mich dabei keiner anderen als der von mir ausdrücklich bezeichneten Quellen und Hilfen bedient habe. Die Dissertation wurde in der jetzigen oder einer ähnlichen Form noch bei keiner anderen Hochschule eingereicht und hat noch keinen sonstigen Prüfungszwecken gedient.

Marburg, den ....

Alexandra Jung